Collection of Abstracts for UKNC Winter Conference, Jan 2016

ORALS

Multi-Microscopy Techniques for the Investigation of Fully Coalesced Boundaries in GaN

T. J. O'Hanlon, F. C.-P. Massabuau and R. A. Oliver
Department of Materials Science and Metallurgy, University of Cambridge, UK

The prevalence of threading dislocations (TDs) in nitride semiconductors is well known, but their generation mechanism is not fully understood. Early models [1-2] suggested TDs formed at GaN island coalescence boundaries (CBs) with slightly differing misorientations. Conversely, later work [3-6] using partially coalesced films to directly correlate CBs with dislocation distributions found no evidence of increased TD density at CBs: most dislocations seemed to be carried through from the initial nucleation layer.

However, as these studies were restricted to partially coalesced films, to allow CB identification, the impact of complex late-coalescing boundaries could not be investigated. Here, the development of a multi-microscopy technique allowing direct correlation of CB and TD locations in fully-coalesced films is presented.

A *c*-plane 3D-2D growth GaN-on-sapphire sample was grown with 100 nm thick highly *n*-type silicon-doped GaN marker layers every 750 nm, effectively marking the surface structure at various points during growth. Scanning Capacitance Microscopy (SCM) was used to map the carrier type and concentration on cleaved cross-sections of the material, revealing the surface evolution over time. This allowed CBs to be located after the film had fully coalesced, as seen in the SCM amplitude image in Figure 1 (unintentional doping is also visible).

Lithographic markers and topographic cleavage steps were used to allow the exact areas characterized in SCM to be located in the Focused Ion Beam / Scanning Electron Microscope. The previously characterized cross-sections were then lifted out as lamellae from the cleaved edge by milling from only the back side, with careful preparation and choice of milling angles to avoid exposure of the characterized surface to the ion beam.

Transmission Electron Microscopy defect analysis was then used to compare and correlate observed TDs with known CB locations to shed further light on the contribution of CBs to dislocation origins in the nitrides.

These techniques could also be applied to numerous other problems where direct correlation of observed cross-sectional features between techniques would yield a greater understanding of the behavior observed.

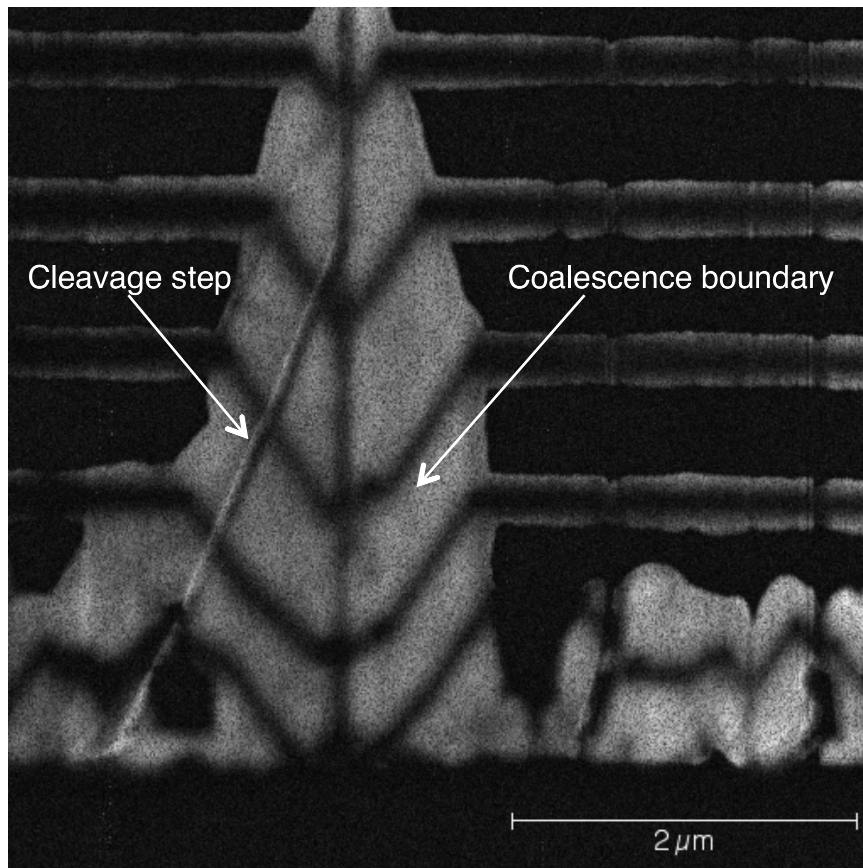

Figure 1: Scanning Capacitance Microscopy dC/dV amplitude image of a late-coalescing boundary. Unintentional doping on inclined growth facets is also seen.

REFERENCES:

[1] Ning, X. J., Chien, F. R., and Pirouz, P. *Journal of Materials Research*, (0001), 1996.
[2] Wu, X. H., Fini, P., Tarsa, E. J., Heying, B., Keller, S., Mishra, U. K., Denbaars, S. P., and Speck, J. S. *Journal of Crystal Growth*, 190:231–243, 1998.
[3] Narayanan, V., Lorenz, K., Kim, W., and Mahajan, S. *Applied Physics Letters*, 78(11):1544, 2001.
[4] Oliver, R. A., Kappers, M. J., and Humphreys, C. J. *Applied Physics Letters*, 89(1):011914, 2006.

[5] Oliver, R., Kappers, M., Sumner, J., Datta, R., and Humphreys, C. *Journal of Crystal Growth*, 289(2):506–514, 2006.
[6] Moram, M. A., Ghedia, C. S., Rao, D. V. S., Barnard, J. S., Zhang, Y., Kappers, M. J., and Humphreys, C. J. *Journal of Applied Physics*, 106(7):073513, 2009.

Nanoscale Tomography of III-nitride devices: Correlating Material Effects and Device Properties.

F. Tang[1], C.X. Ren[1], D. Wang[2], G. Divitni[1], T. Zhu[1], E. Hu[2], R. A. Oliver[1]

[1]Department of Materials Science and Metallurgy, University of Cambridge, 27 Charles Babbage Road, Cambridge CB3 0FS, United Kingdom

[2]School of Engineering and Applied Sciences, Harvard University, Cambridge, MA, 02138, USA

III-nitride materials are perhaps most well-known for their application in high-brightness light emitting diodes (LEDs) [1], however they are also particularly sought after for various optical devices such as laser didoes [2] and single photon sources [3]. In particular, III-nitride microcavities offer an exceptionally versatile platform not only in device related applications, but also as a platform for the investigation of fundamental light-matter interactions and cavity quantum electro-dynamics (cQED) [4]. Despite the expected benefits of III-nitride materials in nano- and micro-scale devices, the performance of said devices can be hindered by issues encountered in top-down fabrication techniques due to the excellent chemical and thermal stability of III-nitride materials [4]. In the development of high-performance nanoscale nitride devices it is thus crucial for optimisation strategies to incorporate techniques for the evaluation of fabrication and material issues.

We report the use of dual-beam focussed ion beam -scanning electron microscope (FIB-SEM) based sample preparation techniques for the analysis of undercut nanoscale nitride photonic crystal cavities using transmission electron microscopy (TEM) and electron tomography (ET). The devices examined in this study are 1-D photonic crystal cavity suspended nanobeam structures fabricated using a method described by Niu *et al.* [5]. Devices fabricated using this method have been shown to exhibit extremely low-threshold lasing behaviour and Q-factors up to 1900. Here, we analyse failed devices to elucidate the materials or fabrication issues leading to failure using electron microscopy techniques following sample preparation.

The nanobeam devices studied here consist of a ridge waveguide design perforated with gratings of circular gaps designed using a deterministic high-Q method [5]. The nanobeam has a total length of 5.2 μm, a width and thickness of 125 nm and 200 nm respectively, and a target hole periodicity of 130 nm .The small dimensions and high aspect ratio of the structures and associated high sensitivity to ion-beam damage render standard FIB-SEM lift-out processes ineffective in producing high-quality samples for TEM analysis. As such, SEM-cured glue was used to perform sample device lift-out and attachment to a tomography holder, providing minimal ion-beam damage and contamination. Scanning transmission electron microscopy with a high-angle annular dark-field detector (STEM-HAADF) revealed the incomplete etching of gaps in the examined device. High resolution tomographic imaging was then performed by recording a series STEM-HAADF images at every 2 degrees for 180 degrees about a tilt axis and 'back-projecting' these to form a 3-D reconstruction of the device, giving detailed information concerning the 3-D geometry of the gaps in the structure as well as potentially revealing surface roughness and tapered features, factors which are key in the performance of the device. These results were then compared to a second tomographic study using a "slice-and-view" technique, in which a nanobeam cross-section is prepared in FIB and imaged in SEM, before a small region of the nanobeam was removed using the ion beam, moving the cross section imaged in SEM along the length of the structure, to produce a series of images for tomographic reconstruction.

In conclusion, we have designed a sample preparation method to minimise the damage and contamination inherent to standard dual-beam FIB/SEM sample preparation methods in order to prepare a fabricated nanobeam photonic crystal device for electron tomography. STEM-HAADF revealed the incomplete etching of the nanobeam holes along the device as well as unetched material on the underside of the nanobeam possibly responsible for device failure, and electron tomography allowed us to access 3-D information concerning the geometry of the device. We envision that this method of analysing fabricated devices can be coupled with theoretical simulations to provide a powerful framework for the characterisation and optimisation of nano-scale photonic devices.

[1] S. Nakamura, T. Mukai, and M. Senoh, "High-Power GaN P-N Junction Blue-Light-Emitting Diodes," *Jpn. J. Appl. Phys.*, vol. 30, no. 12A, pp. 1998–2001, 1991.
[2] S. Nakamura, "The Roles of Structural Imperfections in InGaN-Based Blue Light-Emitting Diodes and Laser Diodes," *Science (80-.).*, vol. 281, no. 5379, pp. 956–961, Aug. 1998.
[3] S. Kako, C. Santori, K. Hoshino, S. Götzinger, Y. Yamamoto, and Y. Arakawa, "A gallium nitride single-photon source operating at 200 K.," *Nat. Mater.*, vol. 5, no. 11, pp. 887–92, Nov. 2006.
[4] T. J. Puchtler, A. Woolf, T. Zhu, D. Gachet, E. L. Hu, and R. A. Oliver, "Effect of Threading Dislocations on the Quality Factor of InGaN/GaN Microdisk Cavities," *ACS Photonics*, vol. 2, pp. 137–143, 2015.
[5] N. Niu, A. Woolf, D. Wang, T. Zhu, Q. Quan, R. A. Oliver, and E. L. Hu, "Ultra-low threshold gallium nitride photonic crystal nanobeam laser," *Appl. Phys. Lett.*, vol. 106, no. 23, p. 231104, 2015.

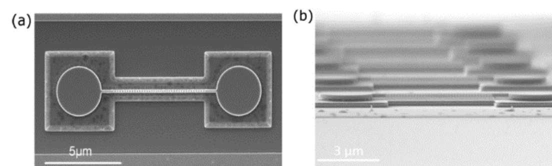

Figure 1: a) SEM image of the photonic crystal b) side-view SEM showing the undercut of the devices.

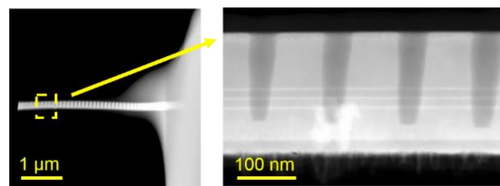

Figure 2: Left: STEM-HAADF overview of the nanobeam, right: close-up view showing the QW active region, and incomplete etching of the holes.

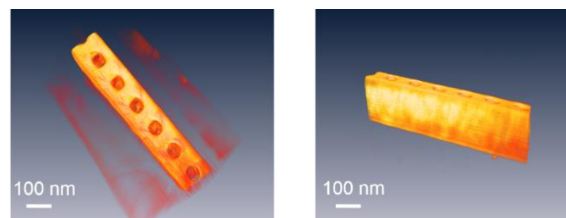

Figure 3: Tomographic reconstruction of the nanobeam.

Room temperature PL efficiency of InGaN QW structures with prelayers as a function of the number of QWs and QW barrier width

George M. Christian[1], Simon Hammersley[1], Matthew J. Davies[1], Phil Dawson[1], Menno J. Kappers[2], Fabien C.-P. Massabuau[2], Rachel A. Oliver[2], Colin J. Humphreys[2]
[1]School of Physics and Astronomy, Photon Science Institute, University of Manchester, M13 9PL, UK.
[2]Department of Materials Science and Metallurgy, 27 Charles Babbage Road, University of Cambridge, CB3 0FS, UK.

The inclusion of prelayer structures, typically low indium composition InGaN layers or InGaN/GaN superlattices underlying InGaN/GaN multiple quantum well (QW) structures in light emitting diodes (LEDs), is frequently associated with an increase in measured photoluminescence intensity and 300 K internal quantum efficiency (IQE) [1-4]. The origin(s) of these improvements in performance, however, remain the subject of debate. Suggested mechanisms include strain relief in the QWs [1], increased electron capture efficiency [2], and a reduction in the density of defects in the QWs [3]. It was previously reported [4] that the increased IQE in InGaN/GaN QW structures containing prelayers could be attributed to the modification of the surface polarisation field between the sample surface and the prelayer. This field opposes the built-in polarisation fields across the QWs leading to a reduced electric field across all of the QWs in a stack. Increased IQEs and reduced photoluminescence (PL) radiative decay times measured for structures containing prelayers compared with those without prelayers were attributed to the reduced spatial separation of the electron and hole wavefunctions, consistent with calculated conduction and valence band profiles.

In this work, we report on the effects of varying the distance between the prelayer and the sample surface in two sets of InGaN/GaN multiple QW structures grown by metalorganic vapour phase epitaxy. Each structure contains a 23 nm thick Si doped ($\sim 5 \times 10^{18}$ cm^{-3}) $In_{0.05}Ga_{0.95}N$ prelayer grown ~ 3 nm below the first QW in the stack. The first set of samples consists of structures containing, respectively, 1, 3, 5, 7, 10, and 15 InGaN QWs and separated by 7 nm GaN barriers. The second set consists of three structures each containing 5 InGaN QWs separated by GaN barriers of thickness 4 nm, 7 nm, and 11 nm, respectively. The electric field across each QW in a stack was calculated for each structure using the device simulation package nextnano^3 [5]. The electric fields were found to be strongly dependent on the total distance between the prelayer and the surface. As this distance decreases, the range over which the surface polarisation field acts is reduced. Therefore the resultant electric field across each QW decreases with either increasing number of QWs or increasing QW barrier thickness. This is supported by a blue shift in the PL emission from the QW(s) with decreasing strength of the mean calculated field across the QWs, as well as reductions in PL radiative decay times, measured at 10 K for both sample sets. Both of these effects are consistent with a reduced resultant electric field across the QWs. The internal quantum efficiency (IQE) at 300K of the samples in the set with varying number of QWs decreases with increasing number of QWs. This is attributed to the increased radiative recombination rate in samples with reduced fields across the QWs. This is in contrast to structures without prelayers, in which the IQE is seen to increase with increasing number of QWs as thermally driven carrier escape effects are reduced [6,7]. The set with varying QW barrier thickness serves to decouple the surface field effect from that of varying the number of QWs and it displays similar trends, with the highest IQE occurring in the sample with the thinnest barriers, suggesting that the effect of the surface field is an important consideration in device design.

[1] N. Nanhui *et al.*, Solid-State Electron., **51**, 860–864, (2007).
[2] N. Otsuji *et al.*, J. Appl. Phys., **100**, 113105, (2006).
[3] A. M. Armstrong *et al.*, J. Appl. Phys., **117**, 134501, (2015).
[4] M. J. Davies *et al.*, Appl. Phys. Lett. **105**, 092106 (2014).
[5] S. Birner, "nextnano GmbH".
[6] P. Hurst *et al.*, Phys. Status Solidi B **228**, 137–140 (2001).
[7] A. Laubsch *et al.*, IEEE Trans. Electron Devices **57**, 79–87 (2010).

Observation of efficiency droop in non-polar InGaN/GaN quantum wells

Simon Hammersley[1], Matthew J. Davies[1], Menno J. Kappers[2], Phil Dawson[1], Colin J. Humphreys[2], Rachel A. Oliver[2]

[1] School of Physics and Astronomy, Photon Science Institute, University of Manchester, M13 9PL.

[2]Department of Materials Science and Metallurgy, 27 Charles Babbage Road, University of Cambridge, CB3 0FS.

Non-polar InGaN/GaN quantum well (QW) structures grown using the *m* (1-100) and *a* (11-20) crystal planes have received a lot of interest in recent years, with the promise to produce high efficiency light emission [1-2]. The major difference between quantum wells using the non-polar *m* and *a*-planes, as opposed those grown using the polar *c*-plane (0001), is the suppression [3] of the strong polarisation-induced electric fields that act across the QWs. This suppression leads to an increase in the electron/hole wavefunction overlap, resulting in faster radiative recombination lifetimes [4] for non-polar QWs when compared to equivalent *c*-plane QWs [5]. Growth using non-polar orientations has also been reported [6-11] to supress the effects of the efficiency droop observed in *c*-plane LEDs, although the reason for this suppression is still under debate.

In this work, the low temperature photoluminescence (PL) of two blue emitting 5 period InGaN/GaN multiple QWs, grown on Ammono [12] *a* and *m*-plane free standing GaN templates respectively, were investigated as a function of excitation power density. The non-polar samples were then compared to a *c*-plane InGaN/GaN single QW. In order to overcome the difference in equilibrium carrier density caused by the vastly different recombination lifetimes, samples were excited using a pulsed laser. The pulse duration was significantly shorter than the recombination lifetime in the samples and the pulse separation was long enough to ensure that all excited carriers had recombined before the arrival of the next excitation pulse. It is therefore possible to estimate the carrier density excited within the QWs. The *a* and *m*-plane samples were found to undergo droop at 10 K, along with an increase in the measured full width half maximum (FWHM) of the PL spectrum. The increase in PL FWHM was caused by a broadening on the high energy side of the PL spectrum. This behaviour is remarkably similar to that observed in the *c*-plane reference sample. The onset of efficiency droop was found to occur at the same value of the density of excited carriers per QW in both the polar and non-polar QWs. We therefore conclude that the process for efficiency droop in polar and non-polar samples is remarkably similar, and is unaffected by the faster recombination lifetime in non-polar samples.

[1] M.C. Schmidt *et al*., J. Appl. Phys. **46**, L126 (2007).
[2] K.-C. Kim *et al*., Phys. Stat. Sol. (RRL), **1**, 125 (2007).
[3] P. Waltereit *et al*., Nature **406**, 865 (2000).
[4] S. Marcinkevicius *et al*., Appl. Phys. Lett. **103**, 111107 (2013).
[5] N.I. Bochkareva *et al*., Semiconductors, **46**, 1032 (2012).
[6] X. Li *et al*., Appl. Phys. Lett. **95**, 121107 (2009).
[7] J. Lee *et al*., Appl. Phys. Lett. **95**, 201113 (2009).
[8] S.-C. Ling *et al*., Appl. Phys. Lett. **96**, 231101 (2010)
[9] S.-H. Chang *et al*., J. of the Electrochemical Society, **157**, H501-H503 (2010)
[10] E. Kioupakis *et al*., Appl. Phys. Lett. **101**, 231107 (2012).
[11] R. Vaxenburg *et al*., Appl. Phys. Lett. **103**, 221111 (2013).
[12] Ammono S.A.

Investigating efficiency droop in InGaN/GaN quantum well structures using ultrafast time-resolved terahertz and photoluminescence spectroscopy

Aniela Dunn[1], Ben F. Spencer[1], Samantha J. O. Hardman[2], Darren M. Graham[1], Simon Hammersley[1], Matthew J. Davies[1], Phil Dawson[1], Menno J. Kappers[3], Rachel A. Oliver[3], and Colin J. Humphreys[3].

[1]School of Physics and Astronomy and the Photon Science Institute, The University of Manchester, Manchester M13 9PL, UK

[2]Manchester Institute of Biotechnology, The University of Manchester, Manchester M1 7DN, UK

[3]Department of Materials Science and Metallurgy, 27 Charles Babbage Road, University of Cambridge, Cambridge CB3 0FS, UK

Understanding the physical mechanism(s) responsible for efficiency droop in InGaN/GaN quantum well light-emitting diodes (LEDs) is critical in developing strategies to mitigate its effect and enable the wide-spread adoption of high power GaN-based LEDs [1]. To date several mechanisms have been proposed to explain efficiency droop, such as Auger recombination [2], carrier escape [3], and the saturation of localised states [4], but no consensus on the precise origin of this phenomenon has yet been reached. Investigations into a reduction in the localisation induced S-shape photoluminescence temperature dependence of InGaN/GaN quantum wells due to increasing excitation power [5] and observation of a high-energy photoluminescence component that decayed more rapidly than localised carrier emission at high excitation power densities [6] suggested that the saturation of localised states may be a contributory factor to efficiency droop.

To further investigate the physical mechanism or mechanisms contributing to efficiency droop, we report on a study of this phenomenon using time-resolved terahertz spectroscopy and ultrafast photoluminescence (PL) spectroscopy. The sample studied consisted of a 10-period $In_{0.18}Ga_{0.82}N$/GaN multiple quantum well structure grown by metal-organic chemical vapour deposition on a 5 μm thick GaN buffer layer on a (0001) sapphire substrate. From power dependent PL studies, a reduction in the room temperature photoluminescence efficiency to 3% of its maximum value was observed for an excitation fluence of 0.96 $mJcm^{-2}$. A correlation was found between the onset of efficiency droop and the emergence of a peak on the high-energy side of the quantum well emission which was found to decay much more rapidly than the localised carrier emission. In line with our previous results [5, 6] we attribute these characteristics to the saturation of localised states and the recombination from higher energy delocalised states at high excitation fluence.

To further understand this behaviour time-resolved terahertz spectroscopy was performed under the same high-fluence excitation. Time-resolved terahertz spectroscopy revealed two decay components: a rapidly decaying component attributed to the emission from delocalised states and a slow nanosecond decay component attributed the recombination involving localised states within the quantum well. In contrast to the PL decays, the magnitude of the nanosecond decay component measured with terahertz spectroscopy was found to increase for increasing excitation power. Due to the effective masses in GaN, terahertz spectroscopy is predominantly sensitive to photoexcited electrons in the structure. These results may therefore suggest that the saturation of localised hole states may be playing a part in the onset of efficiency droop.

[1] G. Verzellesi *et al.*, J. Appl. Phys. 114, 071101 (2013);
[2] K. T. Delaney *et al.*, Appl. Phys. Lett. 94, 191109 (2009);
[3] M. F. Schubert *et al.*, Appl. Phys. Lett. 94, 081114 (2009);
[4] T. Mukai *et al.*, Jpn. J. Appl. Phys. 38, 3976 (1999);
[5] S. Hammersley *et al.*, J. Appl. Phys. 111, 083512 (2012);
[6] M. J. Davies *et al.*, Appl. Phys. Lett. 102, 022106, (2013).

The last bound barrier state model for LEDs

Markus Pristovsek[1,*], Tongtong Zhu[1], Yisong Han[1], Fabrice Oehler[1,a], Rachel A. Oliver[1], Colin J. Humphreys[1], Sebastian Bauer[3], Manuel Knab[3], Klaus Thonke[3], Grzegorz Kozlowski[4], Donagh O'Mahony[4], Pleun Maaskant[4], Brian Corbett[4]
[1]*Department of Materials Science and Metallurgy, University of Cambridge, 27 Charles Babbage Road, Cambridge, CB3 0FS, UK*
[4]*Tyndall National Institute, Lee Maltings, Cork, T12 R5CP, Ireland*
[a]*present address: LPN, CNRS, Route de Nozay, 91460 Marcoussis, France*
[3]*Universität Ulm, Institute of Quantum Matter / Semiconductor Physics Group, D-89069 Ulm, Germany*
*Email: mp680@cam.ac.uk

Many efforts are currently under way to improve the quantum efficiency of InGaN based light emitting diodes (LEDs) and lasers. Semi- and non-polar orientations are one approach which dramatically reduces the built-in polarization and piezo-electric fields. We have prepared quantum wells (QWs) on polar (0001), semi-polar (11-22), and non-polar (11-20) and (1-100) orientation, on quasi-bulk and GaN templates on patterned sapphire with low defect density (LDD) , as well as directly on m- or r-plane sapphire.

For all LDD samples the room temperature photoluminescence (PL) signal at similar wavelengths was lower by a factor of 3-5 for semi-polar (11-22), and even by about 10-30 for (11-20) and (1-100) oriented QWs compared to the polar (0001) orientation (fig. 1a). Moreover, this ratio between semi-polar (11-22) and non-polar (11-20) holds also for the more defective hetero-epitaxial samples grown directly on m-plane or r-plane sapphire. Microstructural characterization of the LDD samples did not reveal any obvious defects in the QWs. Additionally, the PL FWHM values were comparable on (11-22) and (0001). Hence, the lower PL efficiency of the semi- and non-polar QWs is not related to crystal defects.

Further investigations discovered a strong impact of the barrier thickness between the QWs. If excited with a laser wavelength above the barrier bandgap, the light is absorbed in both the QWs and the barrier. Hence, increasing the barrier thickness should linearly increase the total amount of carriers available in the active region. Indeed, for (0001) the PL signal increases proportional to the barrier thickness, as does the power dependent wavelength shift. But for semi-polar (11-22) QWs the PL signal as well as the power dependent shift of PL wavelength stays constant for barriers thicker than 3 nm. We infer that many carriers generated in the barrier region do not reach the QWs.

When comparing the power dependent PL at very high excitation densities, the droop reduces the EQEs of polar and semi-polar close to the much lower EQEs of non-polar QWs. A single QW LED showed the same behavior for electroluminescence: The light output of the (11-22) LED became comparable to the (0001) reference LED deep in the droop regime (fig. 1b).

These results suggest a loss channel, which activates at lower polarization fields, no matter if those lower fields are intrinsic (semi-/non-polar) or due to screening at high currents densities on polar. This loss overcompensates the gain from the larger wave function overlap and the resulting shorter radiative lifetimes with lower fields. On the contrary, stronger fields across the active region in more polar orientations could be beneficial, since these would lead to very deep QW ground states compared to the first unbound state above the barrier (fig. 2). This reduces the carrier escape from QWs (e.g. into the Mg doped regions or surface) because the fields provide many bound states in the barrier next to the QW as an easily accessible reservoir to recombine in the QWs.

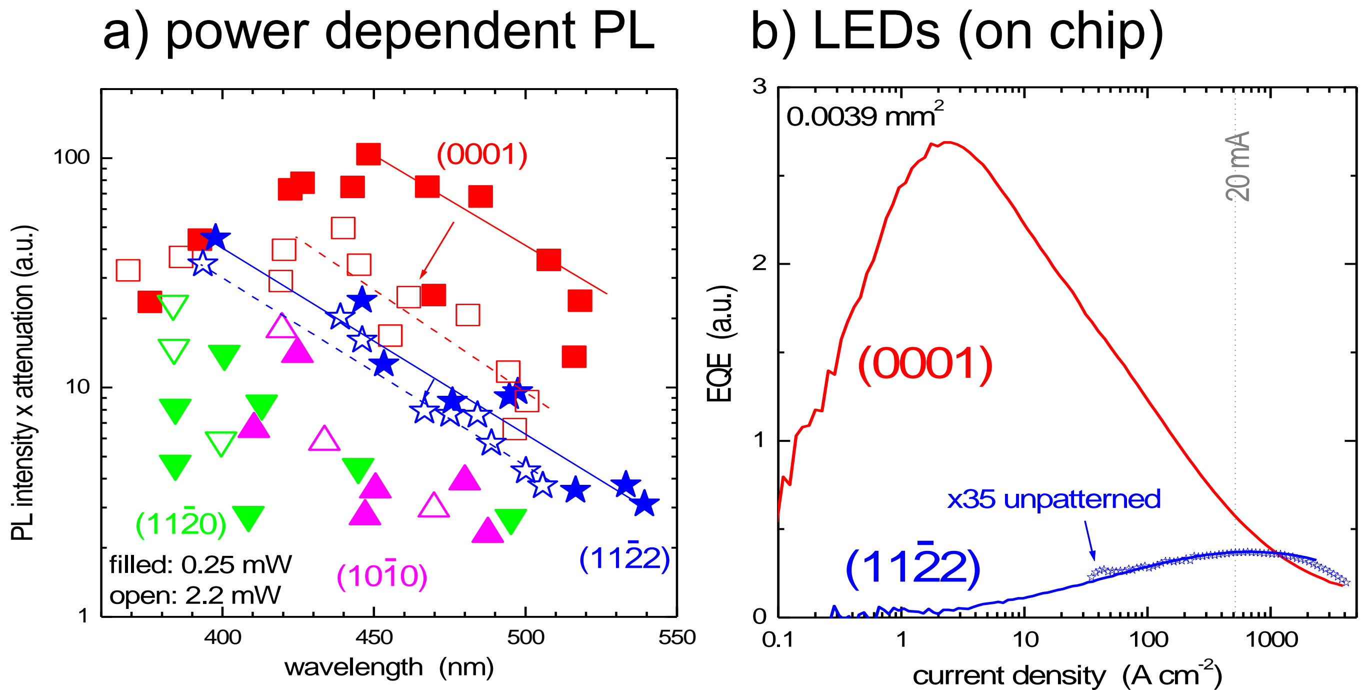

Fig. 1: (a) the power-normalized PL intensity reduces at longer wavelength ("green gap"), less internal polarization from (0001) over (11-22) to (11-20), and power (high power: open symbols). (b) EQE over current density for a single QW LED at 465 nm on (0001) and (11-22) become comparable at very high current densities. The (11-22) was measured on LDD patterned substrates and on more defective unpatterned on m-plane sapphire. The latter was scaled up by a factor of 35 to give the same EQE.

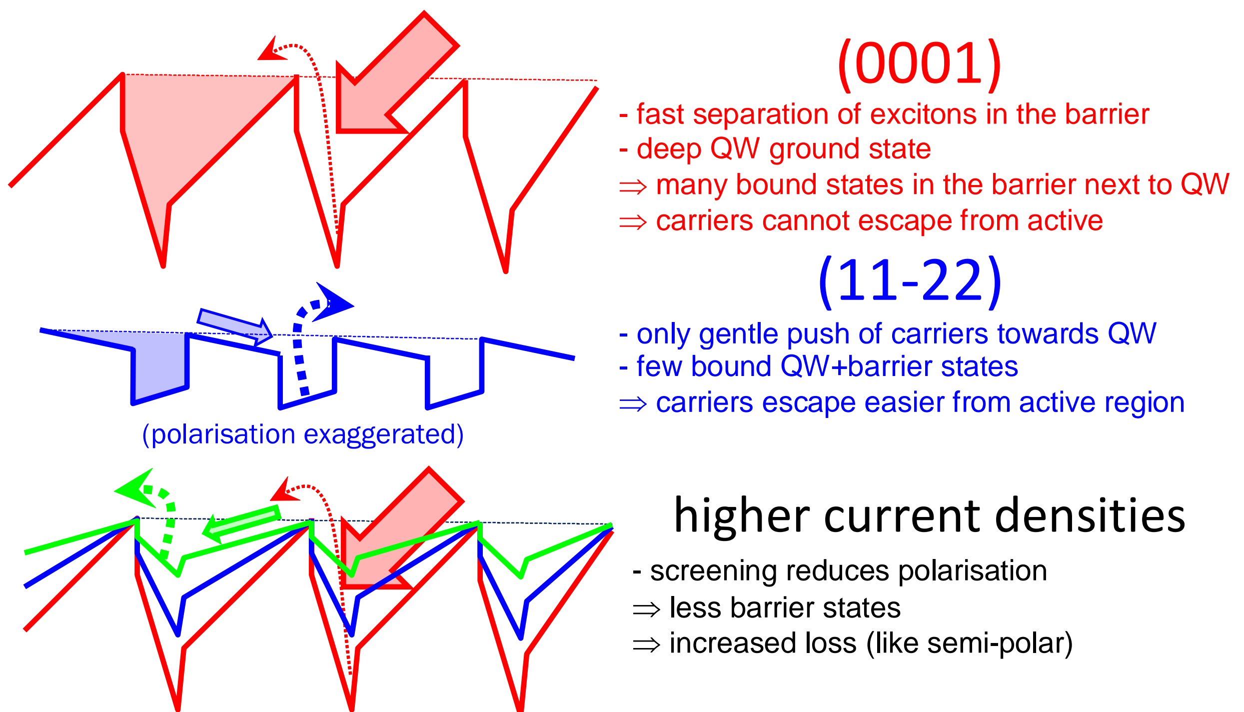

Fig. 2: The last bound barrier state model illustrated.

Electron backscattered diffraction and electron channelling contrast imaging of a cross-section semi-polar GaN on a patterned r-sapphire substrate

G. Naresh - Kumar[1*], A. V. Clemente[2], C. Trager - Cowan[1], A. J. Wilkinson[2], F. Tendille[3], P. de Mierry[3] and P. Vennegues[3]

1.Department of Physics, SUPA, University of Strathclyde, Glasgow G4 ONG, UK
2.Department of Materials, University of Oxford, Parks Road, Oxford OX1 3PH, UK
3.CNRS-CRHEA, rue Bernard Grégory, Sophia-Antipolis, F-06560 Valbonne, France

[*]*naresh.gunasekar@strath.ac.uk*

One method for improving the performance of nitride–based devices is the reduction of the polar and piezoelectric fields which are a result of the wurtzite crystal structure and the strain induced in device structures, respectively. This can be achieved by growing on nonpolar, *m*-plane (1-100) and *a*-plane (11-20), or semipolar (11-22) and (20-21) planes. A range of crystal growth technologies is being developed for the realisation of nonpolar and semipolar GaN substrates, but their size remains small and their cost is too high. Heteroepitaxial growth of semipolar nitrides on sapphire and silicon substrates is highly desirable for the realisation of low cost, high efficiency, and long wavelength (amber and red) light emitting diodes. However, heteroepitaxially grown semipolar nitrides suffer from a high density of extended defects such as threading dislocations (TDs), basal plane stacking faults (BSFs) and associated partial dislocations mainly due to the large lattice mismatch between the heteroepitaxial substrate and the epilayer. In order to optimise the growth and thereby improving the crystal quality, a rapid, non-destructive and cost-effective structural characterisation technique is essential for detailed understanding of extended defects and their formation. Coincident electron channelling contrast imaging (ECCI) [1, 2] and electron backscattered diffraction (EBSD) [3, 4] in a field emission scanning electron microscope (FEG-SEM) can be a route forward to fulfil this requirement.

In our presentation, we will show our preliminary results on a (11-22) semipolar GaN film grown epitaxially on a patterned *r*-sapphire substrate by metal organic vapour phase epitaxy [5]. We were able to produce ECC images (fig. 1a) on a cross section sample revealing extended defects, similar to transmission electron microscope (TEM) images as shown in figure 1b. We have applied cross correlation based high resolution EBSD [3] to evaluate the strain variation (normal and shear strain) in our sample. This is shown in Figure 2. Our preliminary results show both compressive as well as tensile strain around extended defects and strain relaxation is evidenced along the growth direction (see figure 3). Work in progress to corroborate our initial results. Our present work extends the application of ECCI and EBSD for characterising cross section samples to image and quantify the strain around individual defects.

References:

1. G. Naresh-Kumar et al, Phys. Rev. Lett., **108**, 135503 (2012).
2. G. Naresh-Kumar et al, Appl Phys Lett., **102**, 142103 (2013).
3. A. J. Wilkinson, G. Meaden and D.J. Dingley, Ultramicroscopy **106**, 307 (2006).
4. A. Vilalta-Clemente et al, Microsc. Microanal. **21**, 1107 (2015).
5. P. de Mierry et al, Appl Phys Lett., **96**, 231918 (2010).

Acknowledgements: This work was supported by the EPSRC projects EP/J015792/1 and EP/J016098/1.

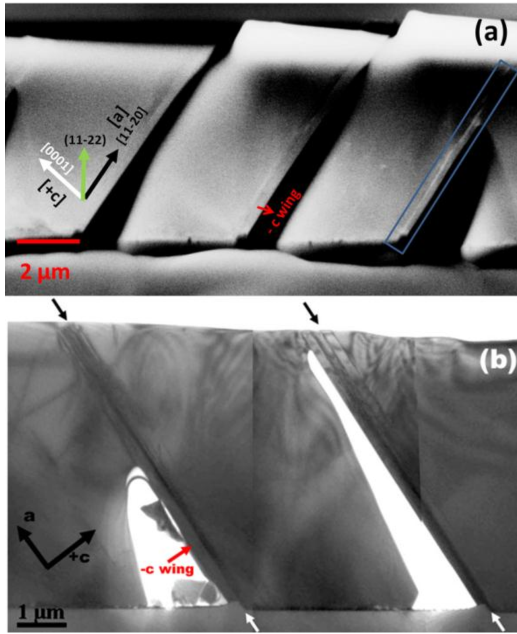

Figure 1: (a) ECCI acquired at 30 keV in a FEG-SEM, the blue box highlights the threading dislocations and (b) cross section TEM image acquired at 200 keV. The black arrow shows areas of threading dislocations and white arrow shows the patterned sapphire substrate.

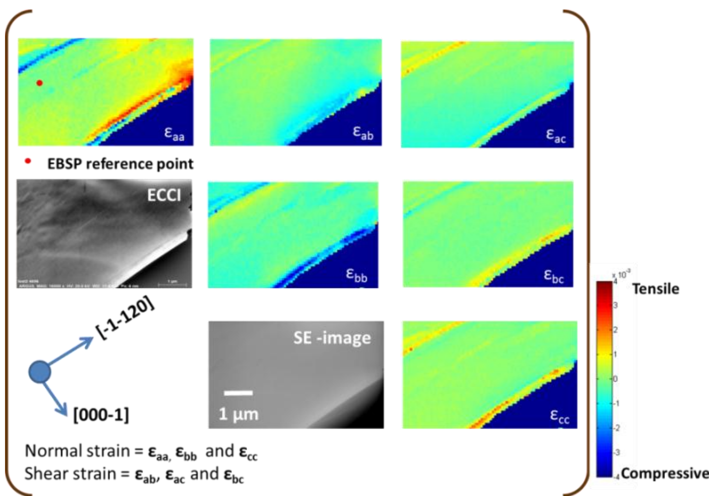

Figure 2: Coincident ECCI and EBSD showing extended defects and strain relaxation along the [0001] as shown in ε_{cc} strain map.

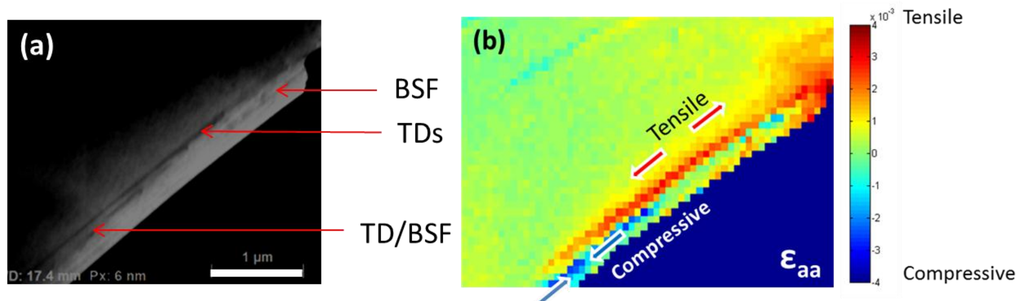

Figure 3: (a) High magnification ECCI showing TD and BSFs and (b) corresponding strain map showing compressive (blue arrow) and tensile (red arrow) strain around extended defects.

Linearly polarised photon emission at 160 K from single non-polar (11-20) InGaN quantum dots embedded in nanopillar structures

Tong Wang[1], Tim J. Puchtler[1], Tongtong Zhu[2], Muhammad Ali[3], Tom Badcock[3], Tao Ding[2,4], Rachel A. Oliver[2], and Robert A. Taylor[1]

[1]*Department of Physics, University of Oxford, Parks Road, Oxford, OX1 3PU, UK*

[2]*Department of Materials Science and Metallurgy, University of Cambridge, 27 Charles Babbage Road, Cambridge, CB3 0FS, UK*

[3]*Nanophotonics Centre, Cavendish Laboratory, University of Cambridge, CB3 0HE, UK*

[4]*Cambridge Research Laboratory, Toshiba Research Europe Limited, 208 Science Park, Milton Road, Cambridge, CB4 0FS, UK*

Email: tong.wang@physics.ox.ac.uk

High-temperature polarised single photon sources have significant applications in quantum information processing and optical quantum computing. Non-polar (11-20) InGaN quantum dots (QDs) are strong candidates for these non-classical light sources due to the large band offsets in nitride materials and the lack of internal fields in the (11-20) crystal direction. The resultant strong exciton oscillator strength and short lifetimes allow these potential single photon emitters to have higher repetition rates and thus better performance. Furthermore, the reduction in acoustic phonon coupling strength allows non-polar (11-20) InGaN QDs to achieve much higher operation temperatures. To further increase the photon extraction efficiency, nanopillar structures can be made with silica nanosphere masks and reactive ion etching.

Polarisation-resolved microphotoluminescence (μPL) is performed at various temperatures on such nanopillar-enhanced single non-polar (11-20) QDs with two-photon excitation from a Ti:Sapphire laser. A closed-cycle cryogenic system is used to cool the sample to 5 K. Sharp emission features from the QDs are observed up to 160 K. As shown in figure 1, the peak emission wavelength gradually redshifts by 3 nm from 5 to 160 K. Although the QD linewidth starts to broaden at higher temperatures, its full width at half maximum remains below 6 meV up to 160 K, thereby making them much more suitable for potential cavity coupling systems than their polar (0001) InGaN QD counterparts.

As shown in figure 2, the nature of linearly polarised photon emission is observed from 5 to 160 K, bringing the operation temperature of non-polar InGaN polarised photon emitters closer to the threshold achievable with commercial thermoelectric cooling systems. To add statistical significance to the investigation, more than 30 QDs have been studied and an average degree of linear polarisation (DOLP) of 0.85 has been found. The dependence of DOLP on temperature and QD energy has also been studied and no correlations can be found. The μPL system has also resolved fine structure splitting (FSS) less than 100 μeV. The relationship between FSS, QD energy, and temperature has been investigated as well. These high temperature polarisation results are a step forward towards the realisation of InGaN-based polarised single photon sources operating at ambient conditions.

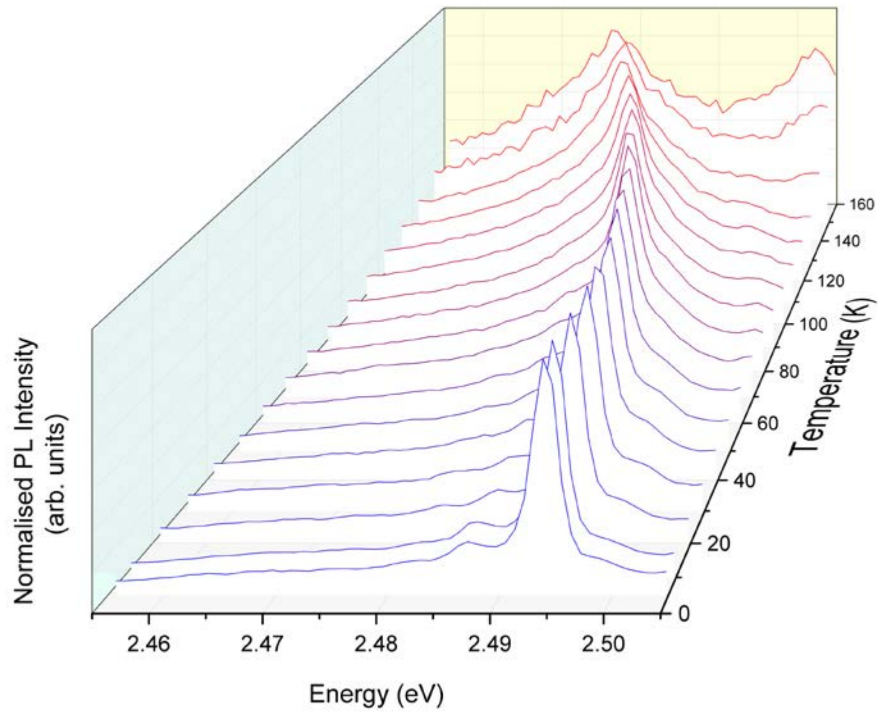

Figure 1: Evolution of QD energy with temperature increase from 5 to 160 K. The PL intensity is normalised to show the corresponding linewidth changes.

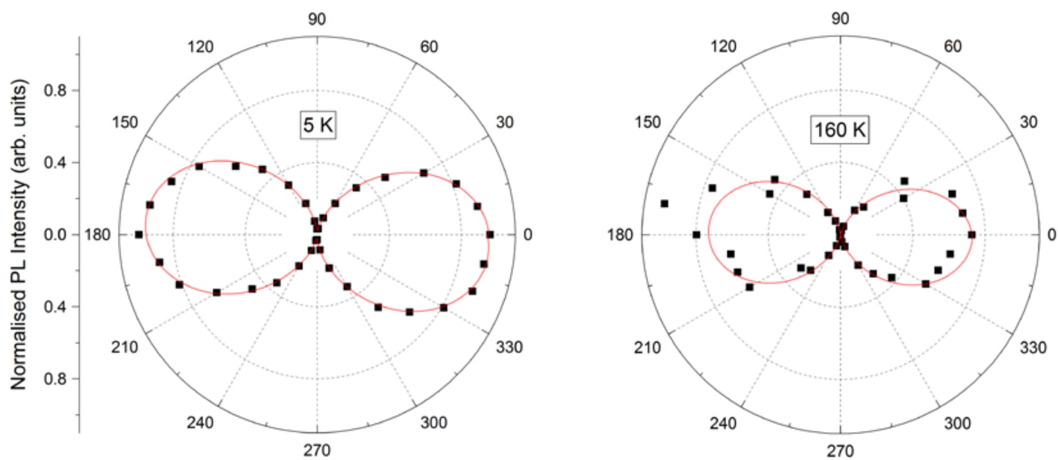

Figure 2: QD PL intensity variations with polariser angle, demonstrating Malus' law of polarisation at both 5 and 160 K.

Polarized White Light Emission From Hybrid Organic / III-nitrides Grating Structures

M. Athanasiou, R. Smith, S. Ghataora and T. Wang*

Department of Electronic and Electrical Engineering, University of Sheffield, Mappin Street, Sheffield, S1 3JD, United Kingdom
* Corresponding author: t.wang@sheffield.ac.uk

Hybrid organic semiconductors/inorganic semiconductors are drawing increasing attention, as a result of uniquely combining their respective advantages from the two major families of semiconductors, potentially fabricating highly efficient white light sources with superior performance over the current "blue LED + yellow phosphor" approach in terms of optical efficiency and color rendering index. Furthermore, it is expected to observe non-radiative energy transfer between organic and inorganic semiconductors as a result of dipole-dipole interaction if they meet requirements. This will also stimulate a lot of new physics. Very recently, we have developed a nanofabrication technique for the fabrication of such a hybrid structure, combining c-plane InGaN/GaN multiple quantum wells (MQWs) and a highly efficient yellow emission polymer (F8BT).[1,2] As a consequence, we have observed a very efficient non-energy transfer between the InGaN MQW and the F8BT.

Polarized white light would be very important for back-lighting applications, and currently it can be achieved by using a polarizer only, leading to extra energy loss. In this presentation, we report a new nanofabrication approach by combining InGaN/GaN MQWs that form one dimensional (1D) gratings with the F8BT, where the polymer molecules can be well aligned with the InGaN/ GaN MQWs gratings in order to intrinsically polarize the emission of the F8BT. With this approach, we have successfully achieved white light polarized emission.

In this work, one dimensional grating structures have been fabricated on a standard InGaN/GaN MQW structure using a confocal microscopy lithography technique, where the spatial resolution of the system can be down to 160 nm. Firstly, a 200 nm thick silicon dioxide (SiO_2) layer was deposited on the top of the standard c-plane MQWs emitting at 460 nm. A photoresist was then deposited on the top of the sample by a standard spin coating method. A commercial confocal microscope from WITec with a 375nm continuous wave (CW) laser was then used to write the grating patterning on the soft photoresist. Reactive ion etching (RIE) technique was then employed to etch the SiO_2 mask, which serves as a second mask for further processing. The grating patterning was then transferred into the sample by etching through the MQWs by means of an inductive couple plasma (ICP) etching technique. As an example, Figure 1 shows a grating structures are shown. By modifying the gaps and periods of the grating, a number of grating structures with a fill factor of 0.5, 0.73 and 0.9 (defined as a ratio of the InGaN/GaN stripe width to the grating period) have been fabricated. Subsequently, the F8BT polymer was deposited by a standard spin coating method, and then fill into the gaps of the grating structures. In order to allow the F8BT molecules align with the underlying MQWs gratings, a high pressure was then applied on the top of the gratings, followed by heating the sample up to 160 ^{o}C for 1 hour in an oxygen free-glove box.

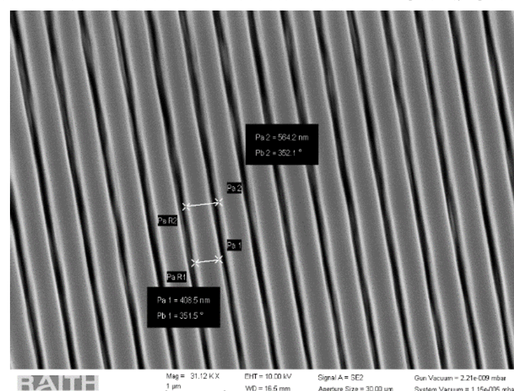

Figure 1. Top view SEM image of the gratings structures fabricated on c-plane InGaN / GaN MQWs.

Polarisation dependent measurements have been performed at room temperature (300 K) using a micro-photoluminescence (PL) system. Figure 2a shows PL spectra of such a hybrid sample with a fill factor of 0.9 as an example, where the emission is collected at two polarisation angles with 90° difference. Figure 2b displays the polarization degree of the F8BT as a function of the fill factor of

the hybrid sample, demonstrating that a high fill factor leads to an increase in the polarisation degree of the F8BT. For example, the sample with a fill factor of 0.9 exhibits an approximately 40% polarisation degree across the whole spectrum, which is almost 8 times higher than that of the sample with a fill factor of 0.5. It means that the polarisation of the F8BT emission would occur and then be enhanced if the gap of the grating structure is small enough to allow the molecules to remain well aligned along the grating.

We have also further measured the polarization of the combined emission (white lighting) from both the InGaN/GaN blue emission and the polymer yellow emission as a function of a fill factor.

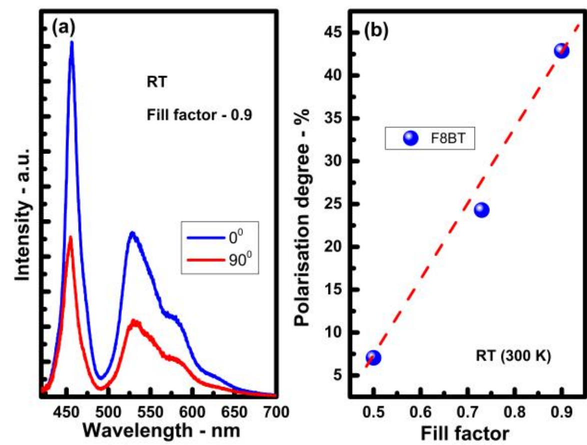

Figure 2a: An example of the polarised white light spectrum for the hybrid grating with 0.9 fill factor; and 2b: Polarisation degree of the F8BT polymer against the fill factor ratio.

In summary, a detailed study of PL polarisation has been performed on a hybrid organic/inorganic grating structures with a different fill factor at room temperature. It was found that the polarisation of the F8BT and thus the hybrid devices, increases with increasing the fill factor of the grating structures due to well alignment of the molecules along the InGaN / GaN MQWs gratings.

References:

1. R Smith, B Liu, J Bai and T Wang, *Nano Lett.* 13, 3042 (2013)
2. R Smith, B Liu, J Bai and T Wang, *Appl. Phys. Lett.* 107,121108 (2015)

Metastable and quasistable Eu^{3+} defects in GaN(Mg)

K.P. O'Donnell[1*], P.R. Edwards[1], M. Yamaga[2], K. Lorenz[3], M.J. Kappers[4] and M. Boćkowski[5]

[1]*SUPA Department of Physics, University of Strathclyde, 107 Rottenrow, Glasgow G40NG, Scotland, UK*
[2]*Department of Mathematical and Design Engineering, Gifu University,Gifu 501-1193, Japan*
[3]*IST, Universidade de Lisboa, CTN, Estrada Nacional 102695-066 Bobadela LRS Portugal*
[4]*Department of Materials Science and Metallurgy, University of Cambridge, 27 Charles Babbage Road, Cambridge CB30FS, England, UK*
[5]*Institute of High Pressure Physics PAS, Sokolowska 29/37, 01-142 Warsaw, Poland*

**e-mail address: k.p.odonnell@strath.ac.uk*

Rare earth (RE) dopants in semiconductors have been studied for decades with the main aim of augmenting the available emission wavelengths of optoelectronic devices [1,2]. Optical spectra of tri-positive rare earth ions in crystals feature sharp lines with half-widths smaller than k_BT, at element-characteristic wavelengths that depend only weakly on the host material. In contrast, the *spectral patterns* of the transitions are rather sensitive to the *symmetry* of the RE local environment. Double doping of epitaxial GaN samples with magnesium and europium introduces defects associated with an extrinsic hysteretic photochromism [3-5]. In an extension of previous studies, RE spectroscopy of such samples reveals the interesting consequences of photo-induced migration of Mg acceptor atoms in GaN.

We monitor photoluminescence (PL) spectra of the simple $^5D_0$ to $^7F_{0,1}$ transitions of Eu^{3+} as a means to study both defect populations and their configurations as a function of temperature. We find, firstly, that the centre into which Eu0, the dominant defect at room temperature, transforms, upon sample cooling below 50 K, is *not* after all the 'real' Eu1 defect, as previously thought, but an analogous one, branded Eu1(Mg), which itself transforms into another centre, Eu1(Mg2) under continuing illumination. We present evidence to support a further level of transformation, yielding Eu1(Mg3), after prolonged sample illumination. The projected endpoint of this *defect cascade* is a centre in which the Mg atom has migrated so far from its initial site, close to the spectator Eu ion, as to form a centre that is *spectroscopically indistinguishable* from the 'real' Eu1. Spectral evidence of the primary photochromic switch, from Eu0 to Eu1(Mg) on sample cooling, is shown in Figure 1.

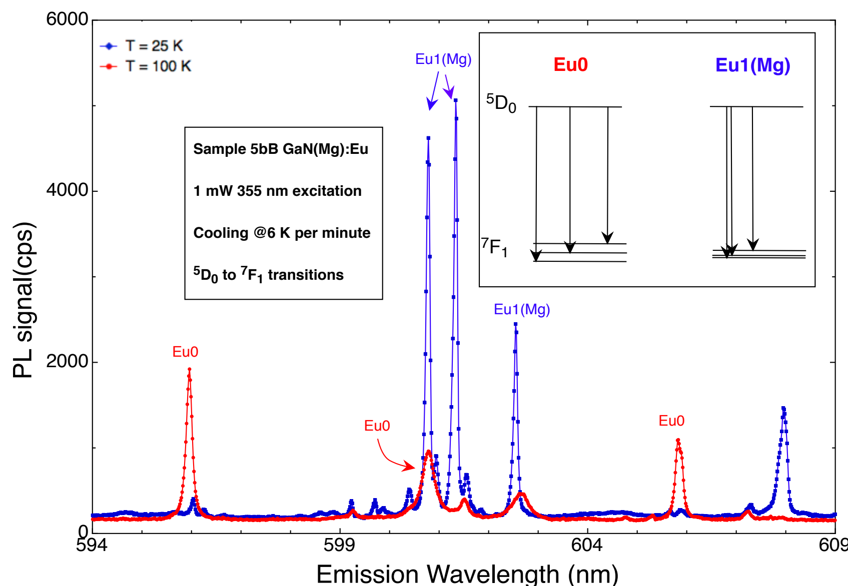

Figure 1: From room temperature down to 100 K, $^5D_0$ to $^7F_1$ spectra of GaN(Mg):Eu feature 3 transition lines of the defect Eu0, widely split by a low-symmetry crystal field. Below ~50 K, this centre transforms into the much more symmetric Eu1(Mg); Eu1(Mg) has *nearly* trigonal symmetry. Inset figures show energy level schemes of the defects (not to scale).

The observation of ongoing spectral changes suggests an extension of the switching model previously advanced for the Eu0 to Eu1(Mg) transformation, based on observation of the stronger, but more complex, $^5D_0$ to $^7F_2$ transitions [3-5]. The photochromism and temperature hysteresis (not shown here) are explained on the basis of the charge-state dependence of the Mg-N bond length, a classic *shallow-deep instability*, described theoretically by several authors [6-7]. This instability acts as a latch, which is *set* by carrier freeze-out and *released* by hole migration: carrier freeze-out of *shallow* centres at low temperature initiates the 'switchdown' that transforms Eu0 to Eu1(Mg), when the Eu-Mg distance spontaneously increases as a hole becomes localized on the intervening N atom; the inverse process ('switchback') is triggered by the release of holes from *deep* acceptors, occurring only at relatively high temperatures. During the first switching stage, from Eu0 to Eu1(Mg), between ~40 K and 10 K, we also observe transient emission lines from a centre, that we describe classically as a metastable intermediate of the Eu0 and Eu1(Mg) configurations. In quantum-optical terms, this resonance can be seen as a *superposition* of the two contributing defects. It may therefore form the basis of a novel solid state *qubit* [5].

Repeated cycling of a sample between high and low temperature, together with prolonged 'blitching' (the combination of bleaching and switching) at low temperature induces the slow formation of other defects, as revealed by the $^5D_0$ to $^7F_0$ spectra of Figure 2. These defects are found to be quasistable at room temperature; their formation and destruction will be described.

By considering the photo-dynamics of the complete excitation and bleaching cycle, we extend the switching model to cases where the Mg atom becomes localised, and sometimes *stuck*, at *distinct* locations ever further from the Eu atom, in line with the measured decreasing magnitude of the off-axis distortion for centres Eu1(Mg2) and Eu1(Mg3).

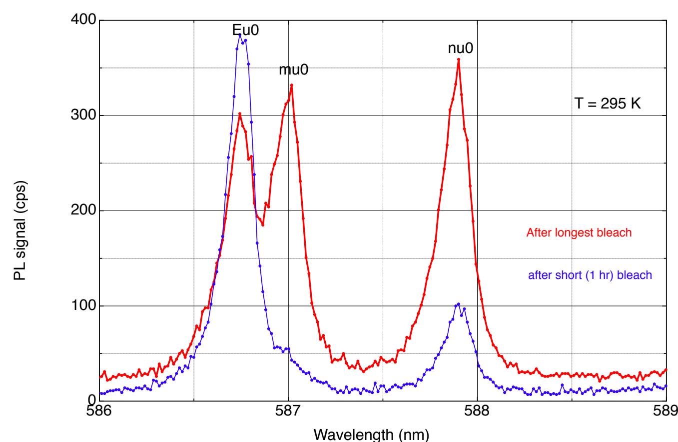

Figure 2: In the $^5D_0$ to $^7F_0$ 'sensitive' region, each Eu^{3+} defect contributes a single resolved spectral line (if there are no overlaps). The singlet belonging to Eu0 is accompanied in this figure by additional lines that are induced by repeated temperature cycling and sample 'blitching' (see text) at low temperature.

Acknowledgment: this work was supported by EPSRC.

[1] P.N. Favennec, H. L'Haridon, M. Salvi, D. Moutonnet and Y. Le Gillou, Electronics Letts. **25**, 718 (1989); see also K.P.O'Donnell, physica status solidi (c). (E-MRS 2014 Spring Meeting Symp. K Proceedings or special issue) (2015)

[2] K.P. O'Donnell and V. Dierolf (eds.), Topics in Applied Physics **124** (Springer, Dordrecht, 2010)

[3] K.P. O'Donnell, UKNC Winter Meeting, Bath, Jan. 2012, unpublished talk

[4] K.P. O'Donnell, R.W. Martin, P.R. Edwards, K. Lorenz, E. Alves, M. Boćkowski, Proceedings of ICPS 2012, Zurich, **1566**, 63 (AIP Publishing, 2013)

[5] K.P. O'Donnell, P.R. Edwards, M.J. Kappers, K. Lorenz , E. Alves and M. Boćkowski, Proceedings of ICNS 2013, Washington, Phys. Status Solidi C **11**, 662 (2014)

[6] S. Lany and A. Zunger, Appl. Phys. Lett. **96**, 142114 (2010)

[7] J.L. Lyons, A. Janotti, and C.G. Van de Walle, Phys. Rev. Lett. **108**, 156403 (2012)

UNRAVELING THE BANDGAP NATURE OF HEXAGONAL BORON NITRIDE

Guillaume Cassabois
Laboratoire Charles Coulomb, CNRS, Montpellier University, France

Hexagonal boron nitride (hBN) is a wide bandgap semiconductor with a large range of basic applications relying on its low dielectric constant, high thermal conductivity, and chemical inertness. The growth of high-quality crystals in 2004 has revealed that hBN is also a promising material for light-emitting devices in the deep ultraviolet domain, as illustrated by the demonstration of lasing at 215 nm by accelerated electron excitation [1], and also the operation of field emitter display-type devices in the deep ultraviolet [2]. With a honeycomb structure similar to graphene, bulk hBN has recently gained tremendous attention as an exceptional substrate for graphene with an atomically smooth surface, and more generally, as a fundamental building block of Van der Waals heterostructures [3].

In spite of this rising interest for hBN and the large number of studies devoted to this material of seemingly simple crystal structure, the very basic question of the bandgap nature is still controversial. There is a strong contrast in the literature between ab initio band structure calculations predicting an indirect bandgap crystal and optical measurements concluding to a direct one [1].

I will discuss our recent experiments by two-photon spectroscopy demonstrating that hBN is an indirect bandgap material. I will show that the optical properties of hBN are profoundly determined by phonon-assisted transitions involving either virtual or real excitonic states. I will present our measurements of the exciton binding energy by two-photon excitation, leading to the estimation of 6.08 eV for the single-particle bandgap in hBN.

REFERENCES:

[1] K. Watanabe, T. Taniguchi, and H. Kanda, Nat Mater 3, 404-409 (2004).
[2] K. Watanabe, T. Taniguchi, T. Niiyama, K. Miya, and M. Taniguchi, Nat Photon 3, 591 (2009).
[3] A. K. Geim and I. V. Grigorieva, Nature 499, 419 (2013).

Band gap engineering in II-IV nitrides

Mikael Råsander, James. B. Quirk and Michelle A. Moram
Department of Materials, Imperial College London

Ultraviolet light-emitting diodes (UV-LEDs) based on wurtzite structure III-nitrides currently have low efficiencies and lifetimes. The light-emitting quantum well (QW) regions of most UV-LEDs are based on AlGaN alloys, but unfortunately it is not possible to achieve lattice-matched and polarization-matched QW heterostructures with appropriate band gaps and band offsets using this alloy system. Therefore, it is motivated to search for alternative wide band gap nitride materials that could introduce additional degrees of freedom for UV-LED device design, either to assist in the lattice-matching or in the polarisation-matching within the active light-emitting region.

The Group II-IV nitride semiconductors are emerging as promising alternatives for these applications. These materials have wurtzite-like orthorhombic crystal structures and can be derived from Group III nitrides by substituting pairs of Group III (e.g. Al, Ga or In) atoms for a single Group II (Be, Mg, Ca or Zn) atom and a single Group IV (C, Si, Ge or Sn) atom. We have recently focused on the II-IV nitride MgSiN2 both from theory and experiment. On the theoretical side, density functional theory has been used to obtain accurate structural properties, elastic constants and piezoelectric properties of MgSiN2. For example, the band structure of MgSiN2 is shown to have a large indirect band gap of similar size as the direct band gap of wurtzite AlN [1]. In this talk, we will present results from both theory and experiment on the variations in the band gaps of II-IV nitride systems. Both when regarding combining different Group II and Group IV elements and for alloying with Group III elements, exemplified by $(MgSi)_{1-x}Al_xN_2$.

[1] J. B. Quirk, M. Råsander, C. M. McGilvery, R. Palgrave and M. A. Moram, Appl. Phys. Lett. **105** 112108 (2014).

Kinetic phase diagrams and universality of surface patterns during growth

B. Hourahine
Department of Physics, SUPA, University of Strathclyde, Glasgow

GaN epitaxial growth can show spontaneous instabilities, leading to self-assembled patterning. One mechanism for this process is due to Ehrlich-Schwöbel barriers leading to asymmetric diffusion of growth species across step edges [1]. This contribution will discuss some more of the range of surface morphologies which can occur in MBE, PAMBE and MOCVD for deposition of nitrides outside of the step-flow regime. The stability regimes for different patterns and the provisional results on post-annealing will be presented. The scaling behaviour of these patterns as a function of growth conditions will be used to categorise the universality classes of these types of pattern.

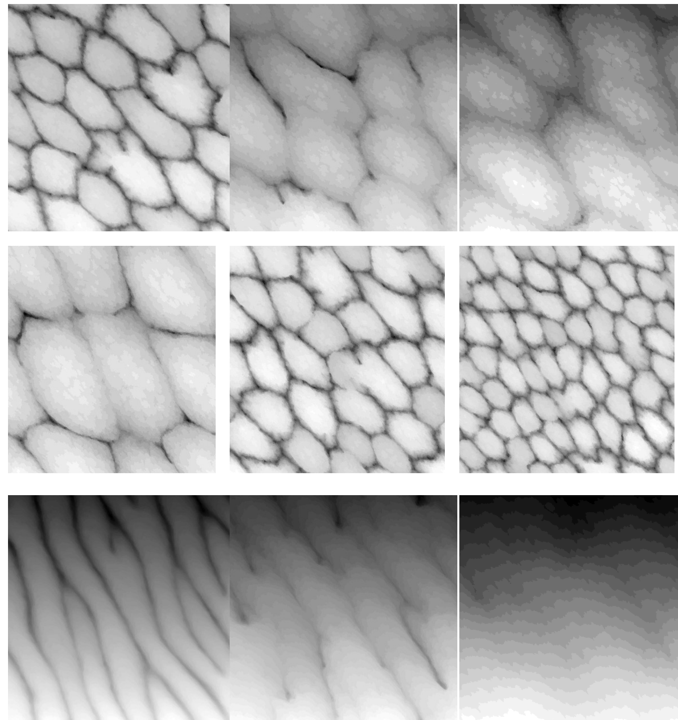

Figure 1: Some of the effects on simulated morphologies changes on scaling the crystal growth temperature (top row), deposition rates (middle) and substrate offcut (bottom).

1. Kaufmann, Lahourcade, Hourahine, Martin and Grandjean *et al.* J. Cryst. Growth **433**, 36–42 (2016)

Terahertz dielectric properties of free-standing non-polar GaN

Morgan T. Hibberd[1], Virginia Frey[1], Abbas A. Roble[1], Ben F. Spencer[1], Peter Mitchell[1], Darren M. Graham[1], Menno J. Kappers[2], Rachel A. Oliver[2] and Colin J. Humphreys[2].

[1]School of Physics and Astronomy and the Photon Science Institute, The University of Manchester, Manchester M13 9PL, United Kingdom
[2]Department of Materials Science and Metallurgy, 27 Charles Babbage Road, University of Cambridge, Cambridge CB3 0FS, United Kingdom

Gallium nitride (GaN) is a direct bandgap semiconductor used for high-frequency and high-power optoelectronic devices that are typically based upon wurtzite GaN grown along the [0001] (*c*-axis) direction. However, strong spontaneous and piezoelectric polarisations exist along the *c*-axis and result in large internal electrostatic fields [1] that have been shown to reduce the efficiency of devices [2]. To avoid these internal fields, GaN can be grown along the $[11\bar{2}0]$ (*a*-axis) and $[1\bar{1}00]$ (*m*-axis), which lie perpendicular to the *c*-axis and consequently possess no polarisation field [3]. The non-polar planes do not therefore suffer from internal electrostatic fields but since the *c*-axis also defines the optic axis of the wurtzite crystal structure, *a*-plane and *m*-plane GaN exhibit birefringence. This leads to a polarisation-dependent anisotropy in the dielectric properties that has been the focus of recent studies in the optical [4,5] and mid-infrared [6,7] spectral regions. The characterisation of the dielectric properties of non-polar GaN within the terahertz regime is however lacking, despite a great deal of recent interest in its use in the development of optoelectronic devices within this spectral range [8-10].

Here we report on the characterisation of the dielectric properties of both *a*-plane and *m*-plane GaN wafers in the spectral region from 0.5 – 5.0 THz, using terahertz time-domain spectroscopy. Terahertz radiation was generated using 50 fs laser pulses incident on a gallium arsenide photoconductive antenna and aligned through a 4F confocal geometry of parabolic mirrors, creating focal spots at the sample position and at a 400 µm thick gallium phosphide crystal in a standard electro-optic detection scheme. The wafers were commercially-available, semi-insulating *a*-plane and *m*-plane GaN crystals, grown by hydride vapour phase epitaxy (Nanowin Ltd.), with a room temperature resistivity of greater than 10^6 Ω.cm and thicknesses of 284 µm and 298 µm respectively. They were attached over an aperture in a rotation mount to allow measurement of the transmitted terahertz electric field (*E*) polarised both parallel and perpendicular to the *c*-axis. By taking a corresponding reference measurement through an identical clear aperture, the complex transmission function for both *a*-plane and *m*-plane GaN was determined, enabling extraction of the refractive index and absorption coefficient.

Figure 1 shows the refractive index of *m*-plane GaN and as expected for a positive, uniaxial crystal, the extraordinary refractive index ($E \parallel c$) was greater than the ordinary refractive index ($E \perp c$), with a difference of 0.18 across the measured frequency range. The results were well-fitted with a pseudo-harmonic approximation of the phonon contribution to the dielectric function, using phonon frequencies obtained from Raman scattering measurements. Furthermore, with an absorption coefficient below 10 cm^{-1} and an average transmission of greater than 50% across the measured frequency range for both *a*-plane and *m*-plane wafers, we have demonstrated the potential for their use in future terahertz optoelectronic devices.

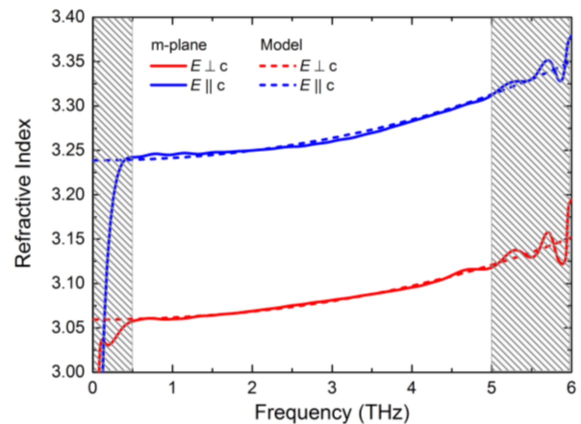

Fig. 1: Refractive index measurements of m-plane GaN with the terahertz electric field polarized both parallel ($E \parallel c$) and perpendicular ($E \perp c$) to the c-axis.

[1] F. Bernardini *et al.*, Phys. Rev. B 56, R10024 (1997); [2] T. Deguchi *et al.*, Jpn. J. Appl. Phys. 38, L914 (1999); [3] P. Waltereit *et al.*, Nature 406, 865 (2000); [4] S. Ghosh *et al.*, Appl. Phys. Lett. 80, 413 (2002); [5] Y. Ding *et al.*, Chin. Phys. Lett. 29, 107801 (2012); [6] S. R. Bowman *et al.*, Opt. Mater. Express 4, 1287 (2014); [7] S. Shokhovets *et al.*, Appl. Phys. Lett. 107, 092104 (2015); [8] A. Pesach *et al.*, Appl. Phys. Lett. 103, 022110 (2013); [9] C. Edmunds *et al.*, Appl. Phys. Lett. 105, 021109 (2014); [10] C. B. Lim *et al.*, Nanotechnology 26, 435201 (2015).

TEMPERATURE DEPENDENT BANDGAP AND BOWING PARAMETER OF INDIUM-ALUMINIUM NITRIDE

S.N. Alam[1,2], V.Z. Zubialevich[1], D.V. Dinh[1], P.J. Parbrook[1,2]

[1] *Tyndall National Institute, University College Cork, Cork, Ireland*
[2] *School of Engineering, University College Cork, Cork, Ireland*

InAlN is an important material system used in many applications including InAlN/GaN high electron mobility transistors, InAlN/GaN Bragg reflectors, InAlN-based photodetectors and more recently as the active region in light emitting structures [1]. Despite this, a significant discrepancy exists in the bandgaps reported for even the most studied and technologically relevant compositions, around the lattice matched to GaN condition (~17%). To estimate bandgap across the whole composition range accurately, a detailed data set for the lowest indium content region is needed, but has been unavailable, mainly due to the difficulty in preparing highly tensile, strained InAlN on GaN templates. Recently InAlN epitaxial layers grown on AlN by MOVPE at different temperatures were investigated and their bandgap E_g was determined by means of photoluminescence excitation spectroscopy (PLE) [2]. Here we describe recent, further developments in this study and comparison of the results to the previously available data.

Initially the composition dependent bowing parameter $b(x)$ was determined from the $E_g(x)$ data using the standard expression: $E_g(x) = x\,E_{g,\mathrm{InN}} - b(x)\,x\,(1-x) + (1-x)E_{g,\mathrm{AlN}}$. Then, combining our low indium content data to the values of $b(x)$ previously available from literature [3] for $x > 8\%$ (Fig. 1), we have managed to obtain an empirical expression shown in the figure for the InAlN bandgap bowing parameter describing well data across the entire composition range.

Using endpoints $E_{g,\mathrm{InN}}$ and $E_{g,\mathrm{AlN}}$ from the literature (0.65 eV for InN [4] and 6.015 eV for AlN [5]) we obtained a good bandgap fit for low and high indium content InAlN with a reasonable compromise between the rather scattered data around compositions lattice matched to GaN (Fig. 2).

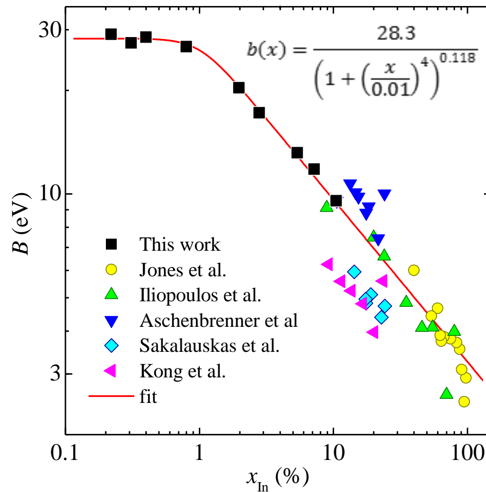

Fig. 1. – InAlN bandgap bowing parameter as a function of In content.

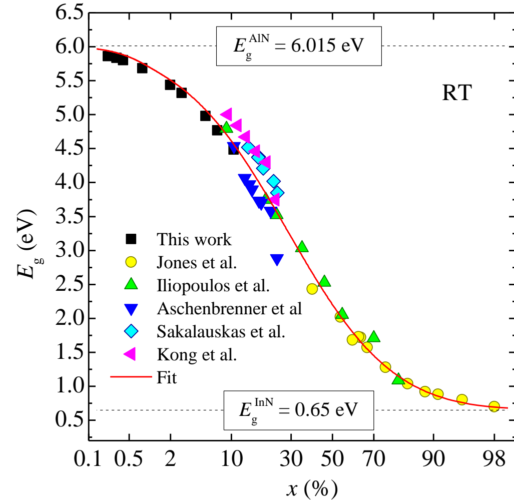

Fig. 2. – InAlN bandgap as a function of In content.

To investigate further, we measured temperature dependence of the InAlN absorption edge of the low indium content samples. It was found that InAlN bandgap shift $\Delta E_g = E_g(10\text{ K})–E_g(300\text{ K})$ does not change monotonically

between AlN and InN, but that ΔE_g initially increases from the 89 meV value of pure AlN, measured using absorption of a specially designed sample, to a value in excess of 110 meV (Fig. 3). The data in this range is challenging to examine due to the impact of valence band interactions (leading to the use of double sigmoidal fits for x_{In}<0.01 and single sigmoidal analysis otherwise as shown in Fig. 4). However, the trend to increasing temperature dependent bandgap shrinkage for these low In content samples is clear, both from the rise in ΔE_g in the range $0.0022 \leq x_{In} \leq 0.0042$ for which a good double sigmoid fit is made, and also from PLE data taken at intermediate temperatures.

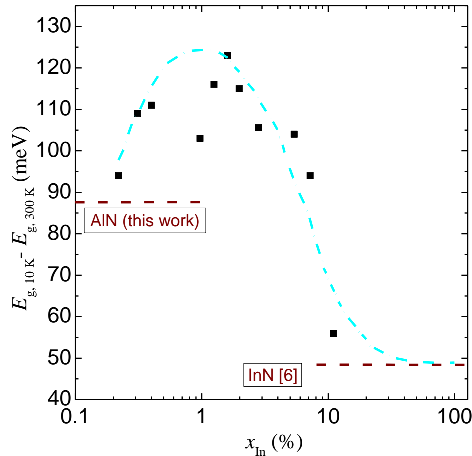

Fig. 3. – Composition dependence of InAlN temperature bandgap shrinkage between 10 K and 300 K (line is guide to the eye).

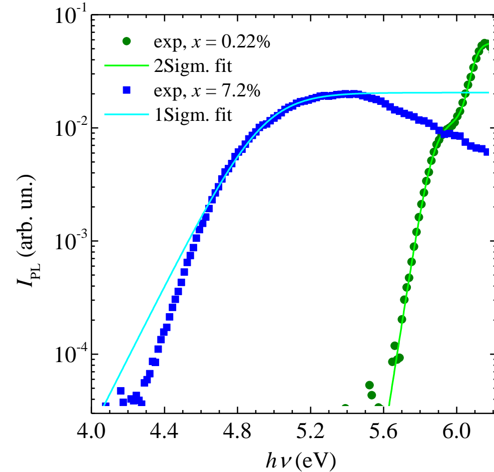

Fig. 4. – Typical PLE spectra of InAlN/AlN samples and their fit using single and double sigmoidal expression.

This behaviour is unlike that reported for other III-nitrides [7], nor can it be explained by the reported bandgap shrinkage observed for dilute nitrides (e.g. GaAsN). While such dilute nitrides also exhibit strong bandgap non-parabolicity with composition, this is typically also associated with a *reduction* rather than *increase* in the bandgap shrinkage with temperature [8]. This unexpected behaviour is currently unexplained but it is another evidence of unusual behaviour of the InAlN alloy and its difference from other III-nitrides materials.

REFERENCES

[1] V.Z. Zubialevich, T.C. Sadler, D.V. Dinh, S.N. Alam, H. Li, P. Pampili, P.J. Parbrook, *J. Lum.* **155** (2014) 108.

[2] V.Z. Zubialevich, D.V. Dinh, S.N. Alam, S. Schulz, E.P. O'Reilly, P.J. Parbrook, *Semicond. Sci. Technol.* (accepted for publication).

[3] R.E. Jones, R. Broesler, K.M. Yu, J.W. Ager, E.E. Haller, W. Walukiewicz, X. Chen, W.J. Schaff, *J. Appl. Phys.* **104** (2008) 123501; E. Iliopoulos, A. Adikimenakis, C. Giesen, M. Heuken, A. Georgakilas, *Appl. Phys. Lett.*, **92** (2008) 191907; E. Sakalauskas, H. Behmenburg, C. Hums, P. Schley, G. Rossbach, C. Giesen, M. Heuken, H. Kalisch, R.H. Jansen, J. Bläsing, A. Dadgar, A. Krost, R. Goldhahn, *J. Phys. D: Appl. Phys.*, **43** (2010) 365102; T. Aschenbrenner, H. Dartsch, C. Kruse, M. Anastasescu, M. Stoica, M. Gartner, A. Pretorius, A. Rosenauer, T. Wagner, and D. Hommel, *J. Appl. Phys.* **108** (2010) 063533; W. Kong, A. Mohanta, A.T. Roberts, W.Y. Jiao, J. Fournelle, T.H. Kim, M. Losurdo, H.O. Everitt, A.S. Brown, *Appl. Phys. Lett.*, **105** (2014) 132101.

[4] S.P. Fu, T.T. Chen, Y.F. Chen, *Semicond. Sci. Technol.* **21** (2006) 244.

[5] M. Feneberg, R.A.R. Leute, B. Neuschl, K. Thonke, M. Bickermann, *Phys. Rev. B* **82** (2010) 075208.

[6] J. Wu, W. Walukiewicz, W. Shan, K. M. Yu, J. W. Ager III, S. X. Li, W. J. Schaff, *J. Appl. Phys.* **94** (2003) 4457.

[7] N. Nepal, J. Li, M.L. Nakarmi, J.Y. Lin, H.X. Jiang, *Appl. Phys. Lett.* **87** (2005) 242104.

[8] K. Uesugi, I. Suemune, T. Hasegawa, T. Akutagawa, T. Nakamura. *Appl. Phys. Lett.* **76** (2000): 1285.

Evolution of the m-plane Quantum Well Morphology within a GaN/InGaN Core-Shell Structure

P.-M. Coulon[1], S. Hosseini Vajargah[2], S.-L. Sahonta[2], E.D. Le Boulbar[1], I. Gîrgel[1], R. A. Oliver[2], C. J. Humphreys[2], D.W.E. Allsopp[1], and P.A. Shields[1]

[1]Department of Electronic and Electrical Engineering, University of Bath, BA2 7AY, UK
[2]Department of Materials Science and Metallurgy, University of Cambridge, CB3 0FS, UK

GaN/InGaN core shell based nanorods (NRs) are promising for optoelectronic applications thanks to the absence of polarization-related electric fields,[1] a lower defect density, a larger emission volume[2] and strain relaxation at the free surfaces.[3] In particular, the growth of high-quality thick InGaN layers on the non-polar surfaces of core-shell structures could be a solution to overcome efficiency droop in III-Nitride LEDs. The increase in the active volume that results from using a thick InGaN layer will have the effect of reducing the average carrier density for a given injection current and thus reduce Auger recombination. Therefore, all these advantages as well as the potential to improve light extraction efficiency[4,5] and absorption[6] have stimulated the interest on GaN NRs for light emitting diodes, laser diodes, solar-cells and other applications, including photodetectors and water-splitting.

In this work, the morphology evolution of the InGaN shell grown on non-polar *m*-plane GaN facets is investigated as a function of the thickness. First, etched GaN NR arrays are obtained by etching a GaN 2D layer down to the silicon substrate.[7,8] Second, a metal organic vapor phase epitaxy (MOVPE) GaN regrowth step was performed to recover the *m*-plane and semi-polar plane facets.[9] Finally, thick InGaN growth is performed at three different growth times, with and without a GaN capping layer.

Scanning electron microscopy and transmission electron microscopy reveal a change in morphology from a two dimensional growth mode to three dimensional striated growth without any additional defect formation. The Indium distribution determined with spatially-resolved energy-dispersive X-ray spectroscopy measurements demonstrate Indium fluctuations along the [10-10] direction, with low and high Indium composition respectively associated with the 2D and 3D layer; and secondly, fluctuations, along the [0001] direction, highly correlated with the change in morphology. Finally, high-resolution transmission electron microscopy indicated the presence of atomic steps at the GaN/InGaN core-shell interface which are suggested to trigger small Indium fluctuations along [0001]. The origin and the impact of atomic steps on the InGaN growth mode of thick layers by seemingly nucleating an elastic relaxation process rather than a plastic one will be discussed.

In conclusion, this study demonstrates that the employed fabrication process of GaN NRs, which results in a +c-miscut, can be employed to avoid misfit dislocation generation during the growth of thicker InGaN shell layers, contrary to the thick InGaN shell grown on selective area grown NRs, opening the possibility of growing light emitting diodes with emissive layers thick enough to mitigate efficiency droop.

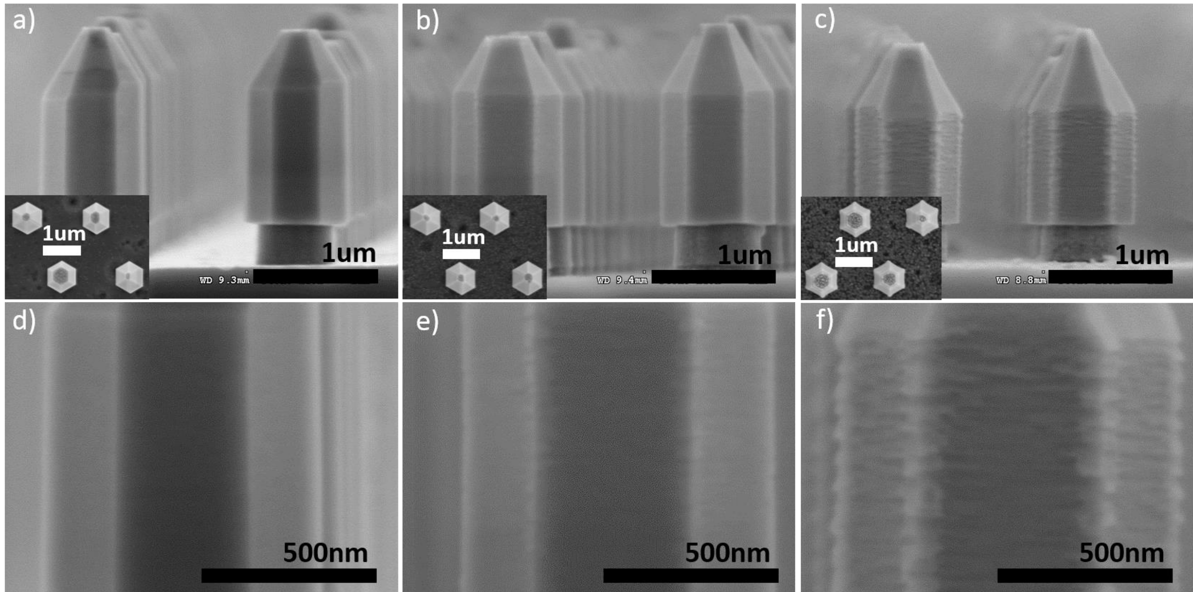

Figure 1. SEM pictures of GaN/InGaN core-shell structures grown by MOVPE without any GaN capping layer for: (a) 2 min, (b) 6 min and (c) 18 min of InGaN growth. The insets show plan-view SEM pictures of the same samples. High magnification SEM pictures of the m-plane facets for: (d) 2 min, (e) 6 min and (f) 18 min InGaN shell growth.

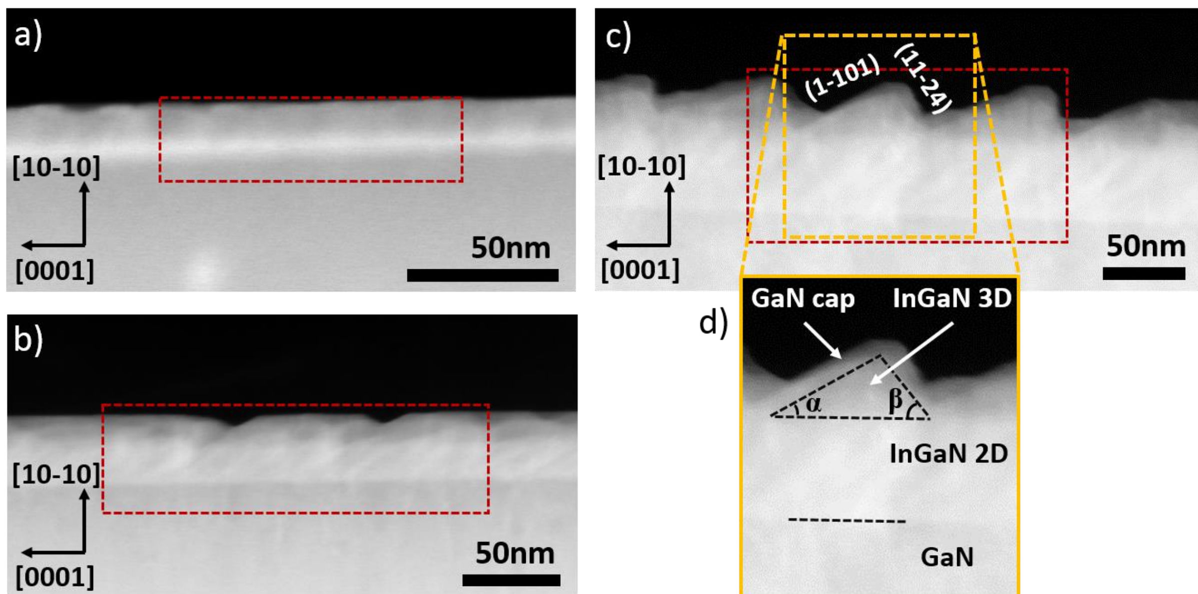

Figure 2. TEM pictures recorded along the [11-20] zone axis of GaN/InGaN core-shell structures grown by MOVPE with a GaN capping layer for: (a) 2 min, (b) 6 min, (c) 18 min InGaN growth. The red dashed rectangle indicates the area where EDX spectra were acquired. (d) Higher magnification TEM pictures showing the various layers in detail.

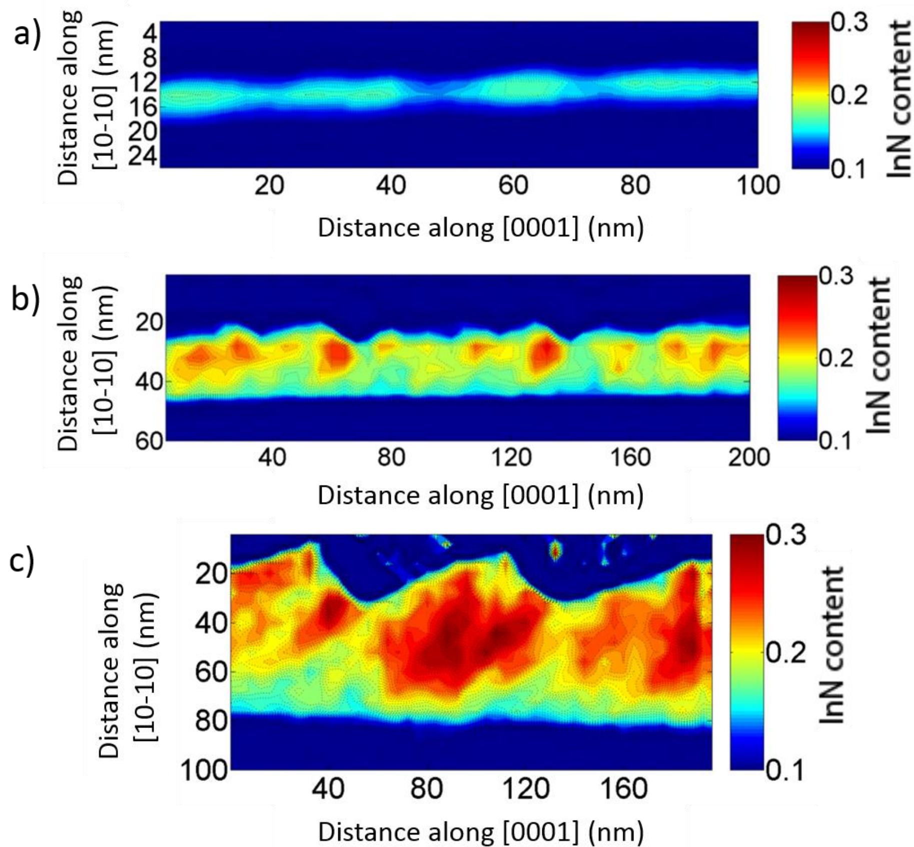

Figure 3. Indium content map obtained by EDX on GaN/InGaN core-shell structures grown by MOVPE with a GaN capping layer for: (a) 2 min, (b) 6 min, (c) 18 min InGaN growth.

REFERENCES:

[1] M. Thomsen, H. Jönen, U. Rossow, A. Hangleiter, "Spontaneous polarization field in polar and nonpolar GaInN/GaN quantum well structures", Physica status solidi (b), 248 (3), 627-631 (2011).

[2] S. Li and A. Waag, "GaN based nanorods for solid state lighting", J. Appl. Phys., 111, 071101 (2012).

[3] M. Hugues, P.A. Shields, F. Sacconi, M. Mexis, M. Auf der Maur, M. Cooke, M. Dineen, A. Di Carlo, D.W.E. Allsopp and J. Zúñiga-Pérez, "Strain evolution in GaN nanowires: From free-surface objects to coalesced templates", J. Appl. Phys., 114, 084307 (2013).

[4] Y.D. Zhuang, C.J. Lewins, S. Lis, P.A. Shields and D.W.E. Allsopp, "Fabrication and Characterization of Light-Emitting Diodes Comprising Highly Ordered Arrays of emissive InGaN/GaN nanorods", IEEE Photonics Technology Letters, 25 (11), 1047-1049 (2013).

[5] C.J. Lewins, E.D. Le Boulbar, S. Lis, P.R. Edwards, R.W. Martin, P.A. Shields and D.W.E. Allsopp, "Strong photonic crystal behavior in regular arrays of core-shell and quantum disc InGaN/GaN nanorod light-emitting diodes", J. Appl. Phys., 116, 044305 (2014).

[6] C. Kölper, M. Sabathil, F. Römer, M. Mandl, M. Strassburg, B. Witzigmann, "Core–shell InGaN nanorod light emitting diodes: Electronic and optical device properties", Physica status solidi (a), 209(11), 2304-2312 (2012).

[7] P.A. Shields, D.W.E. Allsopp, "Nanoimprint lithography resist profile inversion for lift-off applications," Microelectron. Eng., 88(9), 3011–3014, Elsevier B.V. (2011).

[8] P.A. Shields, M. Hugues, J. Zúñiga-Pérez, M. Cooke, M. Dineen, W. Wang, F. Causa, D.W.E. Allsopp, "Fabrication and properties of etched GaN nanorods", Phys. Status Solidi, 9(3-4), 631–634 (2012).

[9] E.D. Le Boulbar, I. Gîrgel, C.J. Lewins, P.R. Edwards, R.W. Martin, A. Šatka, D.W.E. Allsopp, P.A. Shields, "Facet recovery and light emission from GaN/InGaN/GaN core-shell structures grown by metal organic vapour phase epitaxy on etched GaN nanorod arrays", J. Appl. Phys., 114(9), 094302 (2013).

Selective etching of n-type GaN in InGaN/GaN quantum disc nanorod arrays using electrode-less photo-electrochemical etching

C.J. Lewins*, S.A. Fox, A. Sergejevs, P.A. Shields*, and D.W.E. Allsopp
Dept. Electrical & Electronic Engineering, University of Bath, Bath, BA2 7AY, UK
*Email: C.J.Lewins@Bath.ac.uk, P.Shields@Bath.ac.uk

The shape of the sidewall of the nanorods in etched arrays has been shown to be critical to exploiting strong photonic crystal behaviour for the formation of Bloch modes. A quasi-suspended photonic crystal slab can be formed by an area of higher dielectric fill at the top of the nanorods, creating an optical waveguide [1]. Dry etching can be used to shape the sidewalls, but it is constrained to certain geometries and cannot create abrupt interfaces for strong optical confinement.

In GaN, a hot potassium hydroxide (KOH) solution provides an anisotropic etch, highly selective to non-polar facets over c-plane facets. As a result, it is often used to smooth vertical features after dry etching of c-plane GaN, for example for forming reflective laser facets. Etching of GaN for large features has been shown possible using photo-assisted etching with biased electrodes, using UV illumination via mercury lamps to create electron-hole pairs in the GaN; the holes are for assisting with oxidation of the GaN and the paired electrons are removed via the anode. More recently, this has been achieved without electrodes, using an oxidiser such as potassium persulphate ($K_2S_2O_8$) in the solution in place. Due to band-bending at the non-polar surfaces creating a depletion region in doped GaN, holes are not available for the etch mechanism in p-type GaN and so etching is inhibited without additional measures. As a result, it is possible to perform a lateral etch in c-plane GaN, which is selective of n-type over p-type[2]. Electrode-less photo-electrochemical (ElPEC) etching is investigated to shape nanorods for high optical confinement to exploit strong photonic crystal effects.

GaN on sapphire templates with a single quantum well (QW) were patterned with a 600nm pitch hexagonal lattice using nano-imprint lithography and ICP etched to produce nanorods ~1200nm high with a diameter of ~300nm. ElPEC etching is performed using a high power array of UV (~365nm) LEDs, and the effect of solution concentration and illumination intensity on the resulting structures is reported. Selective etching of n-doped GaN in nanorods is shown to be possible without excessive etching of the InGaN quantum disc or higher energy (<310nm) UV light present in a mercury source. An optimised ElPEC etch process after a simple dry etch shows potential as an alternative to exclusively dry etching for shaping nanorod arrays.

[1] *J. Appl. Phys.*, C. J. Lewins et al., vol. 116, no. 4, p. 044305, Jul. 2014.
[2] *Mater. Sci. Eng. R Reports*, D. Zhuang & J. H. Edgar, vol. 48, no. 1, pp. 1–46, Jan. 2005.

Carrier Transport in MOVPE-grown Si:AlGaN material with high aluminum content.

P. Pampili [1, 2], D. V. Dinh [1], V. Z. Zubialevich [1], P. J. Parbrook [1, 2]

[1]*Tyndall National Institute, University College Cork, Lee Maltings, Dyke Parade, Cork, Ireland*
[2]*School of Engineering, University College Cork, Western Road, Cork, Ireland*

The growth of highly conductive n-AlGaN layers is one of the major challenges that need to be addressed in order to realise efficient LEDs emitting in the ultraviolet region, and this challenge becomes even harder as the aluminium content increases, as is required for devices emitting in the UVC range.

For this reason, the MOVPE growth of silicon-doped AlGaN materials by use of different silane (Si_1H_4) or disilane (Si_2H_6) flows into the reactor has been studied in the past by a few different groups [1-4]. More recently, *Mehnke et al.* have found the existence of an optimum, concentration-dependent Si/III ratio [5], but so far no physical explanation of this trend has been proposed.

With the aim of gaining better insight into this topic, we performed a set of temperature dependent Hall measurements of silicon doped AlGaN materials grown with different disilane flows in the range of 0.25 to 3.0 sccm (corresponding to a molar ratio Si/III in the range 0.28—3.35 x 10^{-4}) for 60% and 85% AlGaN materials.

For the 60% AlN content samples, apart from those that were heavily overdoped for which it was not possible to get any conductivity at temperatures lower than 150 K, the clear presence not only of thermally activated carriers, but also of an impurity band conduction which became dominant at very low temperatures but whose contribution was important even at higher temperatures was found (see Fig. 1). The transition between the two regimes is characterised by a typical carrier concentration dip around 100—150 K.

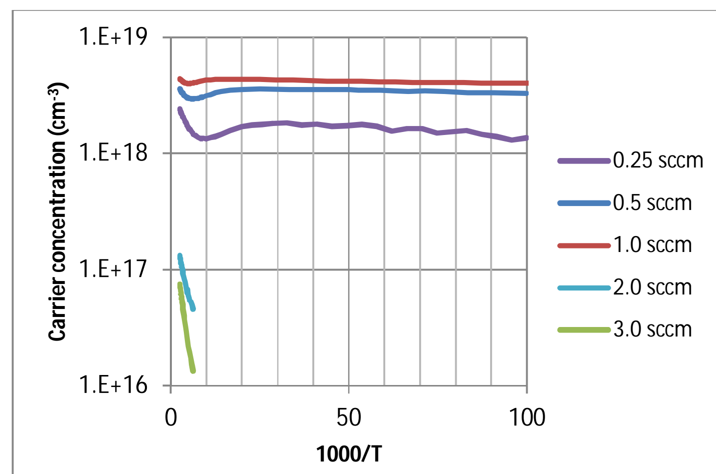

Fig. 1: Variation of carrier concentration with Temperature for $Al_{0.6}Ga_{0.4}N$ with different Si doping concentrations.

As shown in Fig. 2, for the samples close to the optimum condition (0.5—1.0 sccm), the resistivity of the AlGaN remains quite stable with increasing disilane flow as a result of a trade-off between carrier concentration and mobility which increase and reduce, respectively. It is also noted that the change in resistivity with temperature at around 300 K is quite low under optimal doping conditions. At lower temperatures the increase in resistivity is due to the reduced mobility of the mini-band conduction path. For the overdoped samples the both carrier concentration and mobility fall indicative of the formation of significant deep centre complexes and associated carrier scattering.

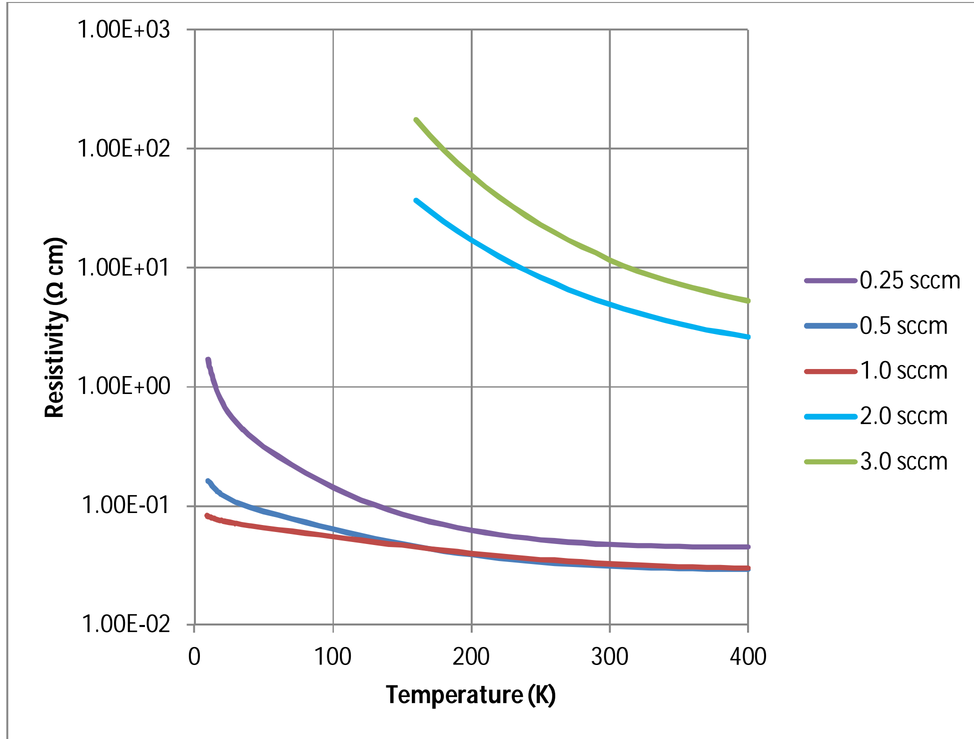

Fig. 2: Variation of resistivity with Temperature for $Al_{0.6}Ga_{0.4}N$ with different Si doping concentrations

A detailed analysis of the results, together with an outline of further investigations on $Al_{0.85}Ga_{0.15}N$ material will be presented in this contribution.

[1] M. L. Nakarmi, K. H. Kim, K. Zhu, J. Y. Lin, and H. X. Jiang, "Transport properties of highly conductive n-type Al-rich $Al_xGa_{1-x}N$ (x≥0.7)," *Applied Physics Letters*, vol. 85, pp. 3769-3771, 2004.

[2] Y. Taniyasu, M. Kasu, and N. Kobayashi, "Intentional control of n-type conduction for Si-doped AlN and $Al_XGa_{1-X}N$ (0.42≤x≤;1)," *Applied Physics Letters*, vol. 81, pp. 1255-1257, 2002.

[3] Y. Taniyasu, M. Kasu, and T. Makimoto, "An aluminium nitride light-emitting diode with a wavelength of 210 nanometres," *Nature*, vol. 441, pp. 325-328, 2006.

[4] R. Collazo, S. Mita, J. Xie, A. Rice, J. Tweedie, R. Dalmau, *et al.*, "Progress on n-type doping of algan alloys on aln single crystal substrates for uv optoelectronic applications," *Physica Status Solidi (C) Current Topics in Solid State Physics*, vol. 8, pp. 2031-2033, 2011.

[5] F. Mehnke, T. Wernicke, H. Pingel, C. Kuhn, C. Reich, V. Kueller, *et al.*, "Highly conductive n-$Al_xGa_{1-x}N$ layers with aluminum mole fractions above 80%," *Applied Physics Letters*, vol. 103, 2013.

III-Nitride Tunnel Junctions for Next-Generation Visible and Ultraviolet Optoelectronics

Siddharth Rajan , Sriram Krishnamoorthy, Fatih Akyol, Yuewei Zhang

Electrical & Computer Engineering, The Ohio State University

e-mail: rajan@ece.osu.edu

A review of recent developments on device engineering and applications of interband tunnel junctions for next-generation III-Nitride optoelectronic devices will be presented. Tunnel junctions can enable significant improvements in the efficiency of visible and ultraviolet emitters, and enable new device functionality for visible and ultraviolet emitters. Multiple active region LEDs cascaded using tunnel junctions could enable a solution to the efficiency droop problem by enabling high power emitters at low current density [1], and overcome intrinsic p-type doping problems in ultra wide band gap AlGaN ultraviolet emitters.

Interband tunnel junctions in wide band gap materials are intrinsically challenging due to the large band gaps and low tunneling probability, but developments in the last few years have led to highly efficient tunnel junctions that can enable a new class of III-nitride optoelectronic devices. We will discuss methods to enable highly efficient interband tunnel diodes to overcome the large band gap and intrinsic low tunneling probability encountered in GaN and AlGaN materials. Polarization engineering [2] can be used to create large dipole charges and electric fields that can enhance tunneling across III-Nitride PN junctions, enabling low-resistance GaN and AlGaN tunnel junctions. We will discuss our recent work on GaN tunnel homojunctions based on extreme doping profiles that enable record low tunnel junction resistance. Demonstration of record low resistance tunnel junction injected light emitting diodes for visible LEDs [3], and recent results demonstrating 3-junction multiple active region LEDs [4] with low resistance losses using tunnel junctions will be discussed. Finally, we will present recent results on tunnel junctions for ultra wide band gap materials, and describe the first demonstration of interband tunnel junctions in AlGaN-based ultraviolet emitters with sub-300 nm emission wavelengths [5].

This work was funded by Office of Naval Research (Program manager: Paul Maki), and the National Science Foundation.

References:

[1] Akyol, F., Krishnamoorthy, S. and Rajan, S., 2013. Tunneling-based carrier regeneration in cascaded GaN light emitting diodes to overcome efficiency droop. Applied Physics Letters, 103(8), p.081107.

[2] S. Krishnamoorthy, D. Nath, F.Akyol, P. S. Park, S. Rajan, Applied Physics Letters, 97, 203502 (2010).

[3] S. Krishnamoorthy, F. Akyol, P. S. Park, and S. Rajan, Applied Physics Letters, 102, 113503 (2013)

[4] Akyol, F., Krishnamoorthy, S., Zhang, Y. and Rajan, S., 2015. GaN-based three-junction cascaded light-emitting diode with low-resistance InGaN tunnel junctions. Applied Physics Express, 8(8), p.082103.

[5] Zhang, Y et al. "Interband tunneling for hole injection in III-nitride ultraviolet emitters." Applied Physics Letters 106, no. 14 (2015): 141103.

A confocal photoluminescence investigation of basal plane stacking faults (BSFs) in (11-22) semi-polar InGaN/InGaN quantum wells on overgrown semi-polar GaN

R. M. Smith, Y. Zhang, J. Bai, K. Xing, X. Yu, B. Xu, Y. Gong, M. Athanasiou, Y. Hou and T. Wang

Department of Electronic and Electrical Engineering, University of Sheffield,

E-mail: t.wang@sheffield.ac.uk

Interest in semi-polar III-nitride materials is increasing due to the potential of superior optical performance compared to polar c-plane. Of the various semi-polar orientations investigated (11-22) is of particular interest due to not only the reduced piezoelectric fields compared to c-plane but also a significantly increased indium incorporation, allowing the development of high efficiency longer wavelength LEDs and Lasers. Many challenges exist in improving the crystal quality of semi-polar III-nitrides grown on cost effective sapphire substrates, our group has recently demonstrated significant improvements in the crystal quality of (11-22) semi-polar GaN on sapphire using a micro-rod overgrowth approach. Using such templates grown with this technique, a series of high indium composition InGaN/InGaN single quantum well LED structures have been grown, with bright emission through the blue to orange spectral regions. The use of our micro-rod overgrowth technique has been shown to significantly suppress the propagation and density of defects in the overlying LED structures. The influence of different types of defects on the optical properties of these (11-22) quantum well structures still requires further investigation, specifically the influence of basal plane stacking faults (BSFs).

In this work, high spatial resolution confocal photoluminescence mapping measurements were used to investigate influence of localized clusters of stacking faults on the optical properties of the quantum wells. TEM measurements indicate that the micro-rod template is effective in blocking propagation of BSFs from the template. The blocking leads to areas with very low BSF density with small clusters of BSFs localized in periodic arrays on the micron scale. Confocal photoluminescence mapping studies of these samples show that there is only a small difference in PL intensity between the BSF free regions and higher BSF density clusters, demonstrating that the BSFs are not acting as non-radiative centres. A lower energy shoulder peak is also observed at the higher BSF density clusters leading to an increase in the photoluminescence centre of mass wavelength as seen in Figure 1. It is therefore proposed that further reduction of BSF density in these LED materials is not expected to lead to significantly enhanced efficiency, but may be important in controlling the emission linewidth of these semi-polar LEDs.

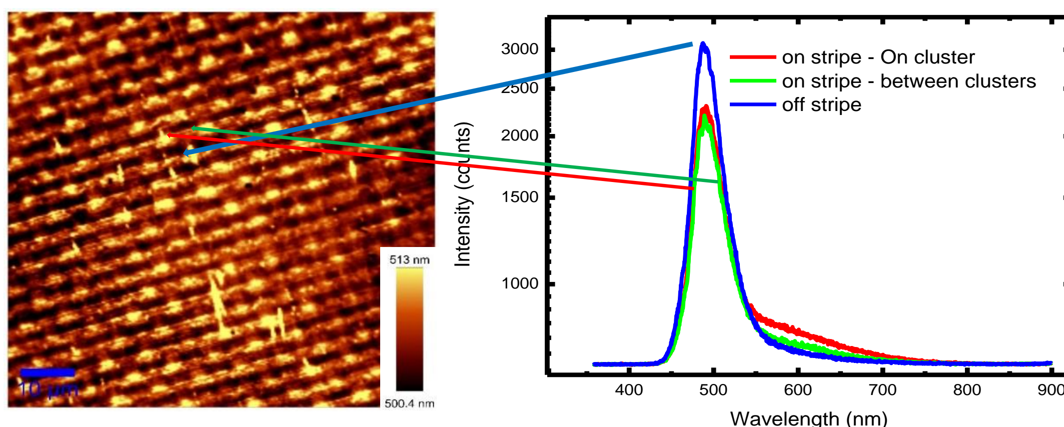

Figure 1: Confocal PL map showing centre of mass wavelength as a function of position. PL spectra taken on the BSF related stripe, on the stripe at a higher BSF density cluster and off the stripe in a low BSF density region.

(11-22) semipolar InGaN emitters from green to amber overgrown on GaN micro-rod templates

Y. Zhang, J. Bai, B. Xu, K. Xing, X. Yu, Y. Gong, Y. Hou, and T. Wang

Department of Electronic and Electrical Engineering, University of Sheffield, Mappin Street, Sheffield, S1 3JD.

1. Introduction

Semi- or and non-polar III-nitrides are becoming increasingly interesting as a result of their advantages of reducing or eliminating the spontaneous and piezoelectric polarizations.[1] Among these planes, the (11-22) semi-polar surface exhibits higher indium incorporation efficiency than the non-polar or polar surface (i.e., c-plane),[2] favoring the growth of ternary InGaN with high indium content. Both advantages make GaN growth along semi-polar (11-22) orientation be a most promising candidate for green and yellow light emitting diodes (LEDs). However, due to the lack of suitable substrates, (11-22) semi-polar GaN on industry-preferred substrates, such as sapphire, usually contains a high density of defects, including basal stacking faults (BSFs) and associated partial dislocations. Recently, our group has successfully achieved (11-22) semi-polar GaN with significantly enhanced crystal quality on sapphire by developing a cost-effective approach of an overgrowth on regularly-arrayed micro-rod templates, where the diameter of micro-rods can be accurately controlled. In this presentation, we will demonstrate high crystal quality (11-22) GaN and then InGaN based LEDs grown on such GaN templates, emitting strong green, yellow, yellow-green and amber emission. Furthermore, the mechanisms of the overgrowth and defect reduction will be explored in detail.

2. Experiments

Micro-rod array structures (Figure 1) are fabricated by a standard photolithography patterning process and subsequent dry etching techniques on single (11-22) GaN layers on *m*-plane sapphire which are grown using our high temperature AlN buffer approach by metal organic chemical vapor deposition (MOCVD). Then, an overgrowth with a thickness of 4 μm is carried out on the semi-polar GaN micro-rod arrays by MOCVD. On such overgrown GaN templates, four InGaN single quantum well LEDs with different indium compositions have been grown. Finally, all the LEDs are fabricated with a 0.33×0.33 mm^2 mesa size.

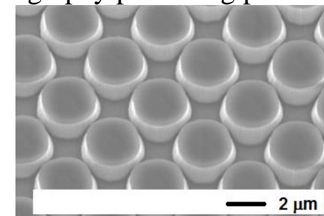

Figure 1

3. Results and discussion

Our cross-sectional TEM studies (Figure 2a) shows the density of dislocations in the overgrown GaN is significantly decreased compared to the GaN micro-rods underneath SiO_2 masks. In addition to blocking by the SiO_2 and the twice coalescence processes. TEM measurements indicate a dislocation density ranging from 1 to $4\times10^8/cm^2$ and a BSF density of 1 to 4×10^4/cm, respectively. XRD rocking curves measured along the on-axis direction show that full-width-at-maximums (FWHMs) are around 330 arcsec and 250 arcsec at 0° and 90° azimuth angle, respectively (Figure 2b). These demonstrate an excellent crystal quality of our (11-22) GaN, approaching the crystal quality of current *c*-plane GaN on sapphire for the growth of ultra-high brightness blue LEDs. Moreover, a model is built up to demonstrate the influence of the pattern on the defect reduction in order to further improve crystal quality.

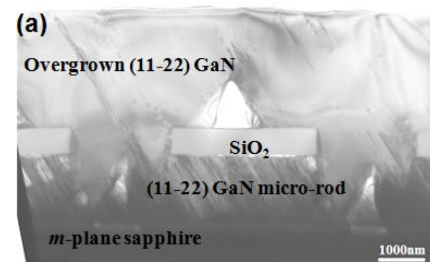

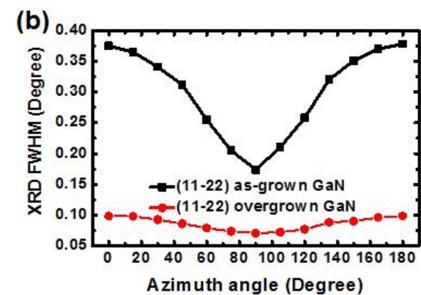

Figure 2

Figure 2 shows a series of Electroluminescence (EL) images for the four LEDs, each taken at 5, 20, 100 mA, respectively, demonstrating bright emissions in green, yellow-green, yellow and amber spectra regions, respectively. On-wafer measurements yield a linear increase in light power with increasing injection current. It is found that the line-width of the EL spectra becomes broader as the emission light moves towards long wavelength (Figure 3a), indicating that higher indium composition leads to more significant indium segregation. With increasing the current from 1 to 100 mA, the blue-shift for the green (11-22) LED, is only 8 nm. The blue-shift slightly increases to 15 nm and 19 nm for the yellow-green and yellow LEDs, respectively. For comparison, the blue-shift of a green LED on *c*-plane is typically about 13 nm. It suggests that the QCSEs in our (11-22) LEDs are effectively suppressed. The EQEs for all the four LEDs increases with increasing the current and reaches maximum at 10-20 mA, then decrease slowly, which is greatly reduce compared to a c-plane green LED. It demonstrates that the efficiency-droop issue could be potentially reduced through growth and fabrication of (11-22) semi-polar LEDs. Furthermore, Figure 3(b) shows the typical current–voltage curves for all the four LEDs, displaying a standard behaviour of InGaN/GaN based LEDs with a typical turn-on voltage of 3.0-3.4 V at 20 mA injection current for the green, yellow-green and yellow LEDs, which are comparable to *c*-plane InGaN based LEDs. For the amber LED, the voltage at 20 mA is relatively higher, which might be related to the growth of p-type GaN.

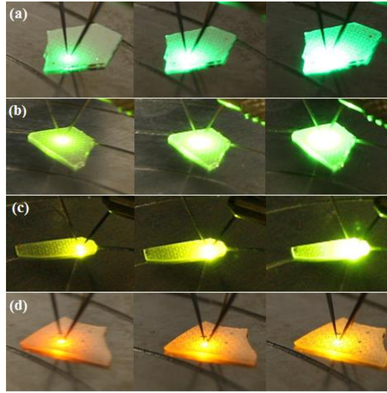

Figure 3

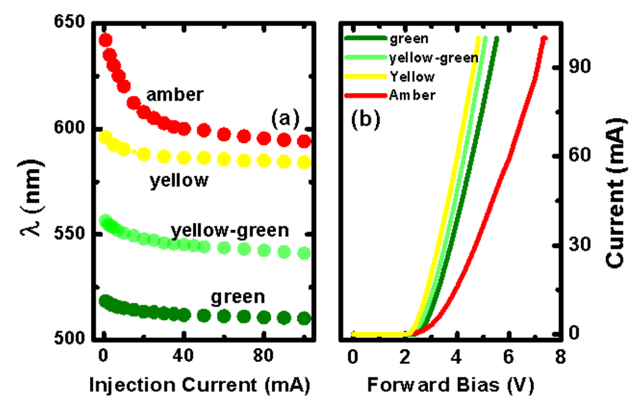

Figure 4

4. Conclusion

We have demonstrated high crystal quality semi-polar (11-22) GaN on *m*-plane sapphire by developing a cost-effective approach of overgrowth on regularly arrayed micro-rod arrays. TEM and XRD measurements show that the crystal quality of our semipolar GaN has approached that of current *c*-plane GaN on sapphire for growth of ultra-high brightness blue LEDs. Furthermore, semi-polar (11-22) InGaN LEDs on our semipolar GaN templates with a wide spectral region of up to amber have been demonstrated, deomonstrating major advantages of semipolar LEDs compared with current c-plane LEDs in terms of suppressing the QCSE, reducing efficiency droop and resolving the "green and yellow" gap issues. The preliminary results suggest that our overgrowth technology is a potentially cost-effective approach to achieving semi-polar GaN emitters with high performance in the long wavelength region, such as green or yellow region.

Reference

1. T. Takeuchi, H. Amano, and I. Akasaki, Jpn. J. Appl. Phys. **39**, 413 (2000).
2. J.E. Northrup, Appl. Phys. Lett. **95**, 10 (2009).

Fast colour conversion of InGaN sources using semiconductor nanocrystals

J. M. Santos[1], M. Leitao[1], C. Foucher[1], S. Rajbhandari[2], H. Chun[2], D. Vithanage[3], B. Guilhabert[1], G. A. Turnbull[3], I. D. W. Samuel[3], G. Faulkner[2], D. O'Brien[2], N. Laurand[1] and M. D. Dawson[1]

1) Institute of Photonics, Department of Physics, University of Strathclyde, Glasgow, G1 1RD, UK
2) Department of Engineering Science, University of Oxford, Oxford OX1 3PJ, UK
3) School of Physics and Astronomy, University of St Andrews, St Andrews KY16 9SS, UK

Visible light communication using InGaN light sources colour-converted with colloidal quantum dot structures is reported. Free-space data transmission up to 500 Mb/s is demonstrated.

Semiconductor nanocrystals, or colloidal quantum dots (CQDs), can act as efficient downconverters for InGaN sources, e.g. LEDs [1]. Advantages of CQDs over other types of converting phosphors for this utilisation include their soft-material processing capabilities, their narrow linewidth photoluminescence (PL) and the fine colour tunability. In turn, CQDs can be combined with blue InGaN LEDs for high performance white light sources having high colour quality [1], and for enabling a wide gamut display technology that is found in CQD-enhanced LCD screens. Applications of InGaN-based light sources other than lighting and displays are also emerging. One of these is visible light communications (VLC), which exploits the relatively high bandwidth of InGaN lasers and/or LEDs in order to transmit data over free space or, in some instances, through fibre and waveguide systems. Here again, CQDs can enable both white and single-colour sources with attractive characteristics. Narrow emission for example will facilitate implementation of wavelength division multiplexing. In addition, CQDs have shorter PL lifetime than the rare-earth phosphors commonly used in commercial LEDs, and are therefore more suited to VLC [2].

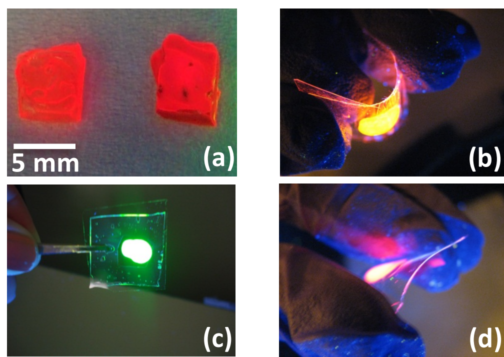

Fig. 1. (a) Red CQD composite converters, and (b), (c) and (d), Flexi-glass CQD converters

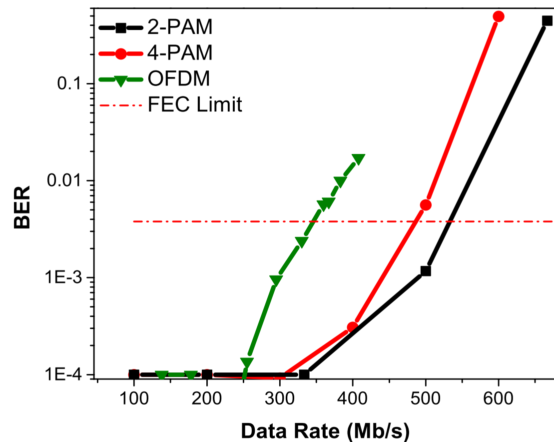

Fig. 2. Free-space transmission; BER vs data rate for different modulation schemes

In this work, we explore two formats of CQD colour-converters for blue-emitting InGaN sources. The CQDs are alloyed-core CdSeS/ZnS structure with a 6nm nominal diameter and emission in the green (540nm), yellow (575nm) and red (630nm). In the solid state, the photoluminescence quantum efficiency is 62%, 54% and 18% for the green, yellow and red CQDs respectively. The first format of converter consists of a polymeric composite film that incorporates the CQDs at weight concentrations of 1% and 10 %. Nanocomposite films with thickness of 1.2 mm were fabricated (see Fig. 1(a)) and the effect of the CQD concentration on the static and dynamic PL characteristics will be discussed. The second format of converter utilises CQDs in neat form that are encapsulated with flexible glass. For this, a 30μm-thick glass sheet was diced into 2 x 2 cm^2 membranes. A CQD/chloroform solution

was drop coated onto one glass membrane and a second membrane was then added to seal the CQD structure. The final flexi-glass CQD colour-converting structures are thin enough to retain flexibility (see Fig. 1(b) and (d)).

Both the composite and flexi-glass colour-converters can be placed in contact with an InGaN source or, alternatively, remotely pumped. A 450nm microLEDs was used as the blue InGaN source in our experiments. The forward power conversion efficiency was measured to be up to 14% depending on the wavelength, the type and the concentration of the converters. We note that there is room for improvement as no light extraction features were utilised. One way to incorporate such feature would be to directly patterned the CQDs by soft-lithography, e.g. with grating structures [3-4].

The -3dB optical modulation bandwidth of the CQD converters is comprised between 10 MHz and 30 MHz, again depending on the exact converter parameters. In turn, we demonstrate free-space data transmission ranging from 200 Mb/s up to 500 Mb/s per wavelength using pulse amplitude modulation (PAM) or orthogonal frequency division multiplexing (OFDM) and considering a forward error correction (FEC) limit of $3.8x10^{-3}$. For the experiment, the 450nm microLED was modulated around a DC-biased point and the converted light from the CQD structures was detected by an avalanche photodiode. Otherwise, details of the experimental set-up are similar to what is described in [5]. Figure 2 represents the data for the red CQD composite. For all the above CQD samples, under the same conditions, PAM leads to superior data rates than OFDM.

In conclusion, we report two formats of CQD downconverters for use with InGaN optical sources and demonstrate free space VLC with data rates up to 500 Mb/s per wavelength.

[1] T. Erdem and H. V. Demir, 'Color science of nanocrystal quantum dots for lighting and displays' Nanophotonics 2(1), pp. 57–81 (2013)

[2] N. Laurand, B. Guilhabert, J. McKendry, A. E. Kelly, B. Rae, D. Massoubre, Z. Gong, E. Gu, R. Henderson, and M. D. Dawson 'Colloidal quantum dot nanocomposites for visible wavelength conversion of modulated signals', Optical Materials Express, 2(3), pp. 250-260 (2012)

[3] J. Herrnsdorf, B. Guilhabert, J. McKendry, Z. Gong, D. Massoubre, S. Zhang, S. Watson, A. E. Kelly, E. Gu, N. Laurand, and M. D. Dawson 'Hybrid organic/GaN photonic crystal light-emitting diode', Applied Physics Letters 101(14), 141122 (2012)

[4] R. Clatyton Shallcross, G. S. Chawla, F. Saneeha Marikkar, S. Tolbert, J. Pyun, and N. R. Armstrong 'Efficient CdSe nanocrystal diffraction gratings prepared by microcontact molding', ACS Nano, 3(11), pp. 3629-3637 (2009)

[5] D. Tsonev, H. Chun, S. Rajbhandari, J. J. D. Mckendry, S. Videv, E. Gu, M. Haji, S. Watson, A. E. Kelly, G. Faulkner, M. D. Dawson, H. Haas, and D. O. Brien, "A 3-Gb / s single-LED OFDM-based weireless VLC link using a gallium nitride μLED," IEEE Photonics Technology Letters, 26(7), pp. 637-640 (2014)

Structured illumination by high-speed micro-LED arrays for imaging and LiFi

J. Herrnsdorf[1], M. J. Strain[1], E. Gu[1], and M. D. Dawson[1]
[1]*Institute of Photonics, Department of Physics, University of Strathclyde, Glasgow G1 1RD*

GaN light-emitting diodes (LEDs) can be modulated at high speeds of typically a few tens of MHz. If the LED size is reduced to below 100×100 µm, the modulation capability is further enhanced to above 100 MHz and also the generation of picosecond optical pulses is possible [1,2]. This is due to the small capacitance and high current density handling capability of such micro-LEDs. Here, we report our recent progress on harnessing this speed in arrays of micro-LEDs where each element has its own electronic driver.
We operate arrays of 16×16 micro-LEDs at a 100 µm pitch at a frame update rate of 2 kfps. See Figure 1 for a micrograph of such a device. The framerate is currently limited by the electronic driver circuit and in the future it will be possible to operate larger arrays at up to 1 Mfps. These devices are applied to imaging with so-called single-pixel cameras and to indoors positioning systems with millisecond time resolution. Both applications are enabled by projecting temporal sequences of suitable spatial illumination patterns onto the illuminated scene.
As a particular example of an application it is shown how the positioning capability can be used in an optical wireless network where up to 16 connected users receive parallel data streams at an aggregate data rate of 1.2 Gb/s.
This work is funded by EPSRC under the grant EP/M01326X/1 “QuantIC”.

[1] McKendry *et al.*, PTL **21**, 811 (2009)
[2] McKendry *et al.*, JLT **30**, 61 (2012)

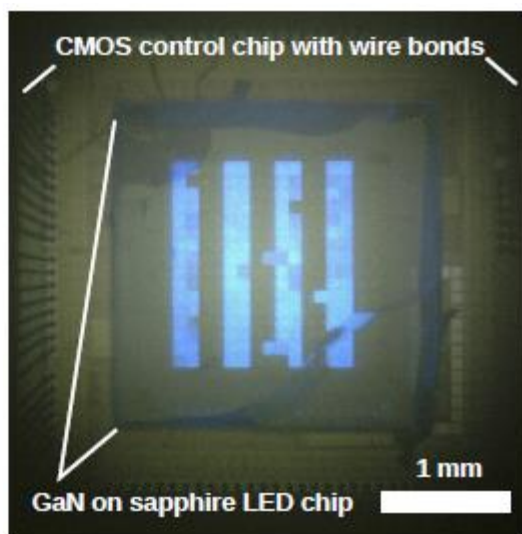

Figure 1: Micrograph of a 16×16 LED array for structured illumination.

1 Gb/s Integrated Visible Light Communication System Comprising CMOS drivers, receivers and GaN micro-LEDs

J.J.D. McKendry[1], S. Rajbhandari[2], H. Chun[2], G. Faulkner[2], K. Cameron[3], A.V.N. Jalajakumari[3], R.K. Henderson[3], D. Tsonev[4], M. Ijaz[4], Z. Chen[4], H. Haas[4], E. Xie[1], J. Herrnsdorf[1], E. Gu[1], M.D. Dawson[1] and D O'Brien[2]

[1] Institute of Photonics, Department of Physics, University of Strathclyde, Glasgow, G1 1RD
[2] Department of Engineering Science, University of Oxford, Oxford OX1 3PJ
[3] CMOS Sensors & Systems Group, The University of Edinburgh, Edinburgh EH9 3JL, U.K.
[4] Institute for Digital Communications, Li-FI R&D Centre, The University of Edinburgh, Edinburgh EH9 3JL, U.K.

The use of Gallium-nitride-based light-emitting diodes for simultaneous illumination and data transmission (which has been referred to as "Li-Fi") is an area of research that has attracted a great deal of interest in recent years. This technology opens up the visible spectrum for use in wireless communications, supplementing existing radio-frequency (RF) wireless communications and can help meet the ever-growing demand for wireless data communication.

Although typical off-the-shelf LEDs have relatively low modulation bandwidths, of the order of 10-20 MHz, data transmission rates over 1 Gb/s have been achieved by the use of spectrally-efficient, though relatively complex, modulation schemes [1]. Micro-LEDs, devices with individually-addressable LED pixels with dimensions < 100 μm, have been reported with modulation bandwidths an order of magnitude higher than their off-the-shelf counterparts [2], which has been attributed to their low device capacitance and operating current densities.

Using such micro-LEDs, data rates of 3 Gb/s over free space [3] and 10 Gb/s bi-directional transmission over polymer fibre [4] have previously been reported. However, these demonstrations used single pixels from their respective micro-LED arrays, and did not utilise the multi-pixel array-nature of these devices. Here we report on a complete integrated system, comprising of micro-LED arrays, a complementary metal-oxide-semiconductor (CMOS) LED driver chip, and a CMOS-based avalanche photodiode (APD) array. This allows each pixel in the micro-LED to be individually-controlled in a flexible fashion. Each micro-LED can either be used to transmit the same data, in order to increase the transmitted power ("ganging" configuration), or different pixels can simultaneously transmit independent data streams ("MIMO"), whilst retaining compatibility with any optical modulation scheme. Similarly, at the receiver, a 3×3 array of high-speed APDs can either be read out independently, or have their inputs summed together. We will present recent results using this system showing data transmission rates exceeding 1 Gb/s over 1 m of free space. This represents an important milestone towards a scalable, flexible and high-speed integrated VLC system.

[1] F.-M. Wu, C.-T. Lin, C.-C. Wei, C.-W. Chen, H.-T. Huang, and C.-H. Ho, "1.1-Gb/s White-LED-Based Visible Light Communication Employing Carrier-Less Amplitude and Phase Modulation," *IEEE Photonics Technol. Lett.*, vol. 24, no. 19, pp. 1730–1732, 2012.

[2] J. J. D. McKendry, D. Massoubre, S. Zhang, B. R. Rae, R. P. Green, E. Gu, R. K. Henderson, A. E. Kelly, and M. D. Dawson, "Visible-Light Communications Using a CMOS-Controlled Micro-Light- Emitting-Diode Array," *J. Light. Technol.*, vol. 30, no. 1, pp. 61–67, Jan. 2012.

[3] D. Tsonev, H. Chun, S. Rajbhandari, J. J. D. McKendry, S. Videv, E. Gu, M. Haji, S. Watson, A. E. Kelly, T. Fath, M. D. Dawson, H. Haas, and D. O. Brien, "A 3-Gb/s Single-LED OFDM-Based Wireless VLC Link Using a Gallium Nitride μ LED," *IEEE Photonics Technol. Lett.*, vol. 26, no. 7, pp. 637–640, 2014.

[4] X. Li, N. Bamiedakis, J. Wei, J. J. D. McKendry, E. Xie, R. Ferreira, E. Gu, M. D. Dawson, R. V Penty, and I. H. White, "μLED-Based Single-Wavelength Bi-directional POF Link With 10 Gb/s Aggregate Data Rate," *J. Light. Technol.*, vol. 33, no. 17, pp. 3571–3576, 2015.

Electrical Characterization of AlGaN/GaN and SiC using Non-contact corona-Kelvin Metrology

A. Findlay[1], J. Lagowski[1], M. Wilson[1], A. Savtchouk[1], Bob Hillard[2]

[1] Semilab SDI, LLC - 10770 N. 46th St., E700, Tampa, Florida, USA
[2] Semilab USA, LLC – 101 Billerica Ave, Building 5 Suite 105, North Billerica, MA, USA
Email: afindlay@semilabsdi.com

Biography

Andrew Findlay is the Director of Global Sales for Semilab, a leading supplier of metrology and characterization equipment for semiconductor materials and dielectrics used in IC and photovoltaic manufacturing. Additionally he is the General Manager of Semilab SDI, a division of the company located in Tampa, FL. He has 25 years' experience in the Semiconductor Industry, primarily in the area of applications and metrology. Since 1996, he worked for Semiconductor Diagnostics, specializing in non-contact electrical characterization of semiconductor materials and dielectrics used in IC processing. In the early years this primarily for silicon, but more recently focus has shifted to wide bandgap semiconductor materials. He graduated from Hertford College, Oxford in 1989, with a MA in Physics, and since then has co-authored more than 25 technical papers, and traveled extensively working with customers around the world.

Abstract

Electrical metrology based on corona charge surface biasing and Kelvin-probe measurement of surface voltage is a powerful approach, proven in production during silicon IC manufacturing [1].

In this work we discuss the extension of "corona-Kelvin" metrology to wide-gap semiconductors such as, AlGaN and SiC. A significant advantage compared to silicon GaN is an excellent retention of corona charge on surfaces of wide-gap semiconductors. This expands the applications to bare wafers enabling the use of "corona-Kelvin" not only as a replacement for MOS characterization but also as a non-contact replacement for Schottkey diode characterization including mercury probe C-V. We demonstrate such capability using a novel, very accurate dopant density determination and dopant profiling in epitaxial SiC and GaN achieved due to development of constant surface potential corona charging [2]. Compared to the capacitance voltage measurement, the corona-Kelvin measurement makes use of three variables (Q,V,C) i.e. the surface charge density, Q, deposited by corona; the surface voltage, V, measured by a Kelvin probe, and the differential capacitance determined from charge and voltage increments $C=\Delta Q/\Delta V$. With an example of AlGaN/GaN heterostructures we demonstrate direct determination of the two dimensional electron gas 2DEG sheet charge using a unique capacitance-charge C-Q characteristic. The carrier concentration profiles of 2DEG within a heterostructure is determined in corona-Kelvin using the static C-V characteristics. Results are presented comparing corona-Kelvin with standard Hg-probe measurement.

Dielectric and interface characterization is demonstrated for GaN and SiC epitaxial layers coated with dielectric films. Corona-Kelvin provides the oxide equivalent dielectric thickness EOT; the total dielectric charge, Q_{tot}; the flatband voltage, V_{FB}, and the spectrum of interface trap density, D_{it} in the energy gap up to about 1eV from the band edge. Corona-Kelvin is equivalent to very low frequency measurement (0.5Hz and less), and therefore enables the observation of slow processes of charge exchange between a semiconductor, and the traps located in the dielectric, referred to as border traps.

Non-contact electrical characterization includes Kelvin-probe surface voltage mapping, SVM, which is used for fast wafer inspection [3]. In combination with whole wafer corona charging to deep depletion, the SVM provides a unique means to identify localized defect spots causing a leakage current in the deep depletion layer.

Keywords: Non-contact, surface voltage, Kelvin probe, corona charge

References

[1] *Will be added in final manuscript.*

Uniformity and robustness of GaN-on-diamond wafer thermal properties for ultra-high power density transistor applications

J.W. Pomeroy, H. Sun, J. Anaya, M. Kuball

H.H. Wills Physics Laboratory, Bristol, U.K.

james.pomeroy@bristol.ac.uk

AlGaN/GaN HEMTs are a disruptive technology in the high-power microwave amplifier field, enabling increased power density with respect to pre-existing technologies, including GaAs pHEMTs. Although the reliability of this technology is now proven, operation is typically de-rated to ensure that parameters remain within a safe operating area. One such critical parameter is channel temperature, which is usually kept below ~200°C to ensure stable long term operation; this must be taken into account when designing microwave integrated circuits. In order to increase the operating power density, but not increase the channel temperature, improved thermal management must be developed, in particular close to the channel where Joule heating is generated. A logical approach is to replace the standard SiC substrate used for high power applications, having a thermal conductivity of 420 W/mK, with the highest thermal conductivity material available, diamond. A process has been developed at Element 6 to achieve this: The substrate is removed from an existing AlGaN/GaN wafer and polycrystalline microwave CVD diamond is grown on the back side of the GaN layer after depositing a thin nitride layer. The GaN-on-diamond wafers up to 4" diameter have been produced using this process, maintaining the electrical properties of the initial wafers

In this work we investigate the thermal properties of the interface between the GaN layer and the diamond substrate, which could be a potential effective thermal barrier resistance (TBR_{eff}). Measurements of the GaN-on-diamond wafer thermal properties have been made using a non-contact thermoreflectance technique developed recently for this material system (Fig. 1), enabling fast screening of wafers without the need for depositing transducers or device structures before measurements; this enables the feedback of the material properties to fabricators to guide process tuning and importantly, allows subsequent device fabrication. The thermal properties of GaN-on-diamond wafers have been characterised over a temperature range encompassing transistor operation, as shown in Fig. 2: the thermal resistance of the GaN/diamond interface decreases with temperature, attributed to the increasing thermal conductivity of the amorphous nitride interlayer. Both the thermal boundary resistance and effective diamond thermal conductivity are consistent with theoretical predictions. Figure 3 shows the result of thermal resistance mapping across a GaN-on-diamond wafer, shown the uniformity of processing. Measured TBR_{eff} values were unchanged after temperature cycling to 950°C, demonstrating the thermomechanical robustness of the GaN/diamond interface. Figure 4 illustrates a comparison between the simulated thermal resistance of a GaN HEMT microwave amplifier on a SiC substrate (benchmark) and diamond, showing that the measured GaN-on-diamond wafer thermal properties enable a >3× increase in RF power density with respect to GaN-on-SiC technology.

Acknowledgement: We are grateful to Element 6 (D. Francis and D. Twitchen) for supplying GaN-on-diamond wafer samples.

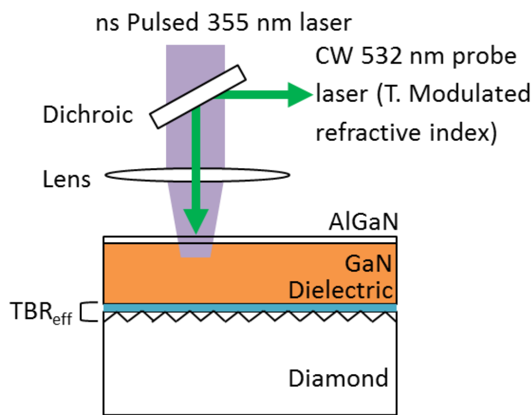

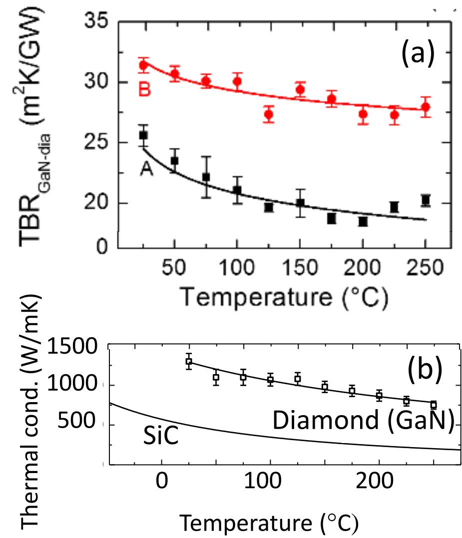

Figure 1: Schematic representation of the non-contact transient thermoreflectance technique developed here. An above bandgap nanosecond pulsed laser heats the GaN surface, while a CW below bandgap laser monitors the transient surface temperature, exploiting the temperature dependency of the GaN refractive index: Both the thermal boundary resistance (TBR_{eff}) and diamond thermal conductivity are determined.

Figure 2: (a) Temperature dependent GaN-on-diamond thermal boundary resistance measured for two wafers, **A** with a higher diamond nucleation layer thermal resistance and **B** with an optimised lower diamond nucleation layer thermal resistance. The TBR_{eff} of wafer **B** is comparable to GaN-on-SiC. (b) Temperature dependence of the diamond substrate effective thermal conductivity, compared with SiC.

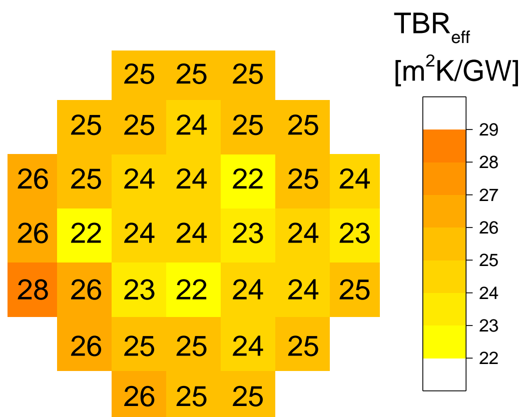

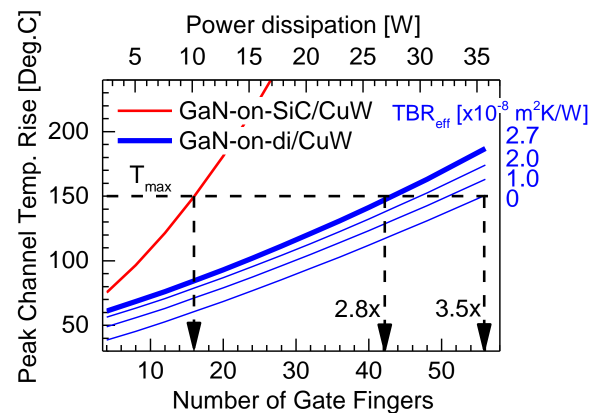

Figure 3: Map showing uniformity of the thermal resistance between the GaN layer and diamond substrate, measured across a 3 inch diameter GaN-on-diamond wafer.

Figure 4: Finite element thermal model, comparing the peak channel temperature rise in a 300×125µm GaN HEMT amplifier cell operated at power dissipation of 5 W/mm and increasing number of gate fingers (decreasing gate pitch). GaN-on-SiC is compared to GaN-on-diamond, considering a range of TBR_{eff} values. A >3× increase in power density can be achieved at a conservative maximum junction temperature (T_{max}).

Development of an atomic layer etch process via repeated cycling of chloride formation in chlorine gas and its argon plasma removal for precision nanometer scale thin layer etch in GaN-based power device fabrications

Xu Li[1], Konstantinos Floros[1], Sung-Jin Cho[1], Ivor Guiney[2], David Moran[1] and Iain G Thayne[1]

[1]*School of Engineering, University of Glasgow, Rankine Building, Oakfield Avenue, Glasgow, G12 8LT, Scotland, UK*

[2]*Department of Materials Science and Metallurgy, University of Cambridge, 27 Charles Babbage Road, Cambridge, CB3 0FS, UK*

phone: +44-141-330-6024, fax: +44-141-330-4907

e-mail: xu.li@glasgow.ac.uk

1. Introduction

ALE (Atomic Layer Etch) as a technique that removes very thin layers of material precisely using sequential self-limiting reactions has been considered one of the most promising techniques for achieving the low process variability necessary in the atomic-scale era [1]. On the other hand, for last decade around, AlGaN/GaN based HFETs have attracted intensive investigation due to their applications in power electronics [2]. Recent device fabrication, e.g. integrated cascode type device, requires very precisely control for etching only a couple of nanometer materials [3]. In this work, an atomic layer etching process for etching group III nitrides has been developed based on a cycled procedure of Cl_2 chlorination and argon plasma removal of the chlorides, which is suitable for fabricating devices based on III-nitrides, such as materials AlGaN, GaN, AlInN, AlN.

2. Experiment and Results

An Oxford Instrument PlasmaLab Inductively Coupled Plasma (ICP) etching system with repeat loop function has been used in this investigation. The etching chemistry was based on the formation of self-limited Al, Ga and In chlorides on the sample surface in Cl_2 gas or Cl_2 plasma and followed by a removal step using Ar plasma at an optimized RF power level at which the plasma only remove the chlorides on the surface but not the nitrides underneath.

The basic devices could be fabricated by this process have been shown in Fig. 1, where A on the left shows an e-mode device in a dual barrier structure for cascade type devices and B on the right also shows a possible e-mode device fabricated on a normal d-mode structure materials. The materials etched were GaN, AlGaN, AlInN, or AlN based materials on Si wafer grown by MOCVD and patterned by Shipley photo resist S1818.

Etching was investigated under various etching conditions including optimizing chlorination in Cl_2 plasma or Cl_2 gas only, such as time of chlorination, gas flow rate, gas concentration, chamber pressure, and optimizing the Ar plasma removal, such as RF power, chamber pressure, and reaction time. Etched surface, etching depth and etching profile were characterised by AFM, SEM, and TEM. The two figures below showed some typical key parameter optimisations. Fig. 2 shows the effect of Ar plasma power on the etch rate for the chloride removal. Under the optimised condition, Ar plasma would only etch the chlorides but not the underneath III-nitrides. Fig. 3 shows the effect of the flow and the dilution of Cl_2 in Ar on the etch rate to achieve a stable and well controlled atomic layer etch process in the etch tool used here.

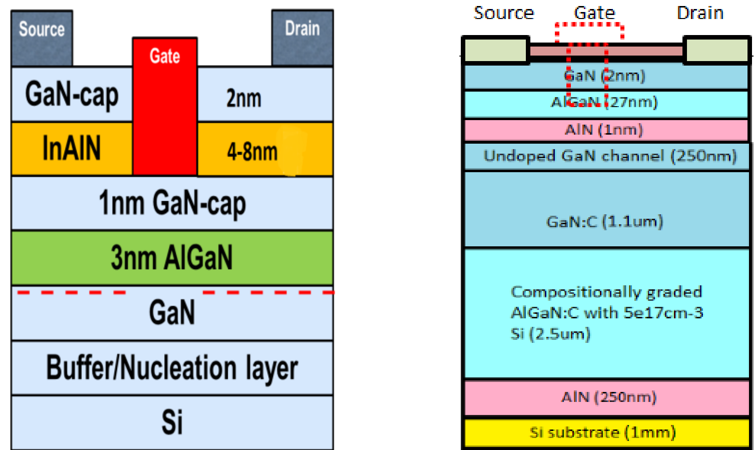

A: Dual barrier structures e-mode device B: Gate recessed for e-mode device

Fig. 1 Scheme of device fabrications requiring precision thin layer etching of III-nitrides

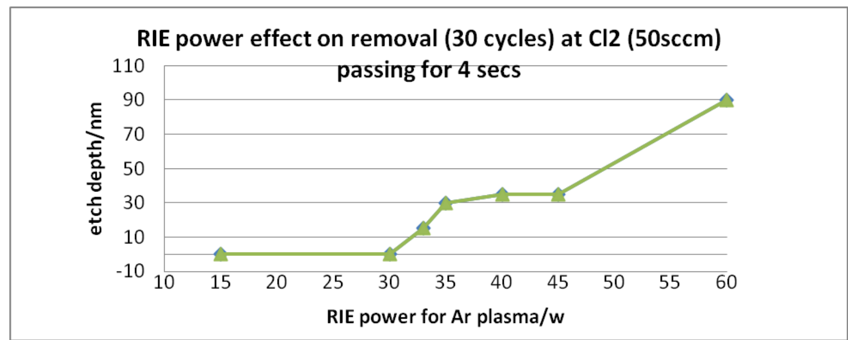

Fig. 2 Effect of RF power on etch depth (fixed 30 cycles) at a fixed chlorination condition

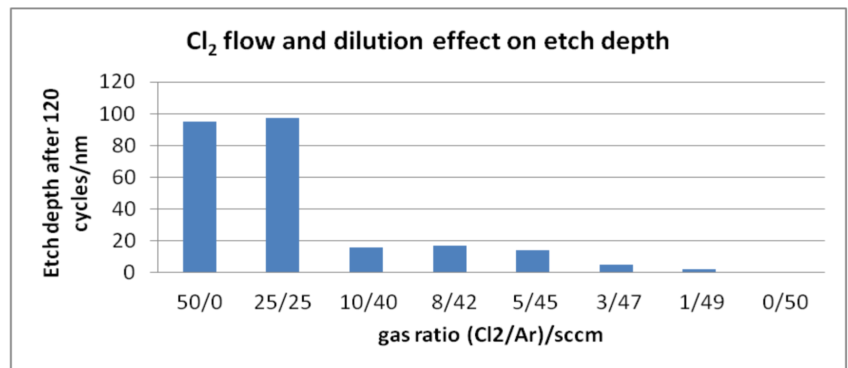

Fig. 3 Effcet of Cl_2 flow and dilution in Ar with passing time of 1 sec (after etching for 120 cycles)

Acknowledgments

This work is a part of UK EPSRC project “Silicon Compatible GaN Power Electronics” EP/K014471/1.

References

[1] K. J. Kanarik, et al.: J. Vac. Sci. Technol. A **33**(2), 020802 (2015).
[2] A. N. Bright, et al.: J. Appl. Phys. **89**, 3143 (2001).
[3] R. Brown, et al.: IEEE Elec. Dev. Lett. **35**(9), 906 (2014)

Subthreshold mobility in AlGaN/GaN HEMTs

William Waller[1], Michael J Uren[1], Kean Boon Lee[2], Peter A. Houston[2], and Martin Kuball[1]
[1]CDTR, H H Wills Physics Laboratory, University of Bristol, United Kingdom
[2]Department of Electronic and Electrical Engineering, University of Sheffield, United Kingdom

We demonstrate that mobility in the AlGaN/GaN 2DEG of AlGaN/GaN power devices can drop rapidly below pinch-off by a factor of as much as ~80 from its value in the on state. The 2DEG mobility was extracted using an innovative method which, in contrast to traditional methods, can extend down to electron densities as low as $2{\times}10^9$ cm^{-2}. This sharp drop in mobility below pinch-off is due to Columbic scattering from ionized impurities [1]. We also demonstrate for the first time that in the sub-threshold regime the mobility becomes independent of electron concentration when the screening of impurities by the 2DEG becomes negligible.

The devices studied were AlGaN/GaN HEMTs grown on Si substrates with an AlN exclusion layer to reduce the alloy scattering in the 2DEG. Mobility is extracted using the frequency dispersion of conductance in a FATFET capacitor structure of 200000 μm^2 area with a long gate length of 200 μm. Hall mobility is 1765 cm^2/Vs and electron concentration $6.50{\times}10^{12}$ cm^{-2} at zero bias. For short channel length FETs dispersion is primarily from any interface traps [2] however when the interface state density is insignificant, as here (less than $5{\times}10^{10}$ cm^{-2}eV^{-1} for these structures), the distributed resistances are dominant [3], allowing the mobility to be extracted from large channel length FATFET devices. By creating an equivalent circuit model for the conductance response of the device at different frequencies, [3,4] the mobility can be used as a free parameter to fit the measured RC response. This approach provides a simple way to probe the mobility at the low electron densities present in the switching regime of power devices.

Figure 1 shows the measured frequency dispersion of the conductance and how the characteristic frequency decreases and then becomes constant as the device is switched off. The prediction of our model is presented in figure 2, and is compared to the measured CV characteristic in figure 3. This simple 1D model has only one fitting parameter, the 2DEG mobility presented in figure 4. The mobility drops sharply as the 2DEG is depleted due to a loss in its ability to screen ionized impurities. This is consistent with other mobility studies on AlGaN/GaN HFETs [1,5] and studies performed on similar heterojunctions [6]. However for the first time we access the regime for channel densities of $< 2 \times 10^{10}$ cm^{-2}, where screening by the 2DEG becomes insignificant and the mobility is limited by the bare Coulomb scatterers.

The limit of the mobility at low electron concentrations defines how fast the final carriers in the channel can be removed and consequently puts a limit on how fast a device can switch. This RC time constant is long for larger gate length devices such as those used as test structures. For the different devices the mobility level at low concentration is a measure of epitaxial quality in the GaN channel. A higher mobility value indicates better control of impurities at this layer. This parameter can be used to test and compare different epitaxial quality using a fast electrical method.

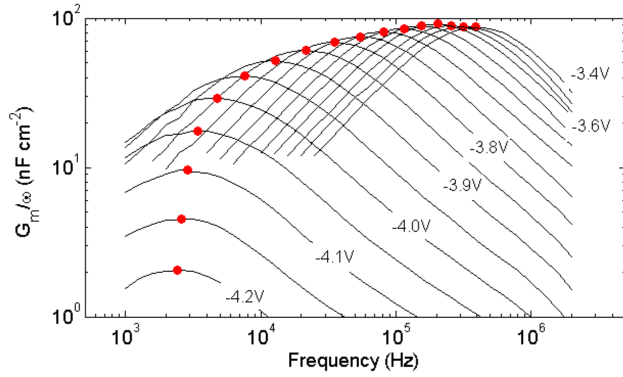

Figure 1: Measured G_m/ω at different gate voltages. Peak position (red points) falls and then becomes constant at -4 V, following the behavior of mobility.

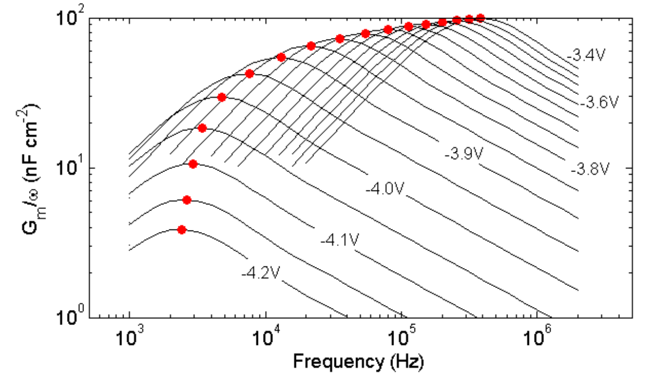

Figure 2: Modelled G_m/ω at different gate voltages. Mobility has been extracted from measurements in Fig. 1

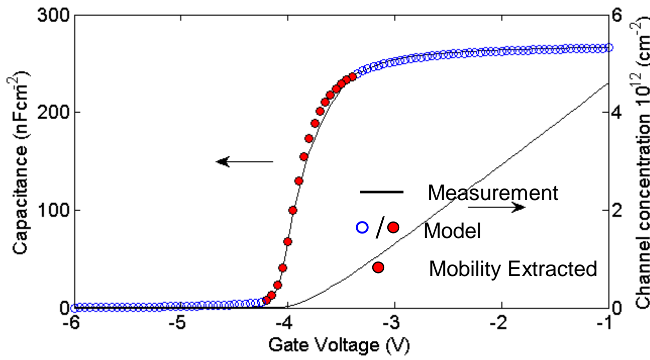

Figure 3: Measured and modelled capacitance at 1 kHz. Red points show where mobility has been extracted.

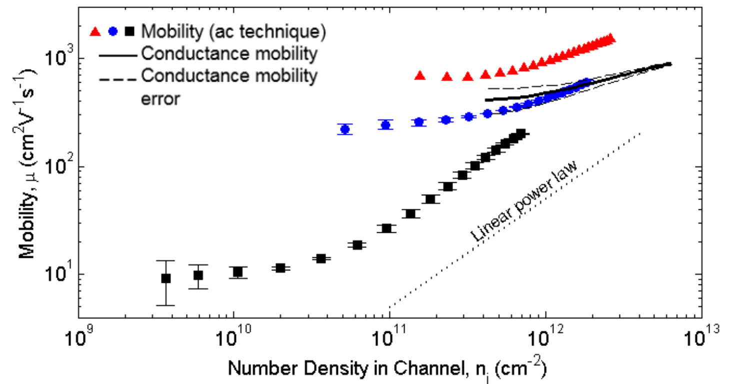

Figure 4: Extracted mobility for different devices demonstrating a drop as the channel is depleted due to reduced screening. The mobility reaches a constant value as screening of Coulombic scattering by the 2DEG becomes insignificant.

REFERENCES:

[1] J. Antoszewski, "Scattering mechanisms limiting two-dimensional electron gas mobility in AlGaN/GaN modulation-doped field-effect transistors", J. Appl. Phys., Vol. 87, p. 3900, 2000.

[2] E. Nicollian, MOS Physics and Technology, Wiley, pp 212-229, 1982.

[3] H. Haddara, "Conductance Technique in MOSFETs: study of interface trap properties in the depletion and weak inversion regimes", Solid State Electronics, Vol. 31, no 8, pp. 1289-1298, 1988.

[4] S. Takagi, "Quantitative Understanding of Inversion Layer Capacitance in Si MOSFETs", IEEE Trans. Electron Devices, Vol. 42. No 12, 1995.

[5] L. Hsu, "Electron Mobility in AlGaN/GaN heterostructures", Phys. Rev. B, Vol. 56, no. 3, pp. 1520, 1997.

[6] K. Hirakawa, "Mobility of the Two Dimensional Electron Gas at Selectively Doped n-type Heterojunctions", Phys. Rev. B, Vol. 33, pp 8291-8303, 1986.

Terahertz magnetospectroscopy studies of an AlGaN/GaN heterostructure

Ben F. Spencer[1], Morgan T. Hibberd[1], William F. Smith[1], Philip Dawson[1], Darren M. Graham[1], Matthias Beck[2], Albrecht Bartels[2], Ivor Guiney[3], Menno J. Kappers[3], Rachel A. Oliver[3], and Colin J. Humphreys[3].

[1]School of Physics and Astronomy and the Photon Science Institute, The University of Manchester, Manchester M13 9PL, United Kingdom

[2]Laser Quantum GmbH, Max-Stromeyer-Str. 116, 78467 Konstanz, Germany

[3]Department of Materials Science and Metallurgy, 27 Charles Babbage Road, University of Cambridge, Cambridge CB3 0FS, United Kingdom

AlGaN/GaN heterostructures have great potential for exploitation in the power electronics market due to their high room temperature electron mobility, large two-dimensional electron gas (2DEG) concentration and wide band gap [1]. To optimize the performance of such AlGaN/GaN high electron mobility transistors, however, requires precise measurements of the two-dimensional electron gas mobility, sheet concentration and electron effective mass. While microwave-based techniques have been developed [2] to enable the determination of the mobility and sheet carrier density, cyclotron resonance is the only noncontact technique able to provide a direct measurement of the carrier effective mass.

We report on a novel table-top terahertz (THz) magnetospectrometer developed to enable contactless measurements using cyclotron resonance absorption in magnetic fields of up to 30 T and its application to characterize the 2DEG confined within an AlGaN/GaN heterostructure. The use of high magnetic fields at national magnetic field facilities has previously been shown to enable precise measurement of the electron effective mass in the 2DEG, thus revealing information crucial for device design on the bandstructure at the heterointerface [3]. Our work enables such measurements to be laboratory based on a tabletop. The heterostructure studied here is made up of a 2.4 μm thick unintentionally-doped GaN channel region, a 1 nm mobility enhancement AlN layer, a 26 nm thick $Al_{0.27}Ga_{0.73}N$ barrier layer, and a 2 nm thick GaN cap grown by metal-organic chemical-vapor deposition on 220 nm thick AlN layer on a c-plane sapphire substrate.

The magnetospectrometer uses an asynchronous optical sampling (ASOPS) THz spectrometer combined with a pulsed magnet capable of generating up to 31 T over a 10 ms duration pulse. The rapidly-varying magnetic field requires fast capturing of the THz spectrum, however THz time-domain spectrometers typically utilize manual scanning of an optical delay line which can take several minutes. The commercial ASOPS spectrometer uses two femtosecond pulsed lasers at a fixed frequency offset, Δf, an electronics control system and an interdigitated photoconductive antenna for THz generation (Taccor power lasers, TL-1000-ASOPS and Tera-SED, all Laser Quantum) [4]. THz spectra were captured on microsecond timescales at a repetition rate of $(1/\Delta f)$, which equates to approximately 100 spectra during the magnetic field pulse.

Initial measurements were performed with pulsed magnetic fields of up to 13 T. The relationship between the cyclotron resonance absorption frequency and magnetic field allowed for the electron effective mass to be precisely determined according to $f = eB / 2\pi m^*$. The complex transmission function, or the ratio of the THz frequency spectrum in a magnetic field to a reference, was then fitted with the Drude model to extract the sheet carrier concentration and scattering time, which is related to the electron mobility according to $\mu = e\tau / m^*$ [5]. A sheet carrier concentration of 8×10^{12} cm^{-2} and a mobility of 9000 cm^2/Vs were determined at 77 K. The in-plane electron effective mass also was determined to be $(0.267 \pm 0.002)m_0$. The implications of these results on device optimization will be discussed.

[1] O. Ambacher *et al.*, J. Appl. Phys. 85, 3222 (1999).
[2] D. Nguyen *et al.*, J. Cryst. Growth 272, 59 (2004).
[3] Y. J. Wang *et al.*, J. Appl. Phys. 79, 8007 (1996).
[4] A. Bartels *et al.*, Rev. Sci. Instrum. 78, 035107 (2007).
[5] X. Wang *et al.*, Opt. Express 18, 12354 (2010).

Buffer Investigations on Substrate Biased AlGaN/GaN HFETs: An Overview

A. Pooth[1,2*], T. Martin[2], M. J. Uren[1], M. Kuball[1]

[1]Centre for Device Thermography and Reliability, University of Bristol BS8 1TL, UK

[2]IQE (Europe) Ltd., Pascal Close, St. Mellons, Cardiff CF3 0LW, UK

*E-mail: A.Pooth@bristol.ac.uk

Applying substrate bias to GaN-based hetero-structure field effect transistor (HFET) structures is a powerful technique for characterising buffer layers [1]. It reveals significant differences in structures that show very good agreement when characterised in a traditional way. These observations can often be linked to unwanted effects like current collapse (CC) or vertical breakdown (vBD), which cause reliability problems. The interpretation of a substrate bias ramp measurement is therefore of great importance, in particular for the implementation of the technique into a commercial production line, but also to understand the charge mechanisms responsible, which have not been explained fully, to date. Since usually several concurrent effects overlay in such a measurement, it can be difficult to derive an immediate explanation of the charge effects. In this paper we give an overview on effects observed on different samples and how they relate to the detrimental phenomena CC and vBD.

Monitoring the 2 dimensional electron gas (2DEG) current while applying a voltage to the conducting substrate of an HFET structure is how the substrate bias technique basically works. The voltage dropped vertically affects the internal electrical fields and this impacts the charge concentration in the 2DEG. Experimentally an ungated structure consisting of 2 ohmic contacts is used (see Fig. 1) with one contact biased at a low voltage to sense the 2DEG current and the conducting substrate being ramped towards high voltages. Figure 2 schematically shows what to expect from such a measurement for different buffer charging effects when ramping to negative substrate bias. If the whole buffer acts like a perfect insulator, 2DEG and substrate are capacitively coupled resulting in the straight line in Fig. 2. As soon as charges in the buffer are moving the curve bends either upwards indicating positive charging, which is holes injected from the 2DEG into the structure and neutralised when the substrate is ramped back to 0V due to the injection of electrons, or downwards corresponding to electron injection from the substrate, a layer starting to conduct or an increase of the capacitive area along a deep interface where lateral conduction is established in form of a 2 dimensional hole or electron gas. Negative charges affecting the 2DEG are not necessarily neutralised on the ramp back to 0V substrate bias and can cause severe reduction of current. Also some of the effects come with a large increase in vertical leakage currents. Figure 3 shows examples for capacitive coupling, positive charging and negative charging with the latter showing behaviour associated with strong current collapse.

An overview of effects observed by the substrate bias technique is given. The occurring effects are explained and how they are linked to device reliability is pointed out.

[1] M. J. Uren, *et al.*, *Appl. Phys. Lett.*, vol. 104, p. 263505, 2014.

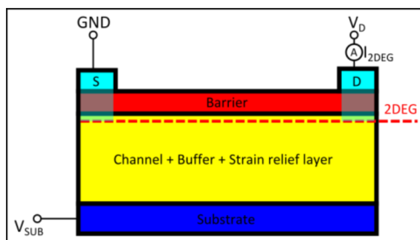

Fig. 1. Experimental setup for substrate bias ramping.

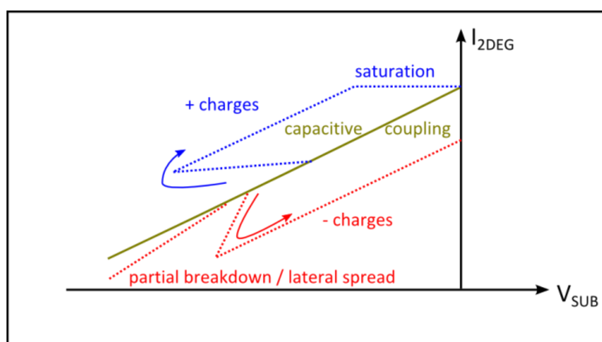

Fig. 2. Schematic plot of 2DEG current vs. substrate voltage, showing how different charging effects alter substrate bias ramp measurements.

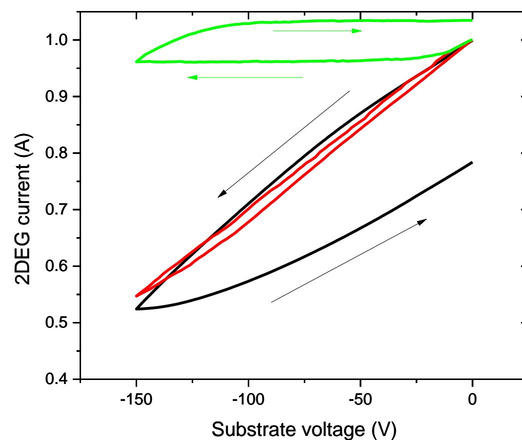

Fig. 3. Normalised substrate bias ramp curves for 3 different HFET samples. Representing negative charging (black), capacitive coupling (red) and positive charging (green).

Simulation of Dynamic R_{ON} Dispersion in GaN Power Transistors

Michael J Uren and Martin Kuball

Centre for Device Thermography and Reliability, H H Wills Physics Laboratory, University of Bristol

We examine the consequences of carbon doping in GaN-on-Si power transistors and show by simulation that dynamic R_{ON} reaches a maximum magnitude at about 150V drain bias before decreasing at higher bias. We also show that there that there are two characteristic time constants for the recovery despite there being only one active trap state. Both these predictions are observed experimentally[1] strongly suggesting that the basic mechanisms for buffer-induced dispersion in carbon doped devices are finally becoming understood.

GaN power devices are being aggressively developed for mass market applications driven by the capability to deliver improved efficiency or higher operating frequency. This is feasible because the GaN-on-Si platform is able to exploit the economy of scale offered by standard 6” or 8” foundries. However when targeted at the mainstream application niche of 600V operation, power devices have proved to be far more vulnerable to dynamic R_{ON} dispersion (an increase in device on-resistance following off-state bias stress) than the RF transistors now widely available. The reason for this serious vulnerability and the variability between processes has not been understood.

Carbon is the GaN dopant of choice for power applications since it delivers higher breakdown voltage and lower leakage than the iron normally used in RF devices. The difference is that the C_N acceptor pins the Fermi level in the valence band whereas Fe pins the Fermi level closer to the conduction band. The result is that the carbon doped buffer is floating with its potential defined by leakage primarily along a proportion of the dislocations[2]. This situation can only be simulated by not only including point defects/trap states but also adding appropriate leakage paths which mimic the experimentally observed leakage paths.

Here we give two examples of the result of such a simulation. Fig. 1 shows the off-state drain bias dependence of the reduction in on-state current. This reduction arises due to ionized acceptors at the top of the GaN:C region in the buffer. The turnover at 100-200V occurs because of the charge balance between the negative acceptor charge and the positive polarization charge once the 2DEG is depleted (Fig. 2), a RESURF effect [3]. The predicted recovery transient is shown in Fig. 3 and it can be seen that it is composed of two distinct contributions with a factor of 50 difference in time constant. The corresponding device cross-sections in Fig. 3 show that initially the hole current in the p-type GaN:C flows vertically cancelling out the vertical dipole, before flowing laterally as the charge dissipates to the contacts. This work indicates that simple analysis of transient spectroscopy to extract time constants does not necessarily directly indicate the presence of multiple trap states. In this case two orthogonal transport paths to the same active trap give two different time constants.

This work was funded by the EPSERC PowerGaN project.

[1] P. Moens*, et al.*, "Impact of buffer leakage on intrinsic reliability of 650V AlGaN/GaN HEMTs," *IEDM*, 2015, accepted.

[2] M. J. Uren*, et al.*, "Buffer design to minimize current collapse in GaN/AlGaN HFETs," *IEEE Trans. Elec. Dev.,* vol. 59, pp. 3327-3333, 2012.

[3] M. J. Uren*, et al.*, "Electric Field Reduction in C-Doped AlGaN/GaN on Si High Electron Mobility Transistors," *IEEE Elec. Dev. Lett.,* vol. 36, pp. 826-828, 2015.

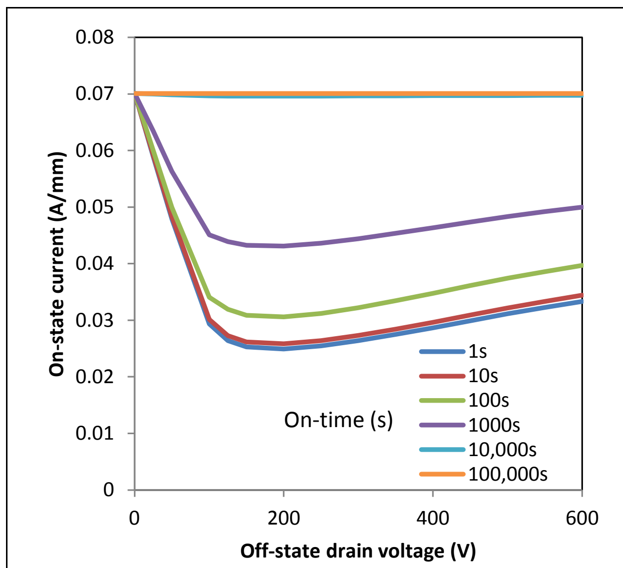

Fig. 1. Simulated reduction in drain current following switching from off-state to on-state. Lines correspond to increasing on-state time. V_{GS}=-5V in the off-state, V_{DS}=1V, V_{GS}=0V in the on-state.

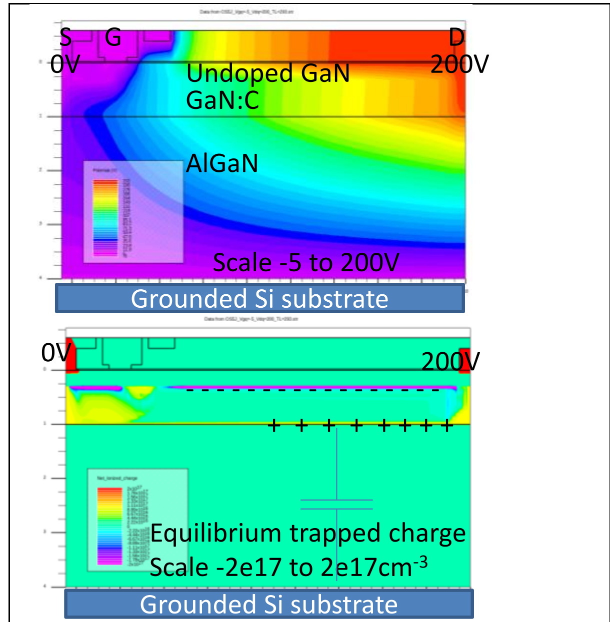

Fig. 2. Device cross-sections in the off- state (V_{GS}=–5V, V_{DS}=200V). The layer structure is 0.3um UID GaN, 0.7um GaN:C, 3um AlGaN strain relief layer. (a) Potential distribution showing resistive voltage drop in the GaN:C. (b) Trapped charge showing ionized acceptors and compensating donors at top and bottom of GaN:C.

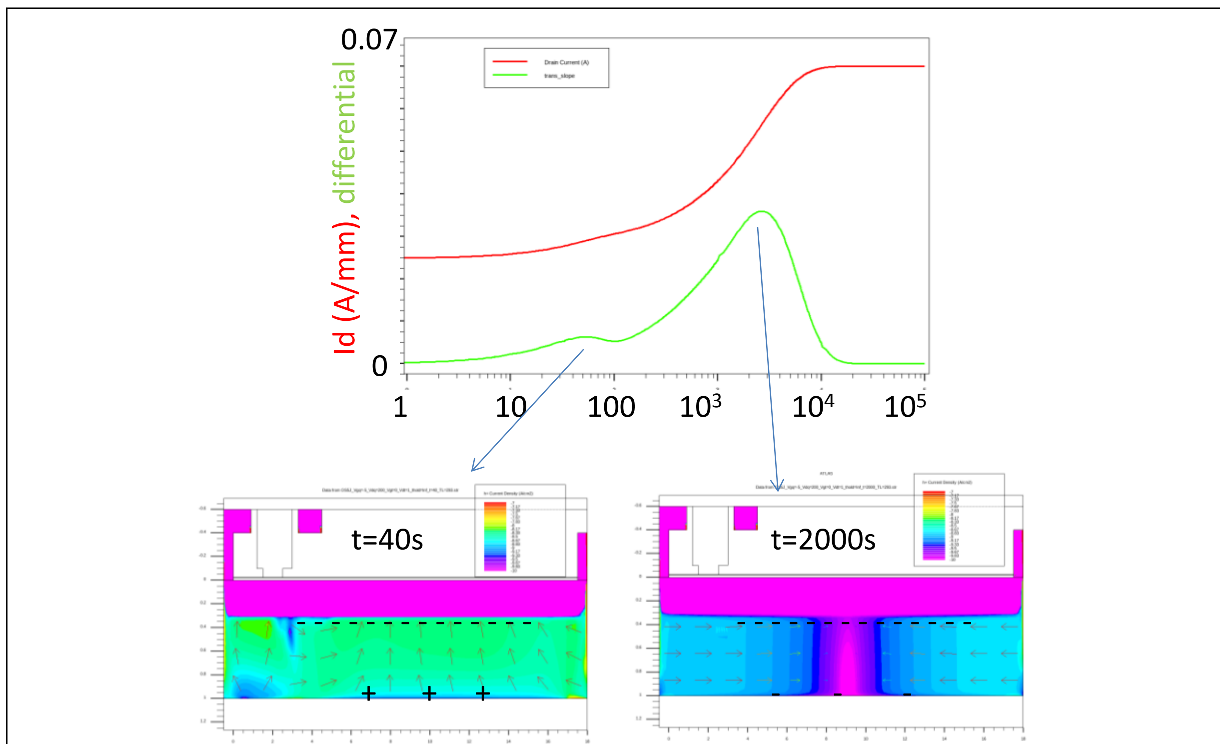

Fig. 3. Transient simulation, drain current and dI_D/dlog(t) as a function of log time after switching from off-state at V_{DS}=200V, V_{GS}=-5V to on-state. Two characteristic recovery time constants seen. Lower plots show hole current density (current density scale is up to 10^{-7}A/cm^2) and demonstrate that the two peaks correspond to charge redistribution initially vertically to cancel out the dipole seen in Fig. 2b, and then laterally as holes flow from leakage paths under the contacts to neutralize the remaining ionized carbon acceptors. Only one active trap level is required for the explanation.

Reduced Hysteresis in E-mode AlGaN/GaN Metal-Semiconductor-Insulator (MIS)HEMT after in-situ N_2 plasma pre-treatment

Zaffar H. Zaidi[1], Kean B. Lee[1], J.W. Roberts[2], Sheng Jiang [1], Ivor Guiney[3], Hongtu Qian[1], David J. Wallis[3], Colin J. Humphreys[3], P.R. Chalker[2] and Peter A. Houston[1]

[1]*Department of Electronic and Electrical Engineering, The University of Sheffield, Mappin Street, S1 3JD Sheffield, United Kingdom*

[2]*Centre for Materials and Structures, University of Liverpool, The Quadrangle, Brownlow Hill, Liverpool L63GH, United Kingdom*

[3]*Department of Materials Science and Metallurgy, The University of Cambridge, 27 Charles Babbage Road, CB3 0FS Cambridge, United Kingdom*

Due to their favorable characteristics, GaN based transistors are excellent candidates for power electronics and RF applications. Enhancement mode transistors are more desirable for power switching applications due to their fail safe operation and simpler circuit configuration. Inserting a dielectric layer between the gate and the III-nitride semiconductor is useful in suppressing the gate leakage current, allowing a larger gate voltage swing and enabling a more positive E-mode threshold voltage. However, the gate dielectric can add additional interface (dielectric/III-nitride) trap states and give rise to threshold voltage hysteresis [1] in double sweep gate transfer characteristics where electrons get trapped in the interface/bulk dielectric states under high forward gate bias conditions. Here, we present studies on the effects of the interfacial traps and their mitigation.

In this work, all devices were implanted with fluorine ions together with 20nm of atomic layer deposition (ALD) Al_2O_3 to achieve enhancement mode operation with V_{TH} > +2V. Before the dielectric deposition, we performed different surface pre-treatments to assess their effects on the interface states and threshold voltage hysteresis. These included 150W N_2 plasma (5min in-situ), 50W Ar plasma (5min in-situ) and 1min KOH plus 1min HCl wet treatment. After the Al_2O_3 deposition, all samples went through a forming gas anneal (FGA) at 430^0C for 30 minutes. In addition, post gate metal (PMA) annealing at 500 ^{0}C for 5 minutes was used to reduce plasma damage due to the fluorine implant. We found that this second anneal reduced the hysteresis in V_{TH}. The lowest hysteresis was obtained with N_2 plasma pre-treatment. This was previously reported to improve interface quality by forming a thin nitridation interlayer between Al_2O_3 and III-N interface [2]. Figure 1 shows double sweep gate transfer characteristics with N_2 plasma pre-treatment (solid line) and reference sample (dotted) with no pre-treatment. The hysteresis is significantly reduced from ~2.5V to 0.6V after N_2 plasma pre-treatment. Also, a considerable increase in the drain current and transconductance (g_m) is obtained, suggesting improvement in the barrier crystal quality as well as mitigation of the interface traps.

We characterized the trapping and de-trapping times [3] for interface/bulk oxide traps for N_2 plasma and reference sample as shown in figure 2 and 3. A large shift in the threshold voltage is observed within the smallest gate forward bias time of 20msec (V_{GS}=+10V, V_{DS}=+10V) after which the threshold voltage increases only gradually with further positive gate bias. The device is fully recovered or de-trapped with negative gate bias (V_{GS}=-10V, V_{DS}=+10V) applied for 20 minutes before each positive gate bias step to avoid charge accumulation. The initial rapid change in the threshold voltage for both samples could be due to the charge trapping in the interface states and the observed further slower drift could be due to a slower trapping process such as trapping in the bulk oxide layer. The reduced initial drift in threshold voltage after N_2 plasma (~0.5V) compared to the reference sample (~2V) suggests that the N_2 plasma pre-treatment has reduced the interface trap density significantly. The de-trapping process is, as expected, much longer than the trapping process. With a negative gate bias (V_{GS}=-10V, V_{DS}=+10V) it took nearly 20 minutes to fully recover the threshold voltage

(figure 3).

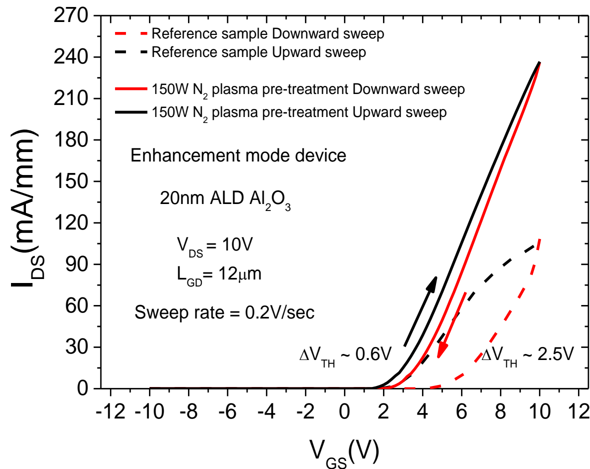

Figure 1 Double sweep gate transfer characteristics with reference and N_2 plasma pre-treatment.

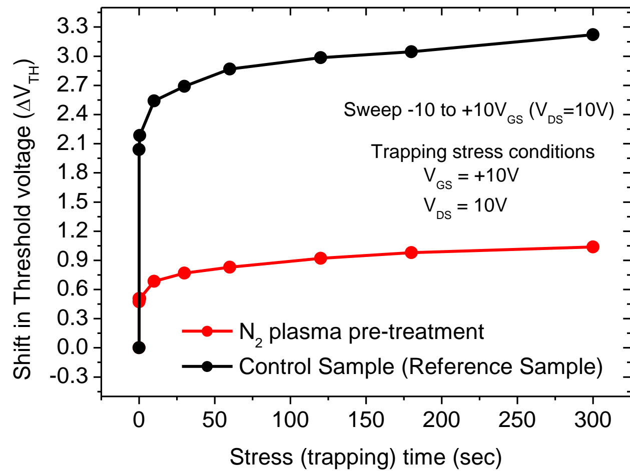

Figure 2 Shift in threshold voltage with positive (V_{GS}=10V) gate bias stress (trapping) time.

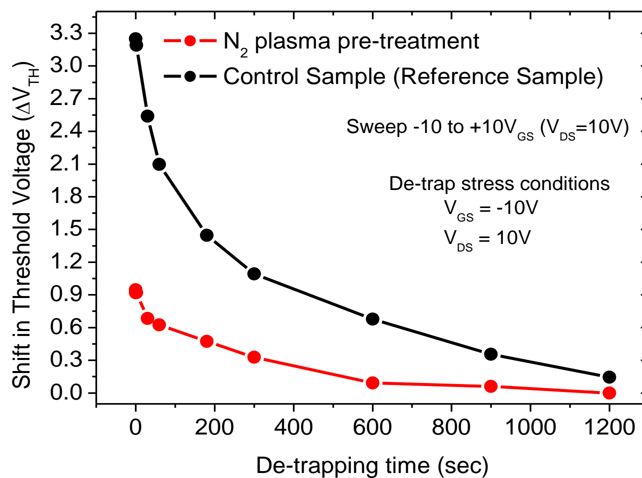

Figure 3 Shift in threshold voltage with negative (V_{GS}=-10V) gate bias stress (de-trapping) time.

References

[1] "Threshold Voltage Instability in Al_2O_3/GaN/AlGaN/GaN Metal–Insulator–Semiconductor High Electron Mobility Transistors," Sen Huang, Shu Yang, John Roberts, and Kevin J. Chen, Japanese Journal of Applied Physics, October, 2011.
[2] "High-Quality Interface in Al_2O_3/GaN/AlGaN/GaN MIS Structures With *In Situ* Pre-Gate Plasma Nitridation," Shu Yang, Zhikai Tang, King-Yuen Wong, Yu-Syuan Lin, Cheng Liu, Yunyou Lu, Sen Huang, and Kevin J. Chen, IEEE electron device letters, vol 34, no. 12, December, 2013.
[3] "Comprehensive study of the complex dynamics of forward bias-induced threshold voltage drifts in GaN based MIS-HEMTs by stress/recovery experiments," Peter Lagger, Maria Reiner, Dionyz Pogany and Clemens Ostermaier, IEEE transaction on electron devices, vol. 61, no. 4, April 2014.

All GaN Integrated Cascode Heterojunction Field Effect Transistors

S. Jiang[1], K. B. Lee[1], I. Guiney[2], P. F. Miaja[3], Z. H. Zaidi[1], H. Qian[1], D. J. Wallis[2], A. J. Forsyth[3], C. J. Humphreys[2] and P. A. Houston[1]

[1]Department of Electronic and Electrical Engineering, University of Sheffield, Mappin Street, S1 3JD Sheffield, United Kingdom

[2]Department of Materials Science and Metallurgy, University of Cambridge, 27 Charles Babbage Road, CB3 0FS Cambridge, United Kingdom

[3]School of Electrical and Electronic Engineering, University of Manchester, M13 9PL, Manchester, United Kingdom

Cascode configurations of GaN HFETs plus Si MOSFETs have recently attracted much attention and are now commercially available [1-3]. The layout consists of a series connection of a high voltage depletion-mode (D-mode) GaN device and a low voltage enhancement-mode (E-mode) Si device as shown in Fig. 1. The cascode configuration offers an advantage in switching speed and switching losses because it utilises the load current, rather than the current from the gate drive circuit, to charge and discharge the gate-drain capacitance. However, the use of a Si device as the E-mode element can reduce this speed advantage due to the limitations of the Si devices compared to GaN based devices [1]. In addition, the hybrid nature of this configuration brings challenges in packaging the devices in order to minimise the parasitic inductance within the cascode structure [4]. An all-GaN based integrated cascode structure can eliminate these issues, but only a few studies have been reported and these have been limited to DC and RF performance [5]. In this study, we present an all GaN integrated cascode configuration and explore its static and dynamic performance for power switching applications.

Fig. 2 depicts the integrated AlGaN/GaN metal-insulator-semiconductor (MIS) HFET in the cascode configuration on a Si substrate with gate width of 100 μm and 8 mm. The E-mode element is fabricated with a fluorine-based plasma treatment [6] together with a 20 nm SiN_x gate dielectric. The cascode device exhibits a threshold voltage, V_{TH}, of ~+2 V and a drain current of 200 mA/mm at V_{DS} = 10 V and V_{GS} = 8 V as shown in Fig. 3. The slightly reduced drain current compared to the equivalent standalone E-mode device can be optimised by engineering the threshold voltage of its D-mode element. With a more negative D-mode threshold voltage, the E-mode element is biased at a higher drain-source voltage during on-state, which effectively improves the current drivability of the E-mode part and hence the whole cascode configuration. Fig. 4 shows the improved drain current of the cascode after shifting the threshold voltage of its D-mode part from -5.5 V to -8.5 V by replacing the D-mode Schottky gate with a MIS gate structure. This highlights the importance of current-matching between the E-mode and D-mode parts in order to maximise the current drivability of the cascode configuration.

Inductive load switching measurements were performed using a double pulse tester on PCB mounted devices. Fig. 5 shows the switching comparison between a 8 mm gate width cascode and standalone E-mode devices at a drain bias of 25 V and load current around 1 A. The results are comparable between two devices due to the relatively small output charge at 25 V, while the major advantage of the cascode structure should become evident when the total output charge dominates over the input charge. The 600 V simulation results based on real device parameters clearly indicate the potential speed advantage of high voltage cascode over standalone E-mode device, as shown in Table 1. For practical high frequency power devices at high voltage and current, the integrated cascode structure will always perform faster switching (lower switching losses) compared to the equivalent high voltage E-mode device. The price to pay for this advantage is a higher specific on-resistance, which may not be an issue under high frequency operation.

REFERENCES:

[1] T. Hirose *et al,* Applied Power Electronics Conference and Exposition (APEC), 29th Annual IEEE, pp 174-181, 2014.
[2] M. J. Scott *et al*, Semiconductor Science and Technology **28**, Vol. 7, pp 074013, 2013.
[3] R. A. Alberto *et al*, Power Electronics, IEEE Transactions on **29**, Vol. 5, pp 2428-2440, 2014.
[4] Z. Liu *et al*, Applied Power Electronics Conference and Exposition (APEC), 29th Annual IEEE, pp 168-173, 2014.
[5] R. Wang *et al*, Japanese Journal of Applied Physics **47**, Vol. 4, pp 2820, 2008.
[6] Y. Cai *et al*, IEEE Transactions on Electron Devices **53**, Vol. 9, pp 2207-2215, 2006.

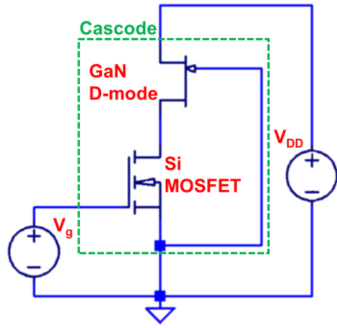

Fig. 1. Circuit diagram of cascode configuration.

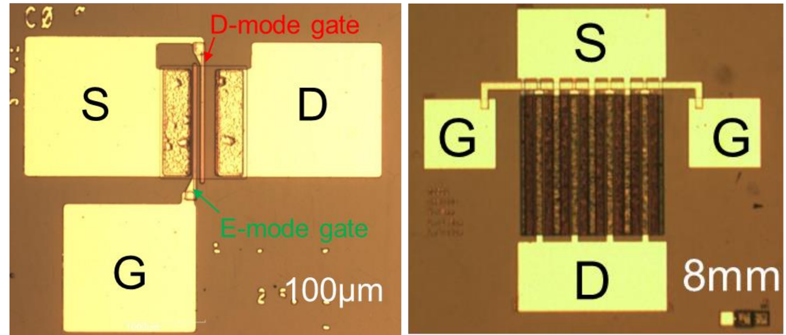

Fig. 2. All GaN integrated cascode device with gate width of (a) 100 μm and (b) 8 mm.

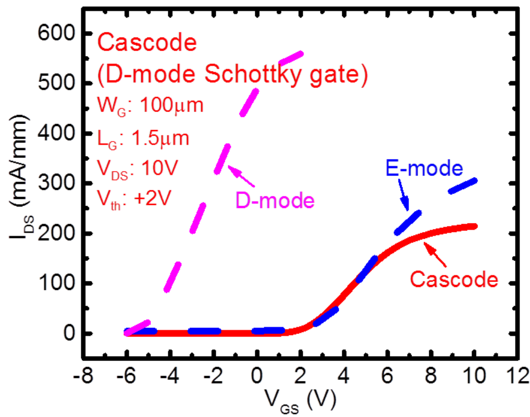

Fig. 3. Gate transfer characteristics of an all-GaN integrated cascode device together with an equivalent standalone E-mode device and standalone D-mode device.

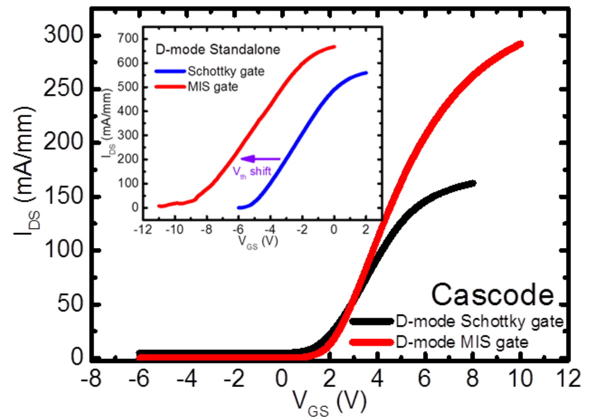

Fig. 4. Gate transfer characteristics of cascode device with a D-mode Schottky gate and a D-mode MIS gate. A higher output current is measured from the cascode device with D-mode MIS gate.

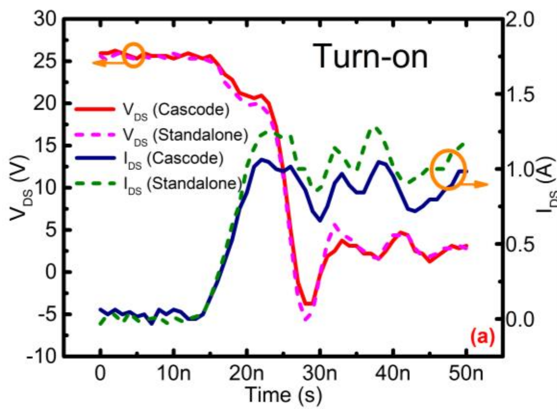

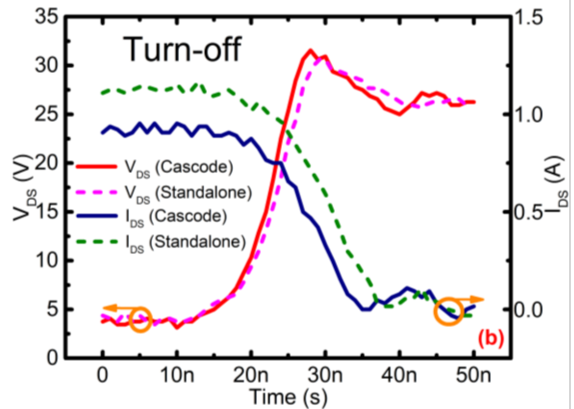

Fig. 5. (a) Turn-on and (b) turn-off 25V switching waveforms for 8mm cascode configuration and 8mm standalone E-mode device.

Table 1. 600 V simulation results show a much reduced switching energy loss for the cascode configuration.

	Turn-on energy loss (E_{on})	Turn-off energy loss (E_{off})
Cascode configuration	5.7μJ	2.3μJ
Standalone E-mode	14μJ	8.7μJ

Recent Advances in High Voltage GaN Power Devices and ICs

T. Paul Chow
Rensselaer Polytechnic Institute
Troy, NY 12180, U.S.A.

GaN photonic devices have revolutionized solid-sate lighting and high-frequency amplifying transistors have substantially impacted communication systems. Now, its power switching devices are impacting power electronics systems with their commercial availability and performance improvement, and hence less power loss and more energy efficient, over conventional silicon and emerging SiC devices. In this talk, we will review the performance potentials and present capabilities, as well as types and structures of GaN power devices and ICs. We will focus on assessing the present commercialization trend in each particular power range (low, medium or high). Also, we will point out the challenges these emerging semiconductor devices are still facing and need to overcome before they can substantially augment existing silicon devices.

Several vertical and lateral, discrete or integrable device structures have been demonstrated for GaN. In the low power (<500W) and blocking voltage (<600V) area, lateral GaN power HEMTs [1] are offering both high power density and lower power loss over both silicon and SiC devices. Besides power ICs, unique monolithic optoelectronic integration is possible, as indicated by recent demonstration of an integrated LED/MOS Channel-HEMT pair [2]. In the medium power (1-100kW) and blocking voltage (1-5kV), vertical GaN power MOSFETs [3] are capable of competing with SiC counterparts and displacing Si IGBTs by increasing the upper limit of switching frequencies and improving the energy efficiency and power density in motor drives and power converters. In the high power (>1MW) and ultra high blocking voltage (> 5kV) range, vertical superjunction (SJ) GaN power FETs [4] can compete with SJ SiC power MOSFETs as well as SiC IGBTs, making possible single-level converter topologies previously not possible in silicon implementations.

The expectations and potentials of these GaN power devices and ICs have not yet gained widespread market acceptance due to concerns on long-term reliability and cost-effectiveness. Nevertheless, we expect these power device technologies will become an important integral part of advanced energy efficient power electronics systems, with a wide range of power levels.

Acknowledgement This work was supported primarily by the ERC Program of the National Science Foundation under Award Number EEC-0812056 and in part by New York State under NYSTAR Contract No. C090145.

1. http://www.semicon.panasonic.co.jp/en/news/contents/2013/apec/panel/APEC2013_GaN_FPD_WEB.pdf.
2. Z. Li, et al., *Appl. Phys. Lett.*, vol. 102, no. 19, pp. 192107-1-3, 2013.
3. S. Chowdhury and T.P. Chow, *International Workshop on Nitride Semiconductors* (IWN 2014), Wroclaw, Poland, 2014.
4. Z. Li and T.P. Chow, *IEEE Trans. Electron Devices*, vol. 60, pp.3230-3237, 2013.

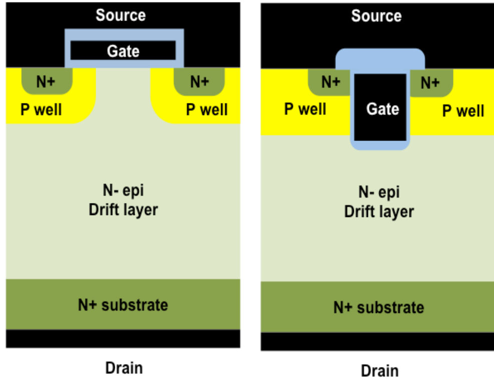

Fig. 1 Vertical DMOS and UMOS FETs.

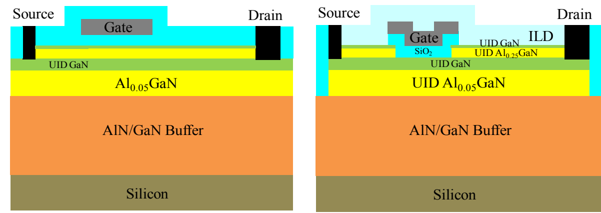

Fig. 2 Lateral GaN HEMT/HFETs

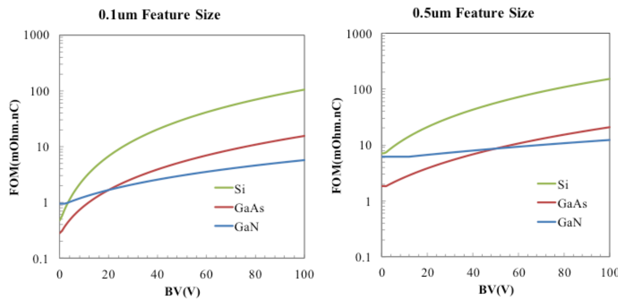

Fig. 3 GaN vs. Si, GaAs power devices

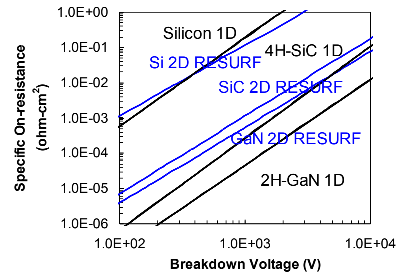

Fig. 4 $R_{on,sp}$ vs. BV for vertical and lateral devices

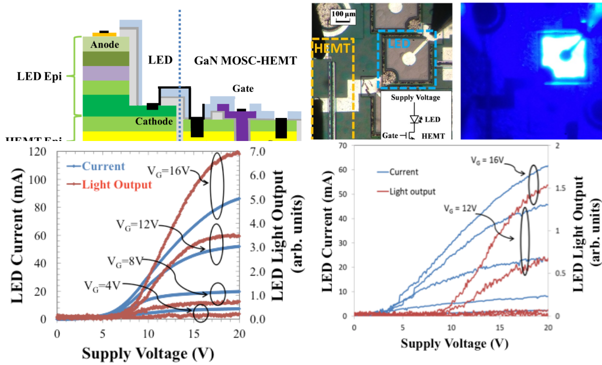

Fig. 5 Integrated GaN LED/HEMT pair.

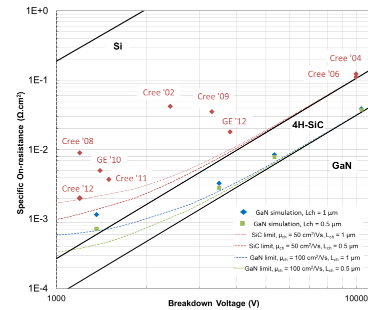

Fig. 6 Performance comparison of high voltage GaN vs. SiC vertical power MOSFETs

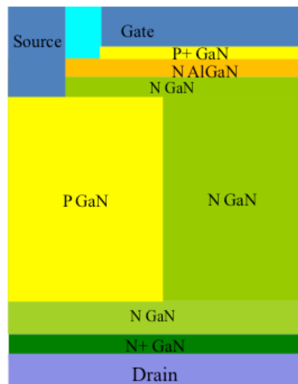

Fig. 7 Vertical Superjunction (SJ) GaN power HEMT

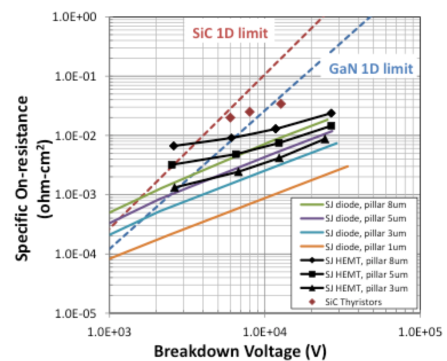

Fig. 8 $R_{on,sp}$ vs. BV for vertical SJ GaN HEMTs and diodes

Collection of Abstracts for UKNC Winter Conference, Jan 2016.

Posters

GaN deposition on Rare Earth Oxide on Silicon

B. Ding, L.Y. Lee, I. Guiney, R.A. Oliver
Department of Materials Science, University of Cambridge, 27 Charles Babbage Road, Cambridge, CB2 3QZ.

Silicon substrates have many potential advantages over sapphire for GaN semiconductor devices. Although the cost of mass production of LEDs on sapphire has been dramatically reduced in recent years, the high price of sapphire wafers is still a limiting factor. Si wafers with low price and high integration capability could provide a potential solution. For GaN high-electron mobility transistors (HEMTs), silicon also has an acceptable thermal conductivity (149 W/mK) whereas the thermal conductivity of sapphire (41 W/mk) severely deteriorates the performance of the device. The potential advantage of Si substrate use, however, is hindered by two main problems: the large thermal expansion mismatch and the large lattice mismatch with GaN. During growth and processing these problems can lead to cracks and high dislocation densities in the GaN thin film.

To mitigate the problems several methods have been developed such as patterned substrates, compliant substrates, AlN interlayers, AlGaN intermediate layers, AlN/GaN superlattices and in-situ SiN_x masking layers [1].

Alternatively, the use of Rare Earth Oxides (REO) such as Er_2O_3, Sc_2O_3 and Gd_2O_3 on Si as substrates for GaN growth have the potential to simplify GaN growth on Si and reduce the density of crystal defects. Er_2O_3 forms a coincidence lattice with Si ($a_{Er2O3} \approx 2a_{Si}$) and hence could form high quality crystal film on Si(111) surface. Er_2O_3 and Sc_2O_3 both have a smaller lattice mismatch with GaN (14.5% Er_2O_3 and 7-9% for Sc_2O_3) compared to Si (17%). In principle, high quality GaN thin film with low dislocation density could be deposited on top of REO buffer layers.

In this research project, buffer layers involving Er_2O_3, Sc_2O_3 and Gd_2O_3 are explored. To prevent the reduction of the oxides in MOCVD chamber with H_2. GaN will be deposited in low temperatures with N_2 ambient, where a Rare Earth Nitride (REN) thin layer could be formed between REO and GaN. As stress relaxation and crystal quality of GaN thin film layer is strongly dependent on the morphology and uniformity of the buffer layer, as a first step AFM was used to examine the surfaces of Er_2O_3, Sc_2O_3 and Gd_2O_3 films grown on silicon before the deposition of GaN.

All the films have a very low RMS surface roughness of less than 1.5 nm for layer thicknesses in the range from 100 to 500 nm. The surface roughness was found to increase as the layer thickness increases. Using an increased oxygen pressure during the deposition also increases the surface roughness. The Er_2O_3 films show a morphology consisting of highly aligned triangular islands. The lateral widths of these islands were measured using a fast Fourier transform (FFT) analysis. It was found that lateral width increases with layer thickness but decreases as oxygen pressure increases. The islands formed on the surfaces have lateral width varying from 40 to 120 nm. Sc_2O_3 and Gd_2O_3 show less strongly oriented surface morphologies.

References

[1] Zhu et al. Rep. Prog. Phys. 76 (2013) 106501

Structural and morphological characterisation of gallium nitride grown on SiC on Si substrates

L.Y. Lee, M. Frentrup, S.-L. Sahonta, M. J. Kappers, L. J. Shaw*, P. J. Ward*, C.J. Humphreys, R.A. Oliver and D. J. Wallis

Department of Materials Science and Metallurgy, 27 Charles Babbage Rd, Cambridge, CB3 0FS

*Anvil Semiconductors Ltd, Windmill Industrial Estate, Birmingham Road, Allesley, Coventry, CV5 9QE

Corresponding author e-mail: lyl24@cam.ac.uk

GaN materials are important for a wide range of applications such as LEDs and laser diodes. Since high quality bulk GaN substrates are difficult and expensive to produce, GaN is grown heteroepitaxially. [1] The most common phase grown on conventional sapphire and silicon carbide substrates is hexagonal wurtzite GaN. Hexagonal GaN is the most thermodynamically stable phase, however it is polar along the usual <0001> growth direction. In common light emitting devices in the hexagonal phase, piezoelectric and spontaneous polarisation fields across the device structure lead to impairment of device efficiency, associated with the quantum-confined Stark effect. [2] One way to eliminate the problem of polarisation and potentially improve device performance is to grow cubic zincblende GaN, which although metastable, is non-polar along the <001> growth direction. [3] Growth of good quality cubic GaN is very challenging, as the hexagonal phase is thermodynamically preferred under most growth conditions, so the growth window for the cubic phase is quite narrow.

In our poster presentation we will report our characterisation studies on a series of cubic GaN layers grown at different temperatures. The GaN epilayers were grown by MOVPE on 3C-SiC on Si substrates from Anvil. Structural and morphologic investigations were done by X-ray diffraction (XRD) and atomic force microscopy (AFM). XRD results reveal that the epilayers become predominantly cubic with negligible amounts of hexagonal by reducing the growth temperature. On the other hand, the ω-FWHM of the symmetric (004) reflection increases with lower growth temperature indicating an increase of the mosaicity and a decrease in crystal quality. AFM measurements were performed to investigate the influence of the growth temperature on the surface morphology, such as the shape of surface features, the height of surface steps and overall surface roughness. The measurements show that RMS roughness of the surface varies with growth temperature partly due to the changing anisotropy of the surface features from elongated to a more square shape. We will discuss these effects in terms of anisotropic surface diffusion of adatoms, and the influence of crystal defects and surface steps.

References

[1] P. Gibart, “Metal organic vapour phase epitaxy of GaN and lateral overgrowth,” *Reports Prog. Phys.*, vol. 67, no. 5, pp. 667–715, 2004.

[2] J. Seo Im, H. Kollmer, J. Off, A. Sohmer, F. Scholz, and A. Hangleiter, “Reduction of oscillator strength due to piezoelectric fields in G a N / A l x Ga 1 − x N quantum wells,” *Phys. Rev. B*, vol. 57, no. 16, pp. R9435–R9438, 1998.

[3] O. Ambacher, J. Majewski, C. R. Miskys, A. Link, M. Hermann, M. Eickhoff, M. Stutzmann, F. Bernardini, V. Fiorentini, V. Tilak, B. Schaff, and L. F. Eastman, “Pyroelectric properties of Al (In) GaN / GaN hetero- and,” *J. Phys. Condens. Matter*, vol. 14, pp. 3399–3434, 2002.

Spectroscopic studies of cubic GaN grown on Si/SiC by metal organic chemical vapour-phase deposition

S. Church[1], M. Davies[1], P. Mitchell[1], D. Binks[1], P. Dawson[1], C.J. Humphreys[2], R.A. Oliver[2], M.J. Kappers[2], P.J. Ward[3], L.J. Shaw[3] and D.J. Wallis[2].

1 - Photon Science Institute & School of Physics and Astronomy, University of Manchester.
2 - Department of Materials Science & Metallurgy, University of Cambridge.
3 - Anvil Semiconductors Ltd, Future Business Centre, King's Hedges Road, Cambridge.

GaN grown in its cubic crystal phase (c-GaN) differs from the hexagonal GaN (h-GaN) currently used in commercial LEDs in a number of ways that promise to improve device performance. Firstly InGaN/GaN quantum wells (QWs) grown on c-GaN will not be susceptible to the strong spontaneous and piezoelectric electric fields across the wells that affects such structures grown along the c-axis of h-GaN [1]. These fields reduce the carrier wave-function overlap in an InGaN QW, decreasing the rate of radiative recombination. The radiative lifetime in a QW is thus expected to be significantly shorter for c-GaN compared to h-GaN, resulting in greater recombination efficiency. Secondly, the bandgap of c-GaN is ~0.2 eV less than that of h-GaN [2], reducing the indium content in a QW required for green emission and thus also decreasing defect-producing strain.

c-GaN is a metastable phase, which makes crystal growth challenging. A number of growth methods have been investigated previously including molecular beam epitaxy (MBE) on substrates with a cubic crystal structure, such as SiC [1], SiC/Si [3] and GaAs [4], and metal organic chemical vapour-phase deposition (MOCVD) on GaAs [5]. More recent developments include the MBE growth of free-standing cubic GaN [6] and the use of microstructured Si substrates [7-8].

In this work, we report a spectroscopic investigation of c-GaN layers grown on to high quality 3C-SiC on large area (100mm) Si (001) using MOCVD. Samples of c-GaN are characterised by both temperature-dependent photoluminescence spectroscopy (PL) and photoluminescence excitation spectroscopy (PLE). The low temperature PL spectra exhibit peaks that are attributed to bound exciton emission and donor-acceptor pair (DAP) recombination, along with a broad defect emission band at lower energies. PLE measurements confirm that these features are due to recombination in c-GaN. Increasing the layer thickness was found to reduce the width of the DAP peak and increase the relative intensity of the bound exciton emission. A weak high energy shoulder is also present in the PL spectra. PLE measurements reveal that this feature may be due to emission from small h-GaN inclusions.

References

[1] Li, S. Schomann, J. As, D. J. and Lischka, K. Appl. Phys. Lett. 90 (2007) 071903.
[2] Vurgaftman, I. Meyer, J. J. Appl. Phys. 94 (2003) 3675-3696.
[3] Feuillet, F. et al. Mater. Sci. Eng. B. 50 (1997) 233.
[4] Fernadez, J. R. L. et al. J. Nitride Semicond. Res. 595 (2000) W3-40.
[5] Wu, J. et al. Appl. Phys. Lett. 71 (1997) 2067.
[6] Novikov S, Foxon CT and Kent AJ, Phys. Stat. Solid C, 8 (2011) 1439.
[7] Stark, C. J. M. et al. Appl. Phys. Lett. 103 (2013) 232107.
[8] Bayram, C. et al. Adv. Funct. Mater. 24 (2014) 4492.

Microstructure of Cubic InGaN Epilayers and Multiple Quantum Well Structures Grown on 3C-SiC (001) Substrates

Suman-Lata Sahonta, Menno Kappers, Martin Frentrup, Rachel Oliver, Jill Shaw*, Peter Ward*, Colin Humphreys and David J Wallis

Department of Materials Science and Metallurgy, University of Cambridge, 27 Charles Babbage Road, Cambridge CB3 0FS

**Anvil Semiconductors Ltd, Windmill Industrial Estate, Birmingham Road, Allesley, Coventry, CV5 9QE*

Abstract

Green-emitting wurtzite InGaN-based LEDs are less efficient than blue-emitting LEDs at a given drive current (known as the *green gap*), possibly due both to the higher point defect densities resulting from the lower growth temperatures required to incorporate higher indium contents into green-emitting devices, and to the higher strain-induced internal electric field within green-emitting QWs[1]. Cubic InGaN-based LEDs may offer a route to efficient green emission, since cubic nitride films are non-polar and therefore the formation of heterostructures does not result in internal electric fields, and therefore a higher carrier wavefunction overlap integral can be achieved in the quantum well. Cubic GaN also has a narrower band gap than wurtzite GaN for a given indium content, facilitating green emission that requires less indium in the active region, and some reports indicate that it is possible to achieve higher *p*-type conductivity than for wurtzite GaN [2]. Additionally, cubic GaN films grown on cubic SiC on silicon (001) substrates may offer a route to integration with silicon (001) electronics.

In this work we investigate the morphology and uniformity of MOVPE-grown cubic InGaN epilayers and multiple quantum well (MQW) structures grown on thick cubic GaN layers deposited on a thick 3C-SiC (001) epilayer grown separately on 4-inch silicon (001) wafers by Anvil Semiconductors Ltd. Electron diffraction patterns show that all films are cubic with no indication of hexagonal inclusions. However a high density of {111}-oriented intrinsic stacking faults is observed at the GaN/SiC interface, which reduces in density as film growth continues, resulting in a stacking fault density of around 10^4 cm^{-1} at the InGaN/GaN interface for both epilayer and MQW structures. Diffraction contrast studies show that there is no relaxation of MQW structures *via* the formation of extended defects. Energy-dispersive X-ray (EDX) analysis in the TEM reveals MQW structures with uniform In composition when viewed with the electron beam along the direction of the SiC substrate miscut. However, MQWs appear rough when viewed perpendicular to the substrate miscut direction, in regions where elastic relaxation may have occurred during growth of the InGaN. Stacking faults do not appear to be related to the variations in In content within the MQW structures.

[1] S. Hammersley, M. J. Kappers, F. C.-P. Massabuau, S.-L. Sahonta, P. Dawson, R. A. Oliver and C. J. Humphreys, Appl. Phys. Lett., 107, 132106 (2015)

[2] DJ As et al., Phys. Rev. A 54 (16), R11118-R11121 (1996)

Structural Studies of Large-Area Thick AlGaN(0001) Films grown on GaAs (111)B Substrates

S-L Sahonta[1], RA Oliver[1], CJ Humphreys[1], CT Foxon[2] and SV Novikov[2]

[1] *Department of Materials Science and Metallurgy, University of Cambridge, 27 Charles Babbage Road, Cambridge, CB3 0FS*

[2] *School of Physics and Astronomy, University of Nottingham, University Park, Nottingham, NG7 2RD*

Commercial AlN- and AlGaN-based ultraviolet optoelectronic devices are typically grown on sapphire substrates, limiting internal quantum efficiencies to around 1 % due to high densities of extended defects. Although bulk GaN and AlN substrates are an improvement over sapphire for the growth of AlGaN- and AlN-based devices, significant lattice mismatch still arises in Al(Ga)N/(Al)GaN heterostuctures, generating defects which limit device efficiency. Ideally, bulk AlGaN substrates grown with an aluminium content tailored to that required for a given UV emission wavelength could dramatically improve device efficiency.

A newly-developed fast molecular beam epitaxy (MBE) growth procedure for nitride growth on 2-inch and 3-inch GaAs (111)B wafers has been recently shown to produce large-area free-standing bulk wurtzite GaN layers [1], where GaAs substrates may be quickly and reliably removed by wet etching, leaving the free-standing GaN ready for further preparation for UV device growth.

In this work we build on the progress made for bulk GaN growth by investigating the microstructure of a series of $Al_{0.2}Ga_{0.8}N$ films, grown up to 100 μm thick on 2-inch and 3-inch GaAs (111)B substrates, to assess their suitability as high-quality bulk AlGaN substrates for subsequent MOVPE device growth. AlGaN films are grown on GaN nucleation layers with relatively high group III beam equivalent pressures to create group III-rich MBE growth conditions. Transmission electron microscopy (TEM) shows that all AlGaN films have high crystallinity with small cubic inclusions at the GaAs/GaN interface, which revert to the wurtzite phase after around 70 nm of growth. Threading dislocation densities range from 10^9 to 10^{10} cm^{-2}, and basal plane I_1 stacking fault densities of around 10^5 cm^{-2} are observed, with defect densities somewhat decreasing with increasing film thickness. The implications for further growth of devices is discussed.

[1] SV Novikov, CT Foxon, AJ Kent, Phys. Stat. Sol. C 8 (2011) 1439.

Raman Spectroscopy of cubic GaN grown on SiC/Si by metal organic chemical vapour-phase deposition

P.W. Mitchell[1*], D. Binks[1], P. Dawson[1], C.J. Humphreys[2], R.A. Oliver[2], M.J. Kappers[2], P.J. Ward[3], L.J. Shaw[3], D.J. Wallis[2]

1 - Photon Science Institute & School of Physics and Astronomy, University of Manchester
2 - Department of Materials Science & Metallurgy, University of Cambridge
3 - Anvil Semiconductors Ltd, Future Business Centre, King's Hedges Road, Cambridge
**- corresponding author*

Cubic GaN (c-GaN, zinc blende structure) may have some advantages over the hexagonal phase (h-GaN, wurzite structure) in improving the performance of LED devices. Being pyroelectric, h-GaN creates strong spontaneous and piezoelectric electric fields across quantum wells (QW) grown perpendicular to the c-axis [1], while c-GaN does not. Such fields reduce the wavefunction overlap between electrons and holes in the QW, increasing the radiative recombination time. QW grown in c-GaN therefore promise greater radiative recombination efficiency than for h-GaN because of the shorter radiative recombination time. Also the smaller bandgap in c-GaN (3.3eV at low T) than in h-GaN (3.5eV) [2] means that for the same wavelength emission, the QW needs less indium, which reduces the lattice mismatch and strain, which produces defects, which promote non-radiative recombination.

h-GaN is the stable phase at all temperatures, which makes the growth of meta-stable c-GaN difficult. Cubic substrates which have been used in MBE growth include SiC [1] and SiC/Si [3], and GaAs has been used with MOCVD [4]. MBE growth of free-standing c-GaN [5] has been developed recently, as has the use of microstructured Si substrates [6,7]. Here we report on Raman measurements used to characterise c-GaN layers grown on 3C-SiC/Si using MOCVD.

TEM and XRD show the main defects to be stacking faults along the cubic {111} planes (stacking faults, SF). Layers adjacent to the SF have hexagonal symmetry locally. Methods which can rapidly assess the c-GaN quality and the amount of h-GaN in samples are useful for the development and refinement of the growth parameters of c-GaN.

Raman spectra show the cubic LO phonon, and also a range of peaks associated with the E_2, E_1(TO), A_1(T0) peaks, and also A_1(TO+LO) and E_1(LO+TO) peaks of the hexagonal phase (see figure). These are consistent with the hexagonal character associated with SF. Use of the Raman intensities is complicated by the dearth of measured values of the Raman tensor components [8,9]. The use of laser wavelengths for which GaN is transparent lead to complications associated with forward scattering Raman and reflection at the substrate interface. Shorter wavelengths with absorption from the GaN band edge run into

complications from the resonant Raman process not obeying the selection rules. Nevertheless, relative intensity measurements have been used to estimate the hexagonal fraction, and the results are consistent with the TEM and XRD results.

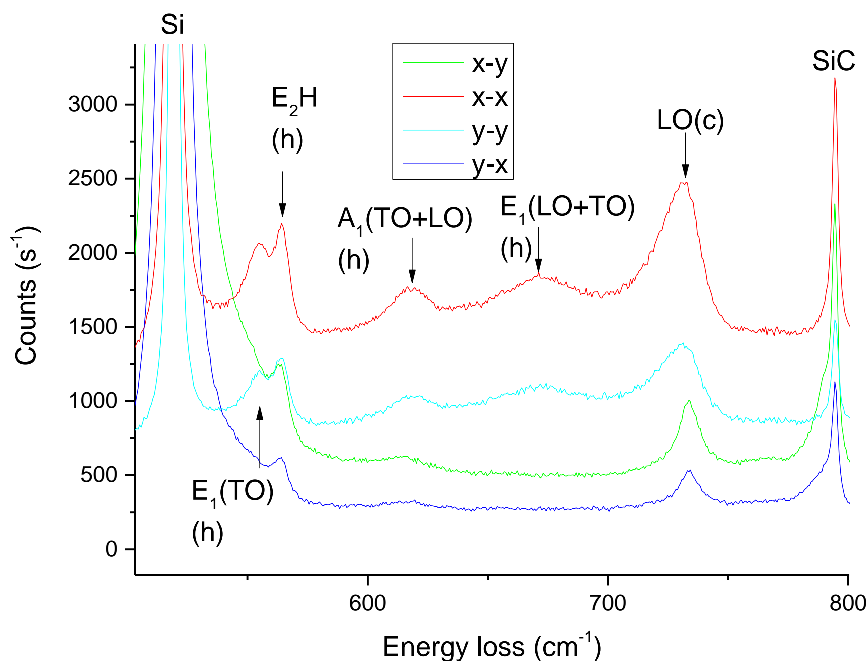

Figure: Polarisation-dependent Raman spectra of c-GaN (LO), showing peaks from hexagonal component (E_1(TO), E_2H, A_1(TO+LO), E_1(LO+TO), using 488nm light. Peaks from the substrate (Si and SiC) are seen as the GaN layer is transparent at this wavelength.

Raman spectroscopy is being used to characterize the relative hexagonal components between samples grown under different conditions, and this is a fast, non-destructive method which may be used to optimise the growth parameters.

References

[1] Li, S. Schomann, J. As, D. J. Lischka, K., Appl. Phys. Lett. **90**, 071903 (2007).
[2] Vurgaftman, I., Meyer, J., J. Appl. Phys. **94**, 3675 (2003).
[3] Feuillet, F. *et al.,* Mater. Sci. Eng. B. **50**, 233 (1997).
[4] Wu, J. *et al.,* Appl. Phys. Lett. **71**, 2067 (1997).
[5] Novikov, S *et al.,* J. Cryst. Growth. **310**, 3964 (2008).
[6] Stark, C. J. M. *et al.,* Appl. Phys. Lett. **103**, 232107 (2013).
[7] Bayram, C. *et al.*, Adv. Funct. Mater. **24**, 4492 (2014).
[8] Loa, I. *et al.*, J. Raman Spec. **29**, 291 (1998)
[9] Irmer, G. *et al.,* J. Appl. Phys. **116**, 245702 (2014)

3D characterisation of novel GaN structures using Raman spectroscopy

Tim Batten[1], Emmanuel Le Boulbar[2], Duncan Allsopp[2], Philip Shields[2]

[1] Renishaw plc, New Mills, Wotton-under-Edge, Gloucestershire

[2] Department of Electronic and Electrical Engineering, University of Bath, Bath

We illustrate the power of Raman mapping for characterising the microstructure and stress/strain in GaN Nano-dash epitaxial lateral overgrowth (ELOG) samples.

Raman spectroscopy provides sub-micrometre resolution information on the vibrational, crystalline, and electronic structures of materials. Raman is a tried and tested tool for analysing nitrides, but in the past, measurements have been slow, with a single spectrum typically taking up to a minute to acquire. Advances in technology have slashed this time to milliseconds, opening up large area mapping measurements in both 2D and 3D and industrial quality control applications. 3D mapping measurements offer significant benefits when studying semiconductor materials as they allow the microstructures in device layers to be imaged and, as a result, defects and their origins can be characterised more comprehensively.

Threading dislocations in GaN act as scattering centres for both light and charge carriers, and can hinder performance in optoelectronic devices, such as LEDs. There is continual research into the growth of epitaxial GaN layers to reduce the density of threading dislocations and improve device material. Here we apply Raman spectroscopy to samples grown with the ELOG technique using growth apertures that comprise a regular array of nano-dashes in order to control the coalescence process. 3D Raman measurements were conducted on the sample after growth and results compared to SEM images collected during growth. Raman intensity images clearly illustrate the microstructure of the sample, reveal regions of increased dislocation density, and show excellent agreement with the SEM images (Figure 1(a) – 1(f)). In addition, the strain in the GaN was imaged and characterised.

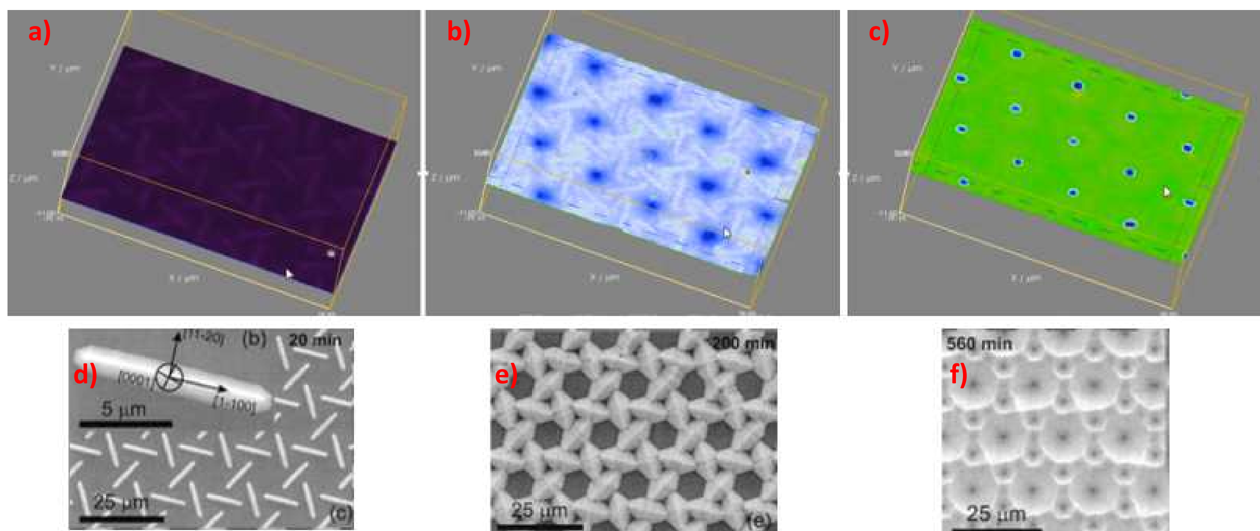

Figure 1 (a) - (c) Raman intensity image slices of the GaN Nano dash layer collected at different depths (extracted from a complete 3D image). (d) - (f) SEM images collected during growth of the Nano-dash layer.

Effect of Growth Temperature on the Internal Quantum Efficiency of InGaN/GaN Quantum Well Structures

Simon Hammersley[1], Menno J. Kappers[2], Fabien C.-P. Massabuau[2], Suman-Lata Sahonta[2]. Phil Dawson[1], Rachel A. Oliver[2], Colin J. Humphreys[2]

[1] School of Physics and Astronomy, Photon Science Institute, University of Manchester, M13 9PL.

[2]Department of Materials Science and Metallurgy, 27 Charles Babbage Road, University of Cambridge, CB3 0FS.

It has been widely reported that as the emission wavelength of InGaN/GaN quantum well (QW) structures is increased there is a corresponding reduction in the internal quantum efficiency (IQE) [1-4]. In order to achieve the higher indium fractions needed for green emission, the growth temperature of the QW layers is reduced in order to reduce the effects of In desorption. This reduction in growth temperature may lead to a significant increase in the density of point defects [5,6]. Point defects have been shown to act as non-radiative recombination centres [7]. In order to test the effect of the QW growth temperature, two series of multiple QW samples, one set emitting in the blue and one set emitting in the green spectral region, were produced in which the QW growth temperature was systematically varied. The indium fraction in each sample set was maintained by adjusting the indium precursor (trimethyl indium) flow rate. X-ray diffraction was used to show that within a sample set emitting at a particular wavelength, the basic structural parameters of the QWs remained unchanged across the different growth temperatures applied.

The optical properties of the both sets were investigated using photoluminescence (PL) measurements as a function of both temperature and excitation power density, and PL time decay measurements. It was found that for both the blue and green-emitting sample sets the measured 300 K IQE was found to vary systematically with the QW growth temperature, with lower temperatures resulting in lower 300 K IQE. The variation in IQE between samples was also found to become more pronounced as the excitation power density was reduced. The 300 K PL decay lifetime was also found to decrease as the QW growth temperature was reduced. Taking into account both the reduced 300K PL lifetime and the variation in the IQE observed in both sample sets we conclude that the reduction in QW growth temperature results in a reduction in the non-radiative recombination lifetime in InGaN QWs.

[1] Z.Lin et al., Japanese J. of Appl. Phys., 54, 0221102, 2015.
[2] K.P.O'Donnell et al., Physica Status Solidi Rapid Research Lett., 6, 49-52, 1996.
[3] S.F.Chichibu et al., Appl. Phys. Lett., 69, 4188, 1996.
[4] T.Takeuchi et al., Japanese J. of Appl. Phys., 36, L382, 1997.
[5] J.Janotti et al. Physica Status Solidi A, 209, 65-70, 2012.
[6] T. Obata, J. Cryst. Growth, 311, 2772, 2009.
[7] T.Langer et al., Proc. SPIE, 8625, 862522-1, 2013.

The effects of an electron blocking layer on recombination in multiple quantum well light emitting diodes

Simon Hammersley[1], Phil Dawson[1], Menno J. Kappers[2], Rachel A. Oliver[2], Colin J. Humphreys[2]

[1] School of Physics and Astronomy, Photon Science Institute, University of Manchester, M13 9PL.

[2]Department of Materials Science and Metallurgy, 27 Charles Babbage Road,
University of Cambridge, CB3 0FS.

Electron blocking layers (EBLs) which consist of a thin layer of *p*-type AlGaN are often included in light emitting diode (LED) designs, inserted between the top most quantum well (QW) in an LED and the *p*-type contact layer, to reduce the spill over of injected electrons. The inclusion of EBLs has been reported to improve the external quantum efficiency (EQE) of an LED, especially at high LED drive currents [1-3]. However despite these reports of a positive impact of the inclusion of an EBL, there are also some reports in which the inclusion of an EBL has led to reduction in EQE [4-6], which were attributed to the formation of an additional confining potential for electrons between the final QW and the EBL.

In this study we have investigated experimentally and theoretically the properties of two LED structures grown by MOCVD, one including an EBL, and one without an EBL. The conduction and valence band profiles of both devices were modelled using the commercial device simulation package nextnano^3 [7] under zero bias to reflect the experimental conditions used to investigate these samples. It was found that the inclusion of the EBL into the device stack leads to a modification of the electric field across each of the QWs in the active region. This results in an increase of the order of 10 % (from 225 to 197.5 mV nm^{-1}) in the electric field across each QW. The modification of the electric field across the QWs leads to a change in the electron/hole wavefunction overlap, which should reduce the radiative recombination lifetime.

The two LEDs were investigated using a combination of temperature dependent photoluminescence measurements and photoluminescence time decay measurements. From these measurements it was found that, as predicted by the modelling of the conduction and valence band profile, the radiative recombination lifetime was of the order 20% longer in the LED structure containing the EBL compared with the sample that did not include an EBL. This increase in radiative recombination lifetime results in a lower 300 K internal quantum efficiency for the sample including an EBL

[1] I.V. Rhozansky et al., Phys. Status Solidi A, 204, 227-230, 2007.
[2] A. Knauer et al., Proc.SPIE, 72310G, 2009.
[3] K.J. Vampola et al., Appl. Phys. Lett., 94 061116, 2009.
[4] J. Piprek et al., Phys. Status Solidi A, 207, 2217-2225, 2010.
[5] J.Y. Chang et al., Opt. Lett., 35, 1368-1370, 2010.
[6] S.-H. Han et al., Appl. Phys. Lett., 94, 231123, 2009.
[7] S. Birner, “nextnano GMBH”.

Identification of loss mechanisms in GaN based Light Emitting Diodes

K Cavanagh[1], C Liu[2], T Martin[3], S Sivaraya[1], M A Hopkins[1], D W E Allsopp[1]

[1]*Department of Electronic and Electrical Engineering, University of Bath, Bath, BA2 7AY, UK*
[2] *IQE-NanoGaN, Department of Electrical and Electronic Engineering, University of Bath, Bath, BA2 7AY*
[3]*IQE, Pascal Close, St Mellons, Cardiff, CF3 OLW*

Corresponding author: *K.Cavanagh@bath.ac.uk*

The efficiency of gallium nitride (GaN) based light emitting diodes (LEDs) has increased significantly in recent years. Unfortunately devices emitting outside of the standard "blue" region suffer from a rapid decrease in efficiency, which increases as wavelength moves away from this standard blue region. Issues arise from reduced crystal quality due to the increased indium or aluminium content required for green or ultraviolet (UV) emission respectively [1].

LEDs were fabricated from a number of different wafers, emitting over a range of wavelengths, all grown by MOCVD. Alongside these, commercially grown wafers were processed and used as controls. The wafers had similar multiple quantum well (MQW) structures, but growth methods varied. The effect of varying drive current on electroluminescence (EL) spectra will be presented. Observations of the EL spectra indicate a shift in peak wavelength in some samples, which is attributed to the quantum confined Stark effect (QCSE).

Temperature dependant forward and reverse current voltage measurements were performed and used to help identify the mechanisms responsible for the observed leakage current. These measurements also allow for the analysis of the series resistance, as well as the voltage and temperature dependence of the ideality factor, all of which will be discussed. Initial analysis provides evidence of Poole-Frenkel emission contributions to the reverse leakage [2][3]. Light output (L-I) measurements were also taken and analysis indicates a slow turn on, which can be correlated with the I-V characteristics. L-I-V measurements show impaired device performance when compared with control samples.

A method for identifying loss mechanisms in GaN based LEDs is to be presented. The mechanisms for leakage currents observed in temperature dependent *I-V* characteristics of the devices will be discussed. It is shown that epitaxial structures that cause a strong QCSE also exhibit increased leakage currents. Such structures result in an increase in the non-radiative recombination rate relative to the radiative recombination rate which results in degraded peak power conversion efficiency [3].

[1] Saito, S., Hashimoto, R., Hwang, J., & Nunoue, S. (2013). InGaN Light-Emitting Diodes on c -Face Sapphire Substrates in Green Gap Spectral Range. *Applied Physics Express*, *6*(11), 111004.

[3] K. Cavanagh, C. Liu, T. Martin, M.A. Hopkins, S. Sivaraya, D.W.E. Allsopp.(2014) Detailed optical and electrical characterisation of green – orange InGaN/GaN LEDs grown by

MOVPE. Proceeding of the 10th International Conference on Advanced Semiconductor Devices and Microsystems, 319-322

[2]Shan, Q. (2012). *Non-Ideal Properties of Gallium Nitride Based Light-Emitting Diodes*. Rensselaer Polytechnic Institute.

A study of defect-related effects in InGaN/GaN LEDs and their impact on efficiency

M.A. Hopkins[1], M.J. Kappers[2], E.J. Thrush[2], A. Philips[2], R.A. Oliver[2],
C.J. Humphreys[2], D.W.E. Allsopp[1]
[1] Dept. of Electronic and Electrical Engineering, University of Bath, UK
[2] Dept. of Materials Science and Metallurgy, University of Cambridge, UK

While it is generally thought that a high threading defect density (DD) is detrimental to the performance of LEDs, effecting especially the peak efficiency, there are few quantitative studies correlating the threading defect density to the external quantum efficiency (EQE) and the wall-plug efficiency (WPE) of light emitting diodes (LEDs). Here, we present a study of defect-related effects in the light emission and current-voltage characteristics of LEDs, notably the effect of changing the density of the threading defects in the growth substrate on the electrical properties and efficiency of InGaN/GaN LEDs.

LEDs structures were grown by MOVPE on sapphire substrates with different densities of threading dislocations in the first-grown GaN buffer layer. Measurements of the EQE as a function of current (figure 1) indicate that for samples with a low to moderate defect density (in the range 10^8 cm^{-2}) the threading defect density has a moderate effect on peak EQE, and a diminishing influence on the EQE as the current is increased. In contrast, increasing the threading DD into the 10^9 cm^{-2} range significantly decreases the EQE over the entire current range measured. It also affects the current-voltage characteristics to have a second influence on the WPE.

However, care must be taken in the interpretation of EQE vs current density graphs. The EQE of any given LED is determined by the interplay of many different mechanisms and to gain an insight from these measurements it is therefore necessary to fit these results to an appropriate analytic model. These results are analysed using the simple but popular 'ABC' recombination model, modified to take account of 'overflow' currents (see ref 1. for a recent review), and the results are discussed in the light of this analysis. Estimates of WPE will also be presented to produce a fuller picture of the full impact of threading dislocations and point defects on LED performance.

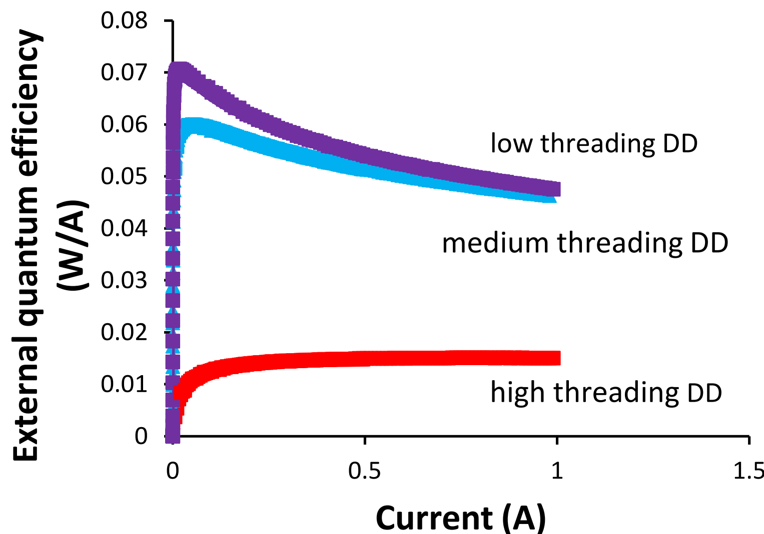

Figure 1. The external quantum efficiency vs current flowing through the device, for LED made on devices with a low (≈ 4×10^8 cm^{-2}), medium (≈8×10^8 cm^{-2}) and high (≈ 4×10^9 cm^{-2}), threading defect density.

Reference:

1. S. Karpov: ABC-model for interpretation of internal quantum efficiency and its droop in III-nitride LEDs: a review. Opt. Quant. Electron (2015) 47:1293 – 1303.

Fabrication of nanostructured III-N growth templates using Displacement Talbot Lithography and Nanoimprint Lithography

E.D. Le Boulbar and P.A. Shields

Department of Electronic and Electrical Engineering, University of Bath, BA2 7AY, UK

Nanostructured templates are the seed for efficient and well-controlled devices properties, for both planar and one dimensional structures. In III-Nitrides growth, nanostructured templates have been used to enhance LED light extraction, to filter propagating defects in c-plane and semipolar material and to grow core-shell devices. For example, both etched nanorod arrays and linear gratings of dielectric have been used in order to filter defects in semipolar materials. For the growth of InGaN/GaN core-shell devices, either holes in dielectric (SiN_x or SiO_2) or Ti can be used for the bottom-up growth of GaN nanorod arrays while etched nanorod arrays can be used as a three-dimensional growth scaffold.

All the above mentioned technologies require a nanopatterned GaN template. As technology increases from 2” to 4” and 6” wafers, there is a need to fabricate nanostructured templates on larger areas. The inherent wafer bowing, created by both the different coefficient of thermal expansion and the lattice mismatch between GaN and sapphire (or silicon), means homogeneous patterning is hard to achieve via conventional lithography techniques.

Displacement Talbot Lithography is a novel lithography technique that is similar to laser interference lithography but easier and simpler to realise. Due to its high depth of focus it is able to pattern on rough and bowed wafers. Nanoimprint lithography, due to its contact method, is also able to transfer various nanoscale shapes and patterns on bowed wafers, but with tighter restrictions on substrate parameters. These two techniques are promising for the large-scale fabrication of patterned substrates.

From a research perspective, one of the attractive attributes of Displacement Talbot Lithography is the ability to modify the filling factor of the pattern, which can be of use when seeking for an optimum template structure. We will present some initial results on the impact of the experimental parameters on the filling factor of a hexagonal pattern with 1 μm pitch and a linear grating with 400 nm period. We show that the hole apertures can be tuned from 300 nm to 500 nm for a fixed 1um pitch hexagonal pattern. Furthermore, we will present the strengths, limitations and applicability of both techniques.

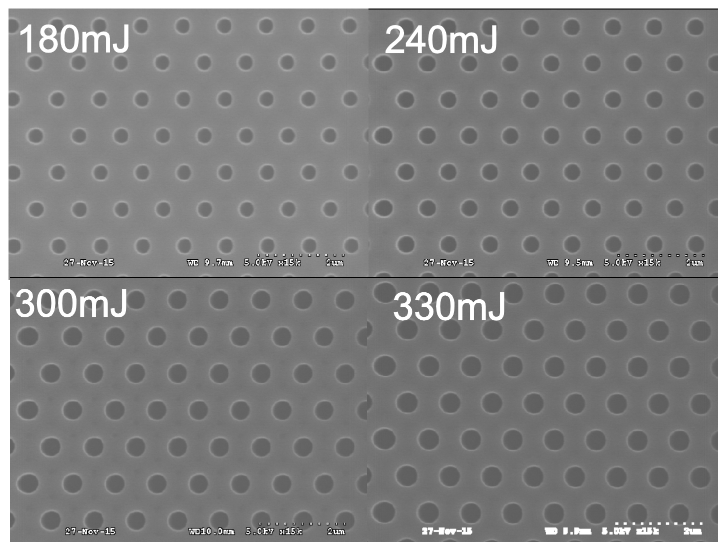

Figure 1: 1 μm pitch hexagonal array hole pattern obtained for different beam exposure

Properties of GaN Nanowires with $Sc_xGa_{1-x}N$ Insertion

A. Bao*[1], L. E. Goff[2], T. Zhu[1], S-L. Sahonta[1], M. Frentrup[1], H. J. Joyce[3], R. A. Oliver[1]

[1] Department of Materials Science and Metallurgy, University of Cambridge, Cambridge, UK
[2] Department of Physics, University of Cambridge, Cambridge, UK
[3] Department of Engineering, University of Cambridge, Cambridge, UK
* Corresponding e-mail Address: ab2115@cam.ac.uk (An. Bao)

ScGaN nanowires are anticipated to combine the unique properties of the nanowire geometry with the advantages of the novel ScGaN material system [1]. A ScGaN nanowire core of suitable composition may, for instance, act as a lattice-matched scaffold for radial m-plane InGaN quantum wells. The nanowire geometry also enables efficient radial strain relaxation, to minimise strain and the associated dislocations at axial ScGaN/GaN interfaces. Thus ScGaN nanowire materials are of considerable interest both for device applications, and for investigations of the fundamental properties of high quality strain-free ScGaN.

GaN nanowires were grown by a self-catalytic method via molecular beam epitaxy (MBE) [2]. A 20 nm $Sc_xGa_{1-x}N$ layer was inserted during the growth process. Scanning electron microscope-cathodoluminescence revealed that the nanowires had an emission at around 3.26 eV (380 nm) at low temperatures (10 K and 77 K), arising approximately from the position of the ScGaN insertion within the nanowires. This emission is more intense than the GaN bandgap emission, perhaps indicating carrier trapping in the vicinity of the ScGaN. The 3.26 eV (380 nm) peak was not observed in the control sample, consisting of GaN nanowires without the $Sc_xGa_{1-x}N$ insertion. The bandgap of $Sc_xGa_{1-x}N$ depends on its crystalline phase and the x value. Therefore, high resolution transmission electron microscopy was used, and confirmed the wurtzite phase of the $Sc_xGa_{1-x}N$ part. The x value in $Sc_xGa_{1-x}N$ is 0.04 ± 0.005, characterised by energy dispersive X-ray spectroscopy mapping in scanning transmission electron microscopy. However, the calculated bandgap in literature at this x value is 3.4 eV [3], corresponding to 365 nm emission rather than the observed 380 nm. One possibility is that the 3.26 eV emission arises from the formation of a heterostructure with type-II band alignment. However, the involvement of defects in the emission cannot be ruled out at this stage.

1. Moram, M. and S. Zhang, ScGaN and ScAlN: emerging nitride materials. Journal of Materials Chemistry A, 2014. **2**(17): p. 6042-6050.

2. Chèze, C., et al., Direct comparison of catalyst-free and catalyst-induced GaN nanowires. Nano Research, 2010. **3**(7): p. 528-536.

3. Tsui, H.C.L., et al., Band gaps of wurtzite ScxGa1−xN alloys. Applied Physics Letters, 2015. **106**(13): p. 132103-132103.

GaN Nanowires Grown on (111) Si Substrate by MOVPE

X Yu[1], S Shen[1], Y Hou[1], Y Gong[1], A Hazari[2], P Bhattacharya[2] and T Wang[1,*]

[1]Department of Electronic and Electrical Engineering, University of Sheffield, Mappin Street, Sheffield S1 3JD, United Kingdom

[2]Department of Electrical Engineering and Computer Science, University of Michigan, Ann Arbor, Michigan 48109-2122, USA

(*E-mail: t.wang@sheffield.ac.uk)

III-nitride nanowires (NWs) have attracted extensive attention very recently, as they exhibit a huge potential to the fabrication of novel optoelectronics which conventional and planar III-nitride devices could not achieve, such as reduced piezoelectric polarisation, reduced efficiency droop, compatibility to integrate electrical circuits on a nanometer scale, etc. Basically, there are two major kinds of approaches to achieving GaN NWs, one based on a post-growth top-down fabrication method, and another on direct bottom-up growth. For the former, we have demonstrated nanowire array LEDs or single nanorod LEDs with significantly improved performance.[1-3] However, the challenge is due to a further reduction in diameter of NWs down to below 100 nm. For the latter, it is mainly based on molecular beam epitaxy (MBE) grown NWs on silicon. A few groups have demonstrated excellent results using MBE grown NWs by vapor–liquid–solid growth or catalyst-free methods.[4] In remarkable contrast, there is no a very impressive report on metalorganic vapour phase epitaxy (MOVPE) grown NWs except using a selective growth approach on pre-patterned templates or substrates, although last two decades have seen major breakthrough in growth of ultra-high brightness GaN-based blue LEDs by using MOVPE techniques. This implies that there exists a major difference in GaN NW growth mechanisms between MOVPE and MBE. Very recently, our group has successfully obtained catalyst-free GaN nanowires on (111) Si by MOVPE, which has been compared with the MBE grown GaN NWs.

Our GaN NWs growth on (111) silicon starts with an initial annealing at 1100 ^{o}C in H_2 ambient for 10 min. Subsequently, a small amount of trimethylaluminum (TMA) precursor is flowing into the reactor at 1145 ^{o}C, and the temperature is ramped down below 900 ^{o}C for GaN NWs growth. Unlike MBE grown NWs where no any metal seed is required prior to NWs growth, the pre-flowing TMAl is crucial for MOVPE NWs growth. However, it is worth highlighting that the pre-flowing TMAl does not serve as metal nanodots for vapor–liquid–solid growth, but form Al-silicon cluster alloys. Without the TMAl pre-flowing or with TMGa pre-flowing, only GaN islands with a random diameter have been obtained. Another difference between MOVPE and MBE grown NWs is due to nitridation, any nitridation process prior to MOVPE growth leads to the growth of only GaN islands with random diameters and orientations. We have also systematically investigated the influences of growth temperature, TMG and ammonia flow rate, respectively.

Eventually, we have successfully achieved GaN NWs grown on (111) silicon as shown in Figure 1, demonstrating our GaN NWs grown using different temperatures. Our preliminary results shows an increase in growth temperature leads to straight and higher NWs with a top flat surface as shown in Figure 1a, while a reduced temperature allow us to obtain better uniformity as shown in Figure 1b. In general, the heights of NWs are ~ 900 nm, with a diameter ranging from 50 nm to 900 nm and

density of ~ 3×10^{8} cm^{-2}.

Crystal quality and morphology of the NWs have been investigated by X-ary diffraction (XRD) and scanning electron microscopy (SEM) measurements. From the XRD scans, it can be found that all the GaN NWs align along c-direction. All the NWs have the same in-plane crystal orientation as well. Room temperature photo-luminescence (PL) measurements show a strong emission at 365 nm.

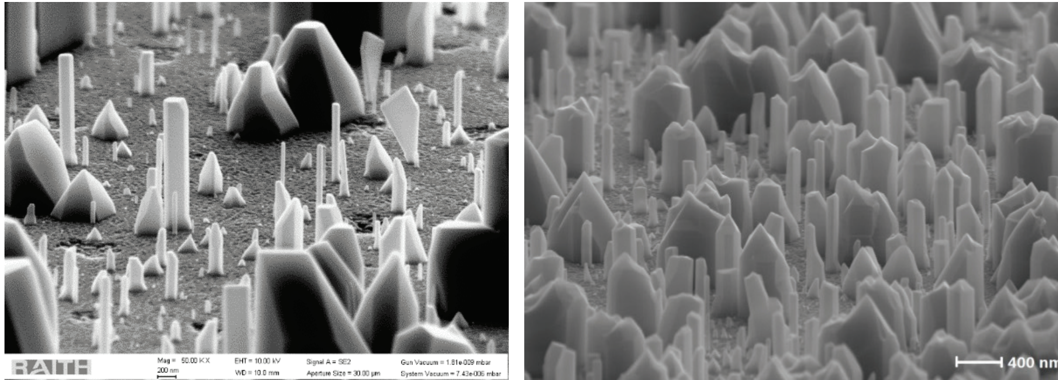

Figure 1. 75°-tilted SEM image of our GaN NWs grown on (111) Si by MOVPE with different growth temperatures (left: high; right: low)

References:

1. J Bai, Q Wang and T Wang, *J. Appl. Phys.* **111**, 113103 (2012)
2. J Bai, Q Wang and T Wang, *Phys. stat. Sol.* A **209**, 477(2012)
3. Y Hou, P Renwick, B Liu, J Bai and T Wang, *Sci. Rep.* **4**, 5014; DOI:10.1038/srep05014 (2014).
4. For an example, W. Guo, M. Zhang, A. Banerjee and P. Bhattacharya, *Nano Letters*, **10**, 3355 (2010).

Characterisation of GaNAs/GaN PN junction diode with scanning probe microscopy

F.S. Choi[1]*, S. Hosseini Vajargah[1], S. Zhang[1], J. Griffiths[1], S.V. Novikov[2], I. Guiney[1], D.J. Wallis[1], C. T. Foxon[2], R.A. Oliver[1], C.J. Humphreys[1]

[1] Department of Materials Science and Metallurgy, University of Cambridge, Cambridge CB3 0FS, UK
[2] School of Physics and Astronomy, University of Nottingham, Nottingham NG7 2RD, UK
* Corresponding email: fsc27@cam.ac.uk

Abstract

It is well known that high hole concentration in GaN is difficult to achieve due to the high activation energy of Mg dopants. Mg-doped p-type GaNAs has been demonstrated to give a high hole concentration up to $10^{20}cm^{-3}$. Additionally, the band gap of this material is smaller than that of GaN [1], thus making Ohmic contacts easier to form. Therefore, good ohmic contacts and low resistivity could be achieved and hence improved device performance can be realised by using this material. GaNAs PN diodes grown under different conditions were characterised with scanning probe microscopy techniques, namely scanning capacitance microscopy (SCM), tunnelling AFM (TUNA) and Kevin probe force microscopy (KPFM). A GaNAs film consisting of elongated As rich and less As rich grains has previously observed in transmission electron microscopy analysis [2]. The phase image in SCM measurements shows formation of a p-type GaNAs layer, confirming earlier device-level studies [3]. TUNA images show substantial regions of reduced conductivity in the GaNAs film on a length scale greater than the grain size which indicates an additional factor controlling the local conductivity. KPFM images show potential variation in different grains. We aims to correlate nanoscale SPM electrical measurements with macroscopic device performance data in order to assist optimisation the performance of future GaN-based devices.

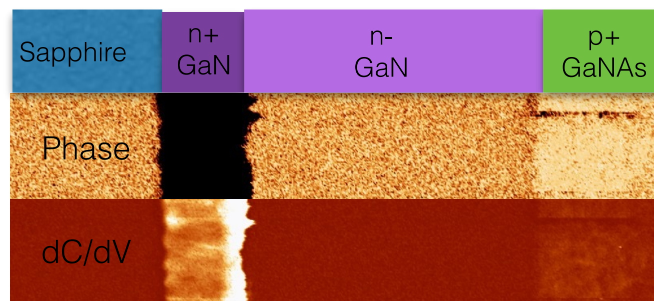

Figure 1. Phase image (top) and SCM amplitude image (bottom) of a GaNAs/GaN PN junction diode with scanning capacitance microscopy.

References:

[1] Novikov, S. V., et al. "Growth by molecular beam epitaxy of amorphous and crystalline GaNAs alloys with band gaps from 3.4 to 0.8 eV for solar energy conversion devices." Journal of Crystal Growth 323.1 (2011): 60-63.
[2] Liliental-Weber, Z., et al. "Microstructure of Mg doped GaNAs alloys." physica status solidi (c) 10.3 (2013): 453-456.
[3] H. Qian, et al."Characterisation of GaNAs/GaN PN junction diodes." Applied Physics Letter (2015): submitted.

Nanocathodoluminescence reveals the mitigation of the Stark shift in InGaN quantum wells by silicon doping

J. T. Griffiths[1], S. Zhang[1], B. Rouet-Leduc[1], W. Y. Fu[1], A. Bao[1], D. Zhu[1,2], D. Wallis[1,2], A. Howkins[3], I. Boyd[3], D. Stowe[4], M. J. Kappers[1], C. J. Humphreys[1], and R. A. Oliver[1]

[1]Department of Materials Science and Metallurgy, 27 Charles Babbage Road, Cambridge, CB3 0FS, United Kingdom

2. Plessey Semiconductors, Tamerton Road, Plymouth, PL6 7BQ, United Kingdom

3. Experimental Techniques Centre, Brunel University, Uxbridge, UB8 3PH, United Kingdom

4. Gatan UK, 25 Nuffield Way, Abingdon, Oxon, OX14 1RL, United Kingdom

InGaN quantum wells (QWs) show high internal quantum efficiencies over the ultraviolet to green spectrum and in white light emitting diodes (LEDs). However a persistent challenge to the development of higher efficiency devices is the strong polarisation field across the across the QWs along the polar axis. The polarisation induced internal electric fields cause the spatial separation of the electron and hole wavefunctions in the QWs, known as the quantum confined Stark effect (QCSE). It has been proposed that the internal electric field can be suppressed by silicon doping the quantum barriers (QBs) [1]. Moreover, Kim *et al*. have theoretically shown that the device efficiency may be improved by variations in the silicon dopant concentration through the QWs [2]. To confirm the simulated properties though, it is crucial to resolve the spectral properties of individual QWs.

In this study [3], nano-cathodoluminescence (nano-CL) reveals for the first time the spectral properties of individual InGaN QWs in a high efficiency LED structure and the influence of silicon doping on the emission properties. A silicon doped underlayer at 5×10^{18} cm^{-3} is included immediately prior to the growth of the 1st QW and the QBs between the QWs are subsequently doped to 1×10^{18} cm^{-3} (sample A). Two further multiple QW InGaN/GaN structures were also grown for reference with no underlayer but QB doping levels of 1×10^{18} cm^{-3} (sample B) and 1×10^{17} cm^{-3} (sample C). Nano-CL reveals variations in the emission wavelength that directly correlate with individual QWs. With QB doping greater than 1×10^{18} cm^{-3}, there is a continuous reduction in the emission wavelength of each of the subsequently grown QWs. The inclusion of a higher doped underlayer immediately prior to the growth of the 1st QW in the LED structure is shown to lead to a blue shift unique to the 1st QW.

The experimental variations in the emission wavelengths were reproduced by Schrödinger-Poisson simulations. The blue shift in emission wavelength through the QWs due to QB doping is found to be caused by screening of the internal electric fields. The reduction in the emission wavelength of the first grown QW due to the underlayer is also found to be the result of screening of the internal electric field. The mitigation of the QCSE and consequently stronger overlap of the electron and hole wavefunction, thus should result in an increase in the radiative recombination. Nano-CL thus may serve as an experimental approach to study and refine the design of future optoelectronic nanostructures, including the effects from doping and lead to improvements in device efficiency and functionality.

References:

[1] T. Deguchi, *et al*., Appl. Phys. Letts. **72**, 3329 (1998)
[2] D. Y. Kim, *et al*., IEEE Photonics. **7**, 1 (2015)
[3] J. T. Griffiths, *et al*., Nano Letts. **15**, 7639 (2015)

Investigation of Directional Light Emission from InGaN/GaN Vertical Light Emitting Diodes using Ordered Nanorod Arrays

S.A. Fox[1], S.M. Lis[1], P.A. Shields[1], D.J. Wallis[2], G. Thompson[3], J. Sarma[1] and D.W.E. Allsopp[1]
[1]*Dept. of Electronic and Electrical Engineering, University of Bath, UK*
[2]*Plessey Semiconductor Limited, Tamerton Road, Roborough, Plymouth, UK*
[3]*Digital Projection Limited, Greenside Way, Middleton, Manchester, UK*

Light emitting diodes (LEDs) employing InGaN/GaN nanorod arrays have been shown to exhibit enhanced light extraction efficiency [1, 2] and improved internal quantum efficiency [2, 3] due to the alleviated strain and reduction of the quantum confined Stark effect. Such devices have also been shown to display improved directionality in the far-field emission [4] making these devices highly suitable for etendue-limited applications such as high brightness projectors [5, 6]. In the work reported here we explore the feasibility of achieving highly directional light emission from vertical structure LEDs with an ordered NR array structure incorporated in place of the surface roughened region and the active region now located below the array and above a reflector contact.

Vertical LEDs were fabricated from commercial GaN-on-silicon epitaxy and the hexagonal nanorod arrays were fabricated via electron beam lithography and inductively coupled plasma etching. Two samples of NR etch depths 1μm and 1.6μm with a pitch of 1μm and base diameter of 0.9μm were processed and the active region is located approximately 130nm above a silver contact mirror (figure 1). Room temperature angular-resolved photoluminescence (PL) was measured for a fixed azimuth to obtain the far-field emission patterns of the two different structures from which Bragg diffraction was observed whereby the nanorod array acted as an optically thick diffraction grating [7] with preferential emission within a ±30° cone, however intensity minima were observed at 0° (surface normal).

Three-dimensional finite-difference time-domain (FDTD) [8] simulations were performed to model the two structures using dimensions from the design schematic. Initial FDTD results predicted strong directionality in the far-field emission as shown in figures 2(a) and 2(b) for nanorod heights of 1μm and 1.6μm respectively. For the etch depth of 1um, 'hyper-directionality' was observed over a spectral range of 40nm, an effect not seen in the experimental PL and found to be highly sensitive to variations in both NR height and pitch by as little as 50nm.

To obtain a better comparison of PL and FDTD results, more accurate FDTD modelling of the NR array vertical LEDs are made to include the optical properties of the AlN, AlGaN and SiO_2 layers inside the NRs and the silver reflector. Increasing the epitaxial thickness to that measured in SEM images and shifting the vertical position of the dipole above the silver reflector by just 20nm (i.e. altering p-GaN thickness) altered the directionality of the emission drastically highlighting the importance of an accurate fabrication process.

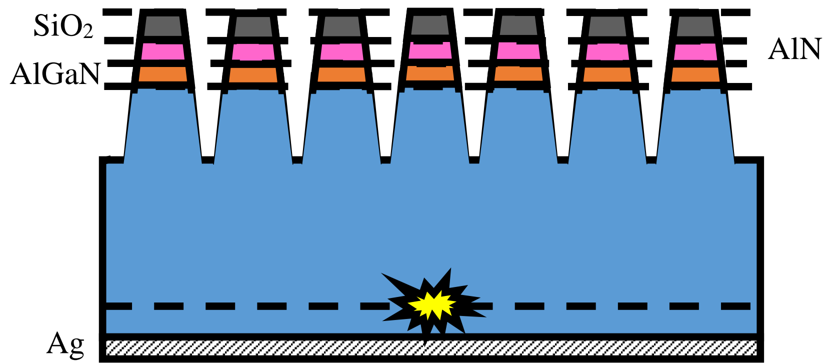

Figure 1: Schematic of vertical structure

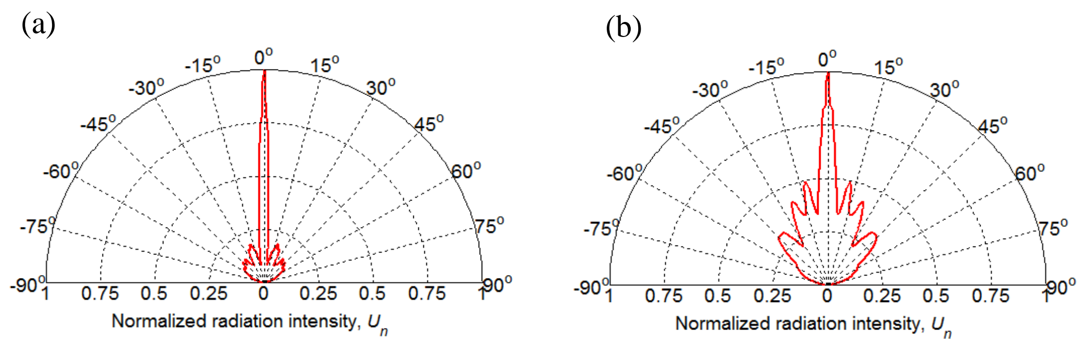

Figure 2: Far-field emission azimuthally and spectrally integrated (421 – 483nm) for NR height of (a) 1µm and (b) 1.6µm

[1] Q. Wang, J. Bai, Y. P. Gong, and T. Wang, *J. Phys. D, Appl. Phys.* **44**, 395102, 2011.
[2] J. Bai, Q. Wang, and T. Wang, *J. Appl. Phys.* **111**, 113103, 2012.
[3] Y.D. Zhuang, C.J. Lewins, S. Lis, P.A. Shields, D.W.E. Allsopp, *IEEE Photonics Tech. Lett.* **25**, 1047, 2013.
[4] Min-An Tsai, Peichen Yu, C. L. Chao, C. H. Chiu, H. C. Kuo, S. H. Lin, J. J. Huang, T.C. Lu, and S. C. Wang, *IEEE Photon. Technol. Lett.* **21**, 257, 2009.
[5] F. Fournier and J. Rolland, *J. Disp. Tech*. **4**, 86, 2008.
[6] G. Harbers, S.J. Bierhuizen and M.R. Krames, *J. Disp. Tech.* **3**, 98, 2007.
[7] R.R.A Syms and J.R. Cozens, *Optical Guided Waves and Devices*, McGraw-Hill Co. 1992.
[8] A. Taflove, *IEEE Trans. Electromagnetic Capability*, **22,** 191 – 202, 1980

Time dependence of cathodoluminescence from InGaN quantum dots grown on non-polar a-plane GaN

J.C. Jarman, T. Zhu, R.A. Oliver, W.Y. Fu

Department of Materials Science and Metallurgy, University of Cambridge
27 Charles Babbage Road, Cambridge CB3 0FS

Corresponding author: John Jarman, jcj27@cam.ac.uk

InGaN quantum dots (QDs) grown in a GaN matrix show promise as practical single-photon sources for operation at room temperature, due to their sharp emission in the blue-green region and deep confinement potential [1]. However, a variation in the wavelength of emission with time (spectral diffusion) is observed in these QDs grown on the polar c-plane of GaN [2]. This makes the coupling of QDs to a resonant optical cavity more difficult, and impairs control of the QD as a qubit for use in quantum information processing. Additionally, for single-photon source use, the spectral diffusion must be smaller than the spacing between adjacent exciton and biexciton peaks, so that the single-exciton emission can be isolated.

This study investigates the cathodoluminescence (CL) from QDs grown by modified droplet epitaxy on non-polar a-plane GaN, where the reduced internal fields mean that QDs are expected to show reduced spectral diffusion [3]. The GaN epilayers used for this study were grown on r-plane sapphire substrates, using epitaxial lateral overgrowth (ELOG) to generate regions of lowered defect density which alternate with regions of high defect density. This allowed us to draw comparisons between the amounts of spectral diffusion observed in regions of differing dislocation and stacking fault density.

We observed that the likelihood of finding a dot that showed a high degree of spectral diffusion was significantly higher in the high-defect-density regions compared to low-defect-density regions. This suggests that spectral diffusion in a-plane InGaN QDs is influenced by stochastic charge trapping in defects, generating local fields which influence emission wavelength by the quantum-confined Stark effect (QCSE) [4]. Additionally, the magnitude of spectral diffusion (measured in terms of standard deviation, deviation from a moving average, and large jump frequency) was determined to be low enough for coupling to an optical cavity for the vast majority of dots measured on the low-defect regions.

These results show that an ELOG defect-reduction growth method could be effective in suppressing spectral diffusion in a-plane InGaN QDs to the extent required for practical single-photon emitters.

1. Kako, S., et al., *A gallium-nitride single-photon source operating at 200K.* Nature Materials, 2006. **5**(11): p. 887-892.
2. Reid, B.P.L., et al., *Origins of Spectral Diffusion in the Micro-Photoluminescence of Single InGaN Quantum Dots.* Japanese Journal of Applied Physics, 2013. **52**(8): p. 4.
3. Zhu, T., et al., *Non-polar (11-20) InGaN quantum dots with short exciton lifetimes grown by metal-organic vapor phase epitaxy.* Applied Physics Letters, 2013. **102**(25).
4. Robinson, J.W., et al., *Quantum-confined Stark effect in a single InGaN quantum dot under a lateral electric field.* Applied Physics Letters, 2005. **86**(21).

Ultraviolet emission from GaN-based metal-insulator-semiconductor diodes

C. Lin[1], K. Kavanagh[2], L. Tsui[1], M.J. Kappers[3], D. Allsopp[2], M.A. Moram[1]

[1] *Department of Materials, Imperial College London, United Kingdom*
[2] *Department of Electric Engineering, University of Bath, United Kingdom*
[3] *Cambridge Centre for Gallium Nitride, University of Cambridge, United Kingdom*

Conventional *p*-*n*-based III-nitride ultraviolet light-emitting diodes (UV-LEDs) typically have low efficiencies, short lifetimes, and high costs relative to LEDs emitting in the blue or red wavelength ranges. The challenges for these devices include the difficulty of achieving high p-type conductivity in III-nitrides, light absorption by the p-type layer and cracking of the device structure during or after growth. Therefore, it is of interest to develop new UV LEDs with simpler, thinner structures, lower process costs and/or higher efficiencies. Therefore, this study aims to assess the feasibility of III-nitride metal-insulator-semiconductor (MIS) structures for UV emission.

The MIS devices were formed by Au electrodes, a 3 nm/5 nm/10 nm/20 nm AlN insulating layer and a 2 μm *n*-doped GaN layer (a schematic diagram is shown in Fig. 1). The effect of the insulating layer thickness on the current-voltage (I-V) characteristic was investigated and a thickness of 5 - 10 nm gave the greatest output power. Electroluminescence (EL) measurements were performed for the MIS device with 10 nm AlN insulating layer and near-band-edge (NBE) emission at 365 nm was observed, shown in Fig. 2. Temperature dependent I-V measurements suggest that the electron and hole transport is governed by hopping, thermionic emission and space charge limited conduction.

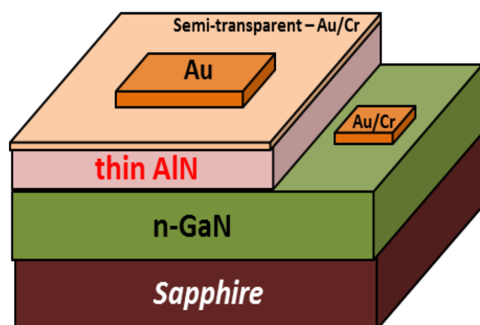

Fig. 1. Schematic of the MIS UV-LED structure.

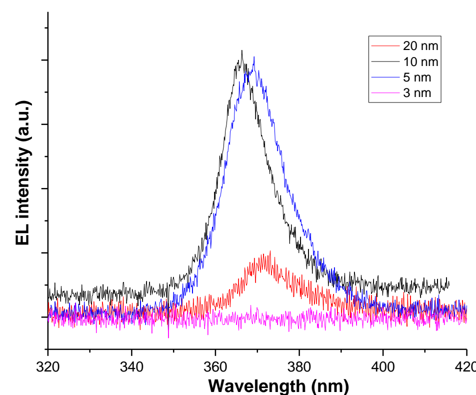

Fig. 2 Room temperature EL emission spectra from MIS structures with different insulator thicknesses.

References

[1] *H. Morkoç, Handbook of Nitride Semiconductors and Devices (2009).*

[2] *Y. Muramoto, M. Kimura, and S. Nouda, Semicond. Sci. Technol.* ***29****, 084004 (2014).*

[3] *K. Balakrishnan, T. Katona, and A. Khan, Nat. Photonics* ***2****, 77 (2008).*

Growth of GaN Epitaxial Films on Polycrystalline Diamond with Metal-organic Vapour Phase Epitaxy via a Si_xC Layer

Quanzhong Jiang[1], Duncan W.E. Allsopp[1] and Chris R. Bowen[2]

[1] Department of Electronic and Electrical Engineering, University of Bath, Bath BA2 7AY, UK

[2] Department of Mechanical Engineering, University of Bath, Bath BA2 7AY, UK

There is a technical need for the epitaxial growth of electronic devices directly on to low-cost polycrystalline diamond (PD) substrates with high thermal conductivity (~2000 W/mK) in order to extract heat efficiently from an operating device to maintain performance stability and increase lifetime. Since a PD surface does not provide sufficient structural periodicity at the wafer scale, there has been limited progress to date. It was demonstrated by Georgakilas et al [1], using molecular beam epitaxy, that GaN layers could be grown on PD substrates. However, the films have tilts up to 2°, which is the full width at half maximum (FWHM) of GaN(0002), and therefore unlikely to be suitable for devices.

This paper reports epitaxial growth of GaN films on polycrystalline diamond substrates with metal-organic vapour phase epitaxy by using a non-single crystal Si_xC layer that is formed during deposition of polycrystalline diamond on a silicon substrate. The Si_xC layer, which is free of Si-Si bonds at its surface, acts to provide sufficient structure ordering information for the formation of single crystal GaN films at the wafer scale. The films appear to have a nitrogen-polarity. The epitaxial relationship between nitrides and the Si(111) substrate, on which the Si_xC layer is formed, can be used to describe the epitaxial relationship between nitrides and the Si_xC layer. It is also shown that a three-dimensional island (3D) growth process is needed to mitigate hexagonal defects that are often observed on GaN surfaces. Intensive 3D growth and curvature engineering act as a means for essential reduction of tensile stress in as-grown GaN layers. With such engineering the GaN epitaxial layer thickness was found to be crack-free up to a thickness of 1.1 microns. The twist and tilt can be as low as 0.65^{o} and 0.39^{o} and are broadly comparable with GaN grown on Si substrates of a similar structure, thereby creating a basis for fabricating GaN based thin-film HFETs with improved heat sinking.

Reference

[1] A. Georgakilas, K.E. Areouli, K. Tsagaraki, A. Kostopoulos, A. Stavrinidis, G. Konstantinidis and A. Adikimenakis, International Workshop on Nitride Semiconductors, Wroclaw, Poland, Aug. 2014, paper TuG09.

Electrical characterisation of InAlN/AlGaN/GaN HEMT on Si substrate with varying InAlN thickness

Konstantinos Floros[a], Xu Li[a], Ivor Guiney[b], Sung-Jin Cho[a], Gary Ternent[a], Dilini Hemakumara[a], Olesya Ignatova[a], David A.J. Moran[a], Edward Wasige[a], Colin J. Humphreys[b] and Iain G. Thayne[a]
[a] School of Engineering, University of Glasgow, Rankine Building, Oakfield Avenue, Glasgow, G12 8LT
[b] Department of Materials Science & Metallurgy, University of Cambridge, Cambridge CB3 0FS UK
e-mail: k.floros.1@research.gla.ac.uk

Introduction

Semiconductor nitrides such as aluminium nitride (AlN), gallium nitride (GaN) and indium nitride (InN) are attractive for high power applications due to their large band gap, high critical electric field and good electron transport properties. These materials and their ternary alloys, especially AlGaN and GaN are widely used in high electron mobility transistors, where 2-D electron gas (2DEG) sheet charge is created by spontaneous and piezoelectric polarisation at the AlGaN/GaN interface [1]. Compared to AlGaN/GaN, InAlN based heterostructures can induce higher quantum well polarisation charges, which in turn result in higher device currents [2].

Hiroki et al [3-4] have demonstrated the growth of InAlN/AlGaN/GaN on sapphire (Al_2O_3) substrates. They tested Schottky gate HEMT based on these structures and reported improved gate leakage current and sub-threshold swing compared to devices that use an InAlN/AlGaN based structure with similar barrier heights. These promising epi-layer structures are limited by the choice of substrate. An extension of the technology to silicon substrates is more cost-effective and important for future commercialisation.

In this work, we have demonstrated InAlN/AlGaN/GaN HEMT on Si substrates and characterised three wafers with different InAlN thicknesses using room temperature Hall measurements and transfer length method (TLM) measurements.

Experiments and Results

The HEMT structures were grown on 6″ diameter silicon wafer by MOCVD. The structures were first isolated by a 600nm deep mesa etch using $SiCl_4$ reactive ion etching (RIE). Consequently, Ti/Al/Ni/Au source and drain ohmic contacts of 30/180/40/100 nm thicknesses were deposited by lift-off and annealed at 770° C for 30s in N_2 atmosphere. This was followed by the formation of Schottky gate Ni/Au contacts of 20/200 nm thicknesses, also using the lift-off technique.

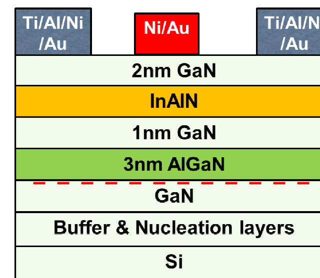

Fig.1. InAlN/AlGaN/GaN HEMT layer structure.

Table 1: TLM and Hall measurements for varying InAlN thicknesses.

x nm InAlN	TLM		Hall measurements		
	R_c (Ωmm)	R_{sh} (Ω/sq)	R_{sh} (Ω/sq)	μ_H (cm^2/Vs)	n_H ($x10^{13}$ cm^{-2})
x = 5nm	0.95	273	277	1540	1.47
x = 6nm	0.67	300	301	1370	1.52
x = 8nm	0.67	306	323	1060	1.82

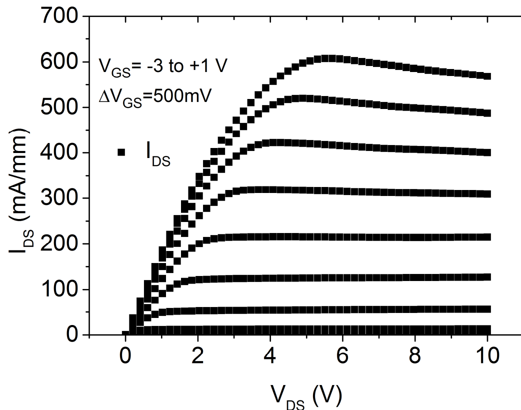

Fig.2. DC output characteristics of 8nm InAlN/3nm AlGaN/GaN HEMT (W_g=100µm, L_{ds}=12µm, L_g=3µm).

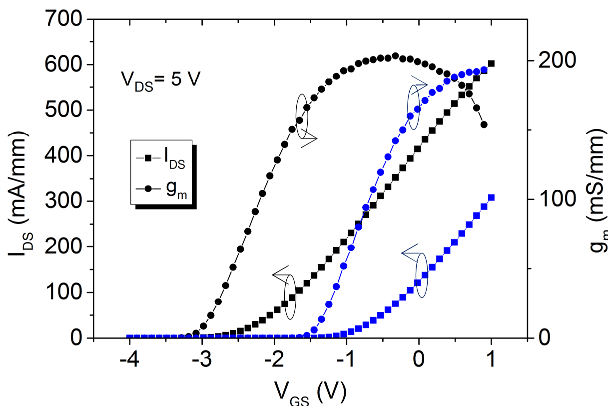

Fig.3. Comparison of transfer characteristics for 8nm InAlN (black) and 5nm InAlN (blue). The increased polarisation-induced charge for thicker (8nm) InAlN, results in a more negative threshold voltage.
(W_g=100µm, L_{ds}=12µm, L_g=3µm)

The low sheet and contact resistances as well as the smooth surface of the wafers grown resulted in high maximum currents I_{DS} > 600mA/mm and transconductance g_m > 200 mS/mm.

Acknowledgments

This work is supported by the EPSRC grant "Silicon Compatible GaN Power Electronics" EP/K014471/1.

References

[1] A. Bykhovski, B. Gelmont, and M. Shur, "The influence of the strain-induced electric field on the charge distribution in GaN-AlN-GaN structure," *J. Appl. Phys.*, vol. 74, no. May 2013, pp. 6734–6739, 1993.

[2] J. Kuzmík, "Power electronics on InAlN/(In)GaN: Prospect for a record performance," IEEE Electron Device Lett., vol. 22, no. 11, pp. 510–512, 2001.

[3] M. Hiroki, N. Maeda, and T. Kobayashi, "Electrical properties and device characteristics of InAlN/AlGaN/AlN/GaN heterostructure field effect transistors," *Phys. Status Solidi Curr. Top. Solid State Phys.*, vol. 6, no. SUPPL. 2, pp. 1–5, 2009.

[4] M. Hiroki, N. Maeda, and T. Kobayashi, "Fabrication of an InAlN/AlGaN/ AlN/GaN Heterostructure with a Flat Surface and High Electron Mobility," *Appl. Phys. Express*, vol. 1, p. 111102, 2008.

High Temperature Performance of 600 V GaN/AlGaN/GaN Heterostructure Field Effect Transistors on Silicon Substrates

K. B. Lee[1], S. Jiang[1], Z. H. Zaidi[1], H. Qian[1], I. Guiney[2], D. J. Wallis[2], C. J. Humphreys[2] and P. A. Houston[1]

[1]*Department of Electronic and Electrical Engineering, University of Sheffield, Mappin Street, Sheffield S1 3JD, United Kingdom*

[2]*Department of Material Science and Metallurgy, University of Cambridge, 27 Charles Babbage Road, Cambridge CB3 0FS, United Kingdom*

AlGaN/GaN heterostructure field effect transistors (HFETs) possess excellent physical and electrical properties, such as wide bandgap, high breakdown field, high saturation electron drift velocity and good thermal stability. These properties make it particularly suitable for high speed and high power switching applications operating at elevated temperatures. It is therefore important to understand the changes in the critical device parameters at high operating temperatures.

In this work, we study the high temperature DC and dynamic operation of 600 V GaN/AlGaN/GaN HFETs on silicon substrates. Figure 1 shows the gate transfer characteristics of the HFET between 25 and 205 ^{0}C. A shift of -0.8 V in the threshold voltage is observed as temperature rises to 205 ^{0}C. The on-resistance (R_{on}) of the device increases from 7 to 21 Ω.mm as the temperature increases from room temperature to 205 ^{0}C (Figure 2). Sheet resistance measured from the transmission line method indicates that the increase of R_{on} with temperature is primarily due to an increase of channel resistance. The deterioration of sheet resistance and R_{on} is believed to be caused by degradation in the polar phonon limited channel mobility with increasing temperature [1].

The device exhibits an excellent off-state blocking voltage capability of 600 V up to 205 ^{0}C as illustrated in Figure 3. It is noted that gate leakage current dominates the off-state leakage across the temperature range studied. Between room temperature and 88 ^{0}C, the gate leakage current shows a negative temperature dependence with an activation energy of 163 meV. Above 88 ^{0}C, the leakage current increase with temperature with an activation energy of 191 meV. The dynamic R_{on} of the device increases with temperature and drain stress bias (Figure 4), indicating the presence of thermally and field-assisted charge trapping on the surface and/or in the carbon-doped GaN buffer region between the gate and drain.

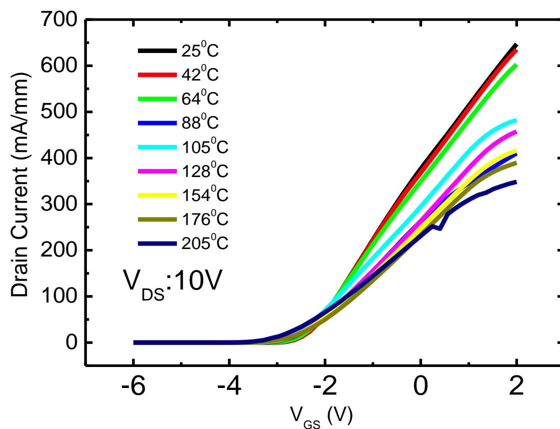

Figure 1: Gate transfer characteristics GaN/AlGaN/GaN HFETs with varying temperature.

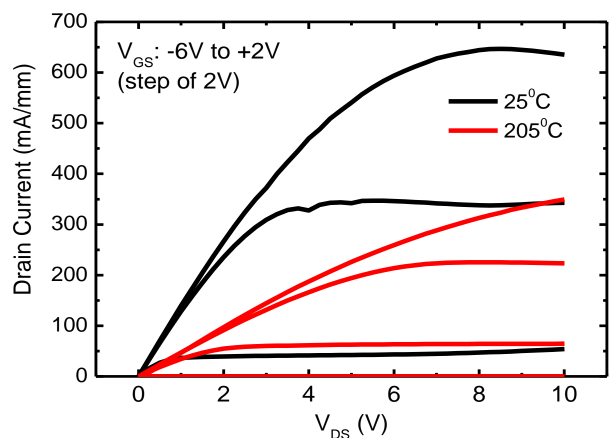

Figure 2: I-V characteristics GaN/AlGaN/GaN HFETs at 25^{0}C and 205^{0}C.

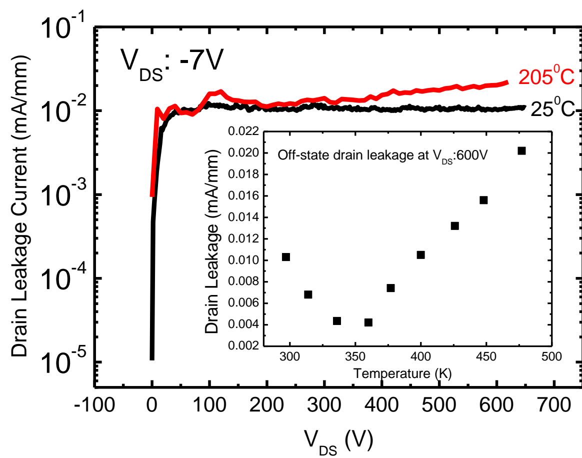

Figure 3: Off-state characteristics of GaN/AlGaN/GaN HFETs at 25^{0}C and 205^{0}C.

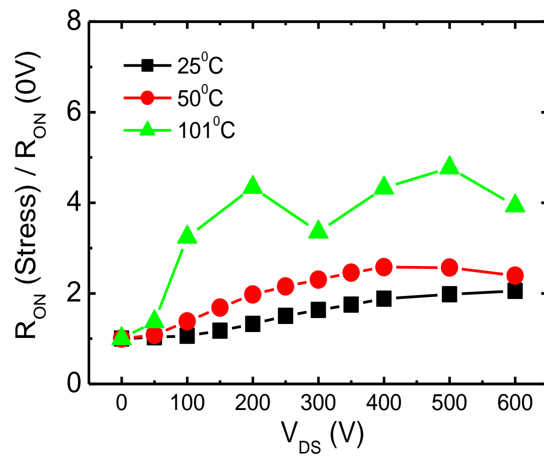

Figure 4: Ratio of dynamic Ron to DC Ron for GaN/AlGaN/GaN HFETs as a function of voltage with varying temperature.

Reference:

[1] N. Maeda, K. Tsubaki, T. Saitoh and N. Kobayashi, *Appl. Phys. Lett.* **79**, 1634 (2001)

Characterization of amorphous and polycrystalline p-$GaN_{1-x}As_x$ / n-GaN diodes

H. Qian [1], K. B. Lee[1], S. Hosseini Vajargah[2], S.V. Novikov[3], I. Guiney[2], Z. H. Zaidi[1], S. Jiang[1], D. J. Wallis[2], C. T. Foxon[3], C. J. Humphreys[2] and P. A. Houston[1]
[1]Department of Electronic and Electrical Engineering, University of Sheffield, Sheffield S1 3JD, UK
[2]Department of Material Science and Metallurgy, University of Cambridge, Cambridge CB3 0FS, UK
[3]School of Physics and Astronomy, University of Nottingham, Nottingham NG7 2RD, UK

MBE grown Mg-doped $GaN_{1-x}As_x$ (0.17<x<0.8) has achieved a hole concentration up to 1×10^{20} cm^{-3}. [1] This high hole concentration can be used to improve the performance of electronic devices such as PN diodes, p-GaN gated HFETs and JFETs. However, reports on the characteristics of the material in electronic devices is still lacking. In this report, we present a study of the electrical characteristics of p-$GaN_{1-x}As_x$/n-GaN junction diodes and include the structural properties.

The n-type GaN templates were grown on sapphire substrates by metal-organic chemical vapour deposition (MOCVD). A 500 nm heavily Si doped n^+GaN contact layer was first grown followed by a 3 μm GaN drift layer with Si concentration of 2×10^{16} cm^{-3}. Subsequently, a 1 um thick Mg-doped $GaN_{1-x}As_x$ layer was grown using plasma-assisted molecular beam epitaxy (PA-MBE) with the Ga beam equivalent pressure (BEP) varied between 2.3×10^{-7} (sample 1) and 2.1×10^{-7} (sample 2) Torr. The detailed growth information is published elsewhere [2]. A hole concentration of 8.5×10^{19} cm^{-3} was measured from a calibration sample with growth conditions similar to sample 1. Fig. 1 shows transmission electron microscopy (TEM) images of the two samples. An all-polycrystalline structure is observed in sample 1 whereas a transition from amorphous to polycrystalline is observed in sample 2. The grown structure depends critically on the Ga BEP.

Fig. 2 and Fig. 3 show the ideality factors and reverse saturation currents, I_0, extracted from the temperature dependent current voltage (I-V-T) characteristics of the two samples in the low forward bias regime (<0.5 V) to determine the carrier transport mechanisms. The results suggest different dominant mechanisms for the two different samples. For instance, recombination dominates in sample 1 throughout the measured temperature range whereas a transition from tunneling at low temperature to recombination at high temperature is observed in sample 2. The transport mechanisms in the high forward bias and reverse bias regimes were also analyzed. The results will be useful for designs of electronics devices using this material.

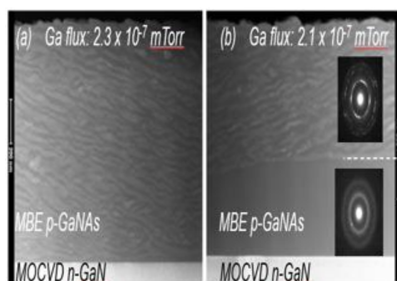

Fig. 1. TEM images with electron diffraction patterns of GaNAs layers showing (a) sample 1 (all-polycrystalline structure), and (b) sample 2 (amorphous/polycrystalline structure).

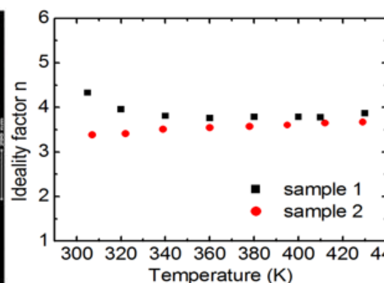

Fig.2. Temperature dependent of ideality factors of sample 1 and sample 2.

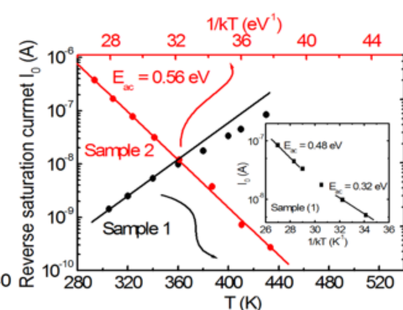

Fig.3. Temperature dependence of I_0 as a function of T (sample 1) and $1/kT$ (sample 2). Inset: I_0 as a function of $1/kT$ of sample 1.

References

[1] A. X. Levander, et. al., "Doping of $GaN_{1-x}As_x$ with high As content", Journal of Applied Physics 110, 093702 (2011)
[2] S.V. Novikov, et. Al., "Growth by molecular beam epitaxy of amorphous and crystalline GaNAs alloys with bandgaps from 3.4 to 0.8 eV for solar energy conversion devices", Journal of Crystal Growth 323 (2011) 60–63